B1: Flows, Fluctuations and Complexity

Toby Adkins

June 19, 2017

Contents

1. *Fluid Flows*

In this chapter, we investigate the physics associated with fluid flows, including:

- Conservation Principles
- Flow Fields
- Rotations and Vorticity
- Some Specific Cases
- Instabilities and Turbulence

The Navier-Stokes equation is the defining equation for this chapter; it can be used to describe how fluids move across a very large range of length-scales, from microscopic, viscous flows on the level of bacteria, to macroscopic flows in planetary atmospheres. As such, we will be careful to introduce it properly, and discuss how it is to be applied in different scenarios.

1.1 Conservation Principles

In order to gain an understanding of how fluids behave, we shall examine some different conservation laws when applied to such systems, in the hope that we will be able to extract interesting physical insights from the resultant equations.

Throughout this chapter, we will be considering *fluid elements*; these are infinitesimal 'pockets' of the fluid within the spatial range $[\mathbf{r}, \mathbf{r} + d\mathbf{r}]$, and with velocities in the range $[\mathbf{u}, \mathbf{u} + d\mathbf{u}]$. That is, we will not be considering individual particle behaviour, only the behaviour of our fluid elements. Suppose that f is some scalar function related to a particular fluid element that depends on both the position and time $f = f(\mathbf{r}(t), t)$ of said fluid element. Then:

$$\frac{df}{dt} = \frac{\partial f}{\partial \mathbf{r}} \cdot \frac{\partial \mathbf{r}}{dt} + \frac{\partial f}{\partial t} = \mathbf{u} \cdot \frac{\partial}{\partial \mathbf{r}} f + \frac{\partial}{\partial t} f \tag{1.1}$$

We thus introduce the operator

$$\boxed{\frac{d}{dt} = \frac{\partial}{\partial t} + \mathbf{u} \cdot \nabla} \tag{1.2}$$

This is known as the *material* or *convective derivative*. This describes the time rate of change of a physical quantity for a fluid element that is subjected to a time and spatially dependent macroscopic velocity field $\mathbf{u}$.

1.1.1 Conservation of Mass

Let the fluid density be $\rho(\mathbf{r}, t)$ be the density of our fluid, and $\mathbf{u}(\mathbf{r}, t)$ be the local fluid velocity field. Consider a volume V bounded by a closed surface $S = \partial V$. In typical conservation law fashion, we argue that the rate of change of mass within this volume will be opposite and equal to the rate at which the mass leaves the volume through the bounding surface:

$$\frac{\partial}{\partial t} \int_V dV\, \rho = -\int_{\partial V} d\mathbf{S} \cdot \mathbf{u}\, \rho = -\int_V dV\, \nabla \cdot (\rho \mathbf{u}) \tag{1.3}$$

where the second equality follows from applying the divergence theorem. As this must hold for all possible volumes, we conclude that

$$\boxed{\frac{\partial \rho}{\partial t} + \nabla \cdot (\rho \mathbf{u}) = 0} \tag{1.4}$$

This is a statement of the conservation of mass. If the fluid is *incompressible*, then ρ is constant in both time and space, giving rise to the condition

$$\boxed{\nabla \cdot \mathbf{u} = 0} \tag{1.5}$$

This is a statement of the fact that pressure changes in the flow will not effect the local density much. Liquids generally have a low compressibility, and so much fluid behaviour can be modelled under these conditions. Similarly for gases with small internal pressure gradients.

1.1.2 Conservation of Momentum

Let us introduce the Newtonian *stress tensor*

$$\sigma_i^j = -\underbrace{p\, \delta_i^j}_{\text{pressure}} + \underbrace{\eta \left(\partial^j u_i + \partial^i u_j\right)}_{\text{viscous stress}} - \underbrace{\frac{2}{3} \eta\, \delta_i^j \nabla \cdot \mathbf{u}}_{\text{compressive stress}} \tag{1.6}$$

where $p(\mathbf{r},t)$ is the pressure of the fluid, and η is the *dynamic viscosity*. This quantity describes the action of forces on fluid elements, which is an important consideration for the conservation of momentum. Specifically, σ_i^j is the i^{th} component of the stress (force per unit area) on an element of surface with normal in the direction j:

$$t_i = \sigma_i^j n_j \tag{1.7}$$

Why does the viscous stress term take this form? Well, we know that it must depend on velocity gradients, from which the largest contribution is linear if the gradients are weak, and that it must be unaffected by a change of coordinate system (symmetric under the exchange $i \leftrightarrow j$). Note that the quantity $\partial^j u_i$ is sometimes referred to as the *velocity gradient tensor*.

Let us suppose that we are considering a fluid that is subject to internal stress forces described by σ_i^j, and some conservative body force per unit volume $\mathbf{f} = -\nabla\chi$. Consider the i^{th} component of the Newtonian conservation equation:

$$\underbrace{\int_V dV\, \rho \frac{du_i}{dt}}_{\text{rate of change of momentum}} = \underbrace{\int_V dV\, \partial_j \sigma_i^j}_{\text{stress forces}} + \underbrace{\int_V dV\, f_i}_{\text{body forces}} \tag{1.8}$$

Again, as this must hold for any volume, we can write that

$$\rho \frac{du_i}{dt} = \partial_j \sigma_i^j + f_i \tag{1.9}$$

Let us now consider the quantity $\partial_j \sigma_i^j$ more closely:

$$\partial_j \sigma_i^j = -\partial_j \delta_i^j p + \eta(\partial_j \partial^j u_i + \partial_j \partial^i u_j) - \frac{2}{3}\eta \partial_j \delta_i^j \nabla \cdot \mathbf{u} \tag{1.10}$$

$$= -\partial_i p + \eta \partial_j \partial^j u_i - \frac{2}{3}\eta \partial_i \nabla \cdot \mathbf{u} \tag{1.11}$$

where we have made use of the fact that $\partial_j \partial^i u_j = \partial^i \partial_j u_j = 0$. Let us now assume that the fluid is incompressible, such that we can ignore the last term in this equation. Substitute (1.11) into (1.9) to obtain

$$\rho \frac{du_i}{dt} = -\partial_i p + \eta \partial_j \partial^j u_i + f_i \tag{1.12}$$

Using (1.2), we can write this in vector form as

$$\boxed{\rho\left(\frac{\partial \mathbf{u}}{\partial t} + (\mathbf{u}\cdot\nabla)\mathbf{u}\right) = -\nabla p + \eta \nabla^2 \mathbf{u} + \mathbf{f}} \tag{1.13}$$

This is the all-important *Navier-Stokes* equation for incompressible fluid flows. This equation is often written when divided throughout by ρ, in which case we define the *kinematic viscosity* $\nu = \eta/\rho$. This, as well as η, are parameters that can be calculated from Kinetic theory. Note that when the force is gravity, we have that $\chi = \rho g z$ such that $\mathbf{f} = -\rho g \mathbf{e}_z$.

The Navier-Stokes equation is a continuum equation, meaning that it is written in terms of the (assumed) continuous functions $\mathbf{u}(\mathbf{r},t)$ and $\rho(\mathbf{r},t)$. We can specify their value at a point, but what we really mean is their average value over a region of size ℓ_0; if we look below this box size, the predictions of the Navier-Stokes equation will break down. Navier-Stokes also breaks down for steep velocity gradients (where higher order terms are important), and for fluids where there are other effects (viscoelastic fluids, magnetised fluids etc).

1.1.3 Conservation of Energy

To round off our consideration of conservation principles, let us take a look at energy. The energy density associated with a fluid can be written as

$$\varepsilon = \frac{1}{2}\rho u^2 + \frac{p}{\gamma - 1} \tag{1.14}$$

where γ is the adiabatic index from Thermodynamics ($\gamma = 5/3$ for an ideal gas). We shall assume the system is subject to no external forces ($\mathbf{f} = 0$). Then, for a volume V bounded by a closed surface $S = \partial V$, we can write that

$$\underbrace{\frac{\partial}{\partial t}\int_V dV\, \varepsilon}_{\text{rate of change of energy}} = \underbrace{-\int_{\partial V} d\mathbf{S}\cdot\mathbf{u}\,\varepsilon}_{\text{flux of energy}} \underbrace{-\int_{\partial V} d\mathbf{S}\cdot\mathbf{u}\,p}_{\text{work done on surface}} \tag{1.15}$$

Using the divergence theorem on the two terms on the right-hand side, and recognising that this relationship must hold for all volumes, it follows that

$$\frac{\partial \varepsilon}{\partial t} = -\nabla(\varepsilon \mathbf{u}) - \nabla(p\mathbf{u}) \tag{1.16}$$

Substituting in our expression for ε, evaluating derivatives, and collecting like terms, we can write this equation as

$$\frac{1}{2}u^2\left(\frac{\partial \rho}{\partial t} + \nabla(\rho\mathbf{u})\right) + \rho\mathbf{u}\cdot\left(\frac{\partial \mathbf{u}}{\partial t} + (\mathbf{u}\cdot\nabla)\mathbf{u}\right) = -\frac{1}{\gamma-1}\left(\frac{\partial p}{\partial t} + \gamma\mathbf{u}\cdot\nabla p + \gamma p\nabla\cdot\mathbf{u}\right) \tag{1.17}$$

The two terms on the left-hand side should be familiar as including expressions for mass conservation (1.4) and momentum conservation (1.13). Substituting these in, we find that

$$-(\gamma-1)\eta\,\mathbf{u}\cdot\nabla^2\mathbf{u} = \frac{\partial p}{\partial t} + \mathbf{u}\cdot\nabla p + \gamma p\nabla\cdot\mathbf{u} \tag{1.18}$$

To write this in a more compact form, we re-introduce ρ by expanding (1.4) and re-arranging for $\nabla\cdot\mathbf{u}$:

$$-(\gamma-1)\eta\,\mathbf{u}\cdot\nabla^2\mathbf{u} = \frac{\partial p}{\partial t} + \mathbf{u}\cdot\nabla p - \frac{\gamma p}{\rho}\frac{\partial \rho}{\partial t} - \frac{\gamma p}{\rho}\mathbf{u}\cdot\nabla p \tag{1.19}$$

which can be re-written into the neat expression

$$\boxed{\frac{\rho^{\gamma-1}}{\gamma-1}\left(\frac{\partial}{\partial t} + \mathbf{u}\cdot\nabla\right)\frac{p}{\rho^\gamma} + \nu\,\mathbf{u}\cdot\nabla^2\mathbf{u} = 0} \tag{1.20}$$

This is our statement of energy conservation; the interaction between pressure and density is balanced by the dissipation due to viscosity. Note that in a system where we take the limit that $\nu \to 0$, we see that there are no energy dissipation; the work done within the fluid causes fluctuations in density, which is a conservative process.

1.2 Flow Fields

The equations conservation equations derived in the previous section should, in principle, allow us to solve any well-behaved fluid system. However, throughout the remainder of this chapter, we will mostly be interested in the solutions to the Navier-Stokes equation (1.13), as we are usually interested in the form of the flow field $\mathbf{u}$.

There are three particularly important flows that one should be familiar with. We shall initially consider only flow fields in the x-y plane. These are as follows:

- Straining flow - This flow type causes compression along one spatial direction, and rarefaction in another. We can describe this by the velocity field

$$\mathbf{u}_{\text{strain}} = \alpha(y, x, 0) \tag{1.21}$$

- Rotational flow - This flow type, as the name suggests, causes a rotation of the fluid with some determined handedness. We can describe this by the velocity field

$$\mathbf{u}_{\text{rotational}} = \beta(y, -x, 0) \tag{1.22}$$

- Shear flow - In such a flow, adjacent layers of fluid move parallel to each other with different speeds that depends on their position in the direction orthogonal to the direction of flow. This is described by the velocity field

$$\mathbf{u}_{\text{shear}} = \gamma(y, 0, 0) \tag{1.23}$$

These are shown in figure 1.1 below. Looking at these graphs, it is clear that the shear flow can actually be decomposed into the sum of a straining and rotational flow; this may have already been obvious to some readers.

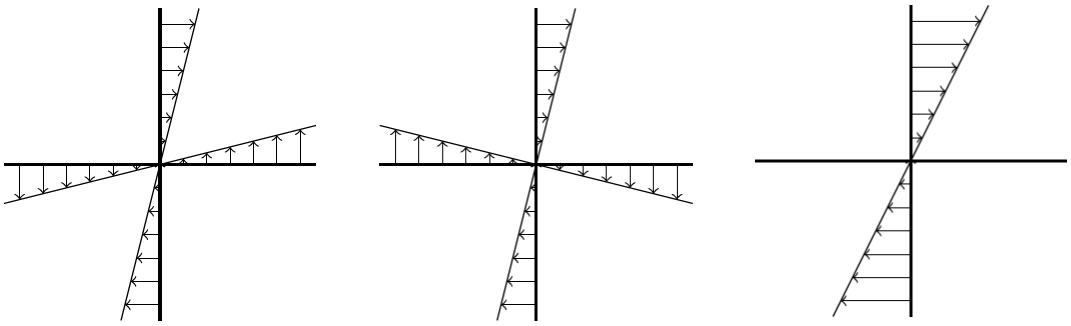

(a) (b) (c)

Figure 1.1: Plots of some flow fields: (a) Straining flow (b) Rotational flow (c) Shear flow

In fact, in the local vicinity to a point in a two dimensional flow, we can decompose any flow into a sum of a straining and rotational flow. Let us consider the flow close to the point $\mathbf{r} = \mathbf{r}_0$. Then, we can expand our flow field $\mathbf{u}$ as

$$\mathbf{u}(\mathbf{r}, t) = \mathbf{u}(\mathbf{r}_0, t) + (\mathbf{r} - \mathbf{r}_0) \left.\frac{\partial \mathbf{u}}{\partial \mathbf{r}}\right|_{\mathbf{r}=\mathbf{r}_0} + \cdots = \mathbf{c}_1 x + \mathbf{c}_2 y + \ldots \tag{1.24}$$

for some spatially constant vectors $\mathbf{c}_1$ and $\mathbf{c}_2$. We can then adopt the $\mathbf{u}_{\text{strain}}$ and $\mathbf{u}_{\text{rotational}}$ as our basis from which we form $\mathbf{u}$.

1.2.1 Streamlines and Scalar Functions

Thus far, we have visualised our flows by simply sketching the velocity field; this is useful for gaining information about the direction and magnitude of the flow. However, the generally preferred method is to sketch the *streamlines* defined by

$$\boxed{\frac{dx}{u_x} = \frac{dy}{u_y} = \frac{dz}{u_z} = dt} \tag{1.25}$$

These are curves in the direction of $\mathbf{u}$ at some time t, which is made obvious when we recognise that $d\boldsymbol{\ell} \times \mathbf{u} = 0$. In a steady flow, the streamlines do not change with time, and fluid particle paths follow the streamlines. Each streamline gives us information about the local direction of the flow, and the density of streamlines gives information about the magnitude of the flow. Note that streamlines cannot intersect; if they did, the direction of the flow would be undefined, as there is no unique tangent to the streamlines. A bunch of streamlines is called a *streamtube.*

Consider a simple shear flow $\mathbf{u} = (\gamma y, 0, 0)$*. Find the streamlines of the flow. At* $t = 0$*, dye is introduced to mark the curve* $x^2 + y^2 = a^2$*. Find the equation for this material fluid curve, and demonstrate that the area inside the curve does not change with time. Provide a reason why this is the case.*

The first part of this question is most simply solved by recognising that $\mathbf{u} = \dot{\mathbf{r}}$, allowing us to write that

$$\frac{dx}{dt} = \gamma y \quad \longrightarrow \quad x = x_0 + \gamma y t \tag{1.26}$$

$$\frac{dy}{dt} = 0 \quad \longrightarrow \quad y = y_0 \tag{1.27}$$

for arbitrary constants x_0 and y_0. This means that the streamlines are simply horizontal lines, as we would expect from a shear flow. Now, we know that at $t = 0$,

$$x_0^2 + y_0^2 = a^2 \tag{1.28}$$

Substituting in the results from above, we find that the curve evolves as an ellipse:

$$x^2 - 2xy\gamma t + [1 + (\gamma t)^2]y^2 = a^2 \tag{1.29}$$

In order to demonstrate that the area inside the ellipse does not change with time, we need to write this in a quadratic form. Defining $\mathbf{r} = (x, y)$, it follows that

$$\mathbf{r}^T \mathrm{A} \mathbf{r} = 1 \quad \text{where} \quad \mathrm{A} = \begin{pmatrix} \frac{1}{a^2} & -\frac{\gamma t}{a^2} \\ -\frac{\gamma t}{a^2} & \frac{1+(\gamma t)^2}{a^2} \end{pmatrix} \tag{1.30}$$

Now, the area of an ellipse is given by $\pi/(\det \mathrm{A})^{1/2}$; it is clear that this is constant with time. The reason for this is that the flow satisfies $\nabla \cdot \mathbf{u} = 0$ (incompressible). This means that the density is constant by (1.4), and so the area enclosed by the curve cannot change, as otherwise this would imply a change in density.

Stream Function

For a two-dimensional flow, we can define a *stream function* ψ such that

$$\boxed{\mathbf{u} = \nabla \times (\psi\, \mathbf{e}_z)} \tag{1.31}$$

Two things are immediately obvious from this definition: any flow described by a stream function must be incompressible, and consequently lines of constant ψ are streamlines of the flow. Let us write out the stream function explicitly in component form:

$$u_x = \frac{\partial \psi}{\partial y}, \quad u_y = -\frac{\partial \psi}{\partial x} \tag{1.32}$$

Under what conditions does a stream function describe an irrotational fluid (see section 1.3)? Using the definition of vorticity and (1.31), we can write that

$$\boldsymbol{\omega} = \nabla \times (\nabla \times (\psi \, \mathbf{e}_z)) \tag{1.33}$$

This is most easily dealt with in index notation form

$$\omega_i = \epsilon_{ijk}\epsilon_{k\ell m}\partial_j \partial_\ell \, \psi e_m = \partial_i \partial_m \, \psi e_m - \partial_\ell \partial_\ell \, \psi e_i = \partial_i(\partial_z \psi) - \partial_\ell^2 \, \psi e_i \tag{1.34}$$

However, we have defined our stream function in two dimensions, meaning that $\partial_z \psi = 0$. It is thus clear that the only possible vorticity component is

$$\omega_z = -\nabla^2 \psi \tag{1.35}$$

This means that if a fluid is both incompressible and irrotational, its associated stream function must satisfy Laplace's equation.

Velocity Potential

Suppose that our flow is irrotational. Then, we have that

$$\nabla \times \mathbf{u} = 0 \tag{1.36}$$

This allows us to define the velocity potential ϕ by

$$\boxed{\mathbf{u} = \nabla \phi} \tag{1.37}$$

Due to its definition, there is no unique velocity potential; it is subject to gauge transformations, as in Electromagnetism. The velocity potential can be written in component form as

$$u_x = \frac{\partial \phi}{\partial x}, \quad u_y = \frac{\partial \phi}{\partial y} \tag{1.38}$$

If the flow is incompressible, then the velocity potential ϕ must also satisfy Laplace's equation, though this is most valid in the *inviscid* limit ($\nu \backsim 0$). In a similar way to the stream function, we can define lines of constant ϕ. These *equipotential* lines are perpendicular to the streamlines. Consider a differential line element $d\ell$. Then, for the stream function ψ and the velocity potential ϕ, we have that

$$d\psi = \nabla \psi \cdot d\boldsymbol{\ell} \quad \longrightarrow \quad \left(\frac{\partial y}{\partial x}\right)_{d\psi = 0} = \frac{u_y}{u_x} \tag{1.39}$$

$$d\phi = \nabla \phi \cdot d\boldsymbol{\ell} \quad \longrightarrow \quad \left(\frac{\partial y}{\partial x}\right)_{d\phi = 0} = -\frac{u_x}{u_y} \tag{1.40}$$

It is clear that the product of these two gradients is equal to -1, meaning that the streamlines and equipotential lines of the flow are perpendicular to one another in two dimensions.

1.2.2 Solving Navier-Stokes

In the material at the start of this section, we have assumed that we already know some flow field $\mathbf{u}$. However, to find the flow field, we must solve the Navier-Stokes equation (1.13). Before we do this for a few simple cases, we should outline an important boundary condition that we shall make use of. Namely, the condition that

$$\boxed{\text{At a solid boundary : } \mathbf{u} = u_\perp \mathbf{e}_\perp + u_\parallel \mathbf{e}_\parallel = 0} \tag{1.41}$$

The fact that $\mathbf{u}_\perp = 0$ follows from the fact that we cannot have sources or sinks at the boundary, while $\mathbf{u}_\parallel$ is an empirically observed fact. The latter of these is often known as the *no-slip condition*. Note that (1.41) only holds at a solid boundary; at a free boundary (such as the surface of a liquid), it is evidently possible to have $\mathbf{u}_\perp \neq 0$, as this simply re-defines the position of the free boundary.

Poiseuille Flow

Consider two parallel solid boundaries separated by a distance a to form a channel, orientated such that the x-axis is along the direction of the channel, and the y-axis perpendicular to it. Suppose further that there is a pressure difference $\Delta p = p_0$ between the channel of the pipe at $x = 0$ and $x = b$.

As there must be translational symmetry along x, we conclude that $\partial_x u = 0$. There can be no flow perpendicular to the plates by (1.41), and so $u_y = 0$. This means that our flow field is given by

$$\mathbf{u} = (u_x(y), 0, 0) \tag{1.42}$$

Assume that the flow has reached the steady state, meaning that $\partial_t u = 0$. Then, the only terms that remain in the Navier-Stokes equation (1.13) are

$$\nabla p = \eta \nabla^2 \mathbf{u} \tag{1.43}$$

Then:

$$\frac{\partial p}{\partial x} = \frac{p_0}{b} = \eta \frac{\partial^2 u_x}{\partial x^2} \tag{1.44}$$

Integrating this expression, and applying the solid boundary condition (1.41) at $y = 0$ and $y = a$ allows us to arrive at the expression

$$u_x = \frac{p_0}{2\rho\nu b} y(y - a) \tag{1.45}$$

where we have used the fact that $\eta = \rho\nu$. The flow profile is thus parabolic, with viscosity causing adjacent 'fluid layers' to slide past one another. End effects become important for higher velocities, as the flow will take some time to develop into this steady state distribution.

Couette Flow

Consider the same geometry as for Poiseuille flow, except instead of having a pressure difference between the ends of the channel, we set up a velocity gradient along the y direction, such that $u = 0$ at $y = 0$, and $u = u_0$ at $y = a$.

We make the same assumptions concerning the flow field, such that (1.42) and (1.43) are still valid. However, as $\nabla p = 0$, we conclude that

$$\frac{\partial^2 u_x}{\partial x^2} = 0 \quad \longrightarrow \quad u_x = \frac{u_0 y}{a} \tag{1.46}$$

Comparison with (1.23) reveals that this is a shear flow parametrised by u_0/a.

Flow under Gravity

Consider a steady, two-dimensional, incompressible, viscous flow down an inclined plane under the influence of gravity, as shown in figure 1.2.

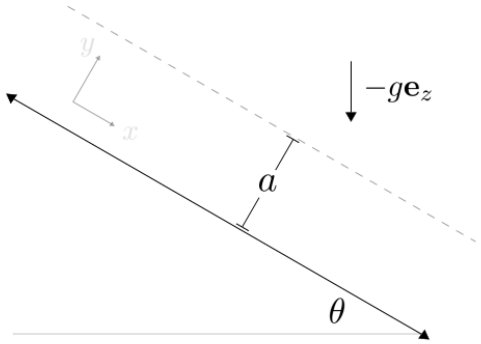

Figure 1.2: Flow down an inclined plane. The dotted line indicates the free upper boundary of the liquid layer

Adopting the axes shown on the figure, translational symmetry along x demands that $\partial_x u = 0$. Applying the incompressibility condition:

$$\nabla \cdot \mathbf{u} = \frac{\partial u_x}{\partial x} + \frac{\partial u_y}{\partial y} = 0 \quad \longrightarrow \quad \frac{\partial u_y}{\partial y} = 0 \tag{1.47}$$

This means that $u_y = 0$ due to the boundary condition that $\mathbf{u} = 0$ at $y = 0$ from (1.41). Now that our flow field is again of the form (1.42), we can also conclude that $u_j \partial^j = 0$. Lastly, we assumed that the flow is *well-developed*, meaning that there are no pressure gradients in the direction of the flow:

$$\frac{\partial p}{\partial x} = 0 \tag{1.48}$$

Taking all of this into account, we are left with the following two components of the Navier-Stokes equation (1.13):

$$0 = \nu \frac{\partial^2 u_x}{\partial y^2} + g \sin\theta \tag{1.49}$$

$$\frac{1}{\rho}\frac{\partial p}{\partial y} = -g\cos\theta \tag{1.50}$$

Let the pressure at the free surface ($y = a$) be $p = p_0$. We can then integrate (1.50) to give

$$p = p_0 + \rho g(a - y)\cos\theta \tag{1.51}$$

Similarly, we can integrate (1.49) to give

$$u_x = \frac{g}{2\nu} y(2a - y)\sin\theta \tag{1.52}$$

In order to obtain this result, we have had to make use of the fact that there is zero tangential stress at the free boundary, as we assume that there is no viscous interaction with the medium that the fluid is flowing in. Mathematically, we can express this as

$$\boxed{\nu \frac{\partial u_\parallel}{\partial \mathbf{r}} \cdot \mathbf{e}_\perp = 0} \tag{1.53}$$

where the directions $\parallel$ and $\perp$ are defined with respect to the free surface.

1.2.3 The Reynolds Number

We can gain a greater understanding of the behaviour of the Navier-Stokes equation (1.13) by the process of non-dimensionaliation. We introduce the variable re-scalings:

$$\widetilde{\mathbf{u}} = \frac{\mathbf{u}}{u_0}, \quad \widetilde{\mathbf{r}} = \frac{\mathbf{r}}{\ell_0}, \quad \widetilde{t} = \frac{t}{t_0}, \quad t_0 = \frac{\ell_0}{u_0}, \quad \widetilde{p} = \frac{p}{\rho u_0^2} \tag{1.54}$$

where u_0 and ℓ_0 are the characteristic velocity and length scales of the system. Note that we have not defined some characteristic density scale for the system as the fluid is assumed to be incompressible, meaning that the characteristic scale is simple the density itself. This gives rise to the operators

$$\frac{\partial}{\partial \widetilde{t}} = t_0 \frac{\partial}{\partial t}, \quad \widetilde{\nabla} = \ell_0 \nabla \tag{1.55}$$

Introducing these into (1.13) with $\mathbf{f} = 0$:

$$\rho \left(\frac{u_0}{t_0} \frac{\partial \widetilde{\mathbf{u}}}{\partial \widetilde{t}} + \frac{u_0^2}{\ell_0} (\widetilde{\mathbf{u}} \cdot \widetilde{\nabla}) \widetilde{\mathbf{u}} \right) = -\frac{\rho u_0^2}{\ell_0} \widetilde{\nabla} \widetilde{p} + \frac{u_0 \eta}{\ell_0^2} \widetilde{\nabla}^2 \widetilde{\mathbf{u}} \tag{1.56}$$

Introducing the definition of t_0, and dividing through by $\rho u_0^2 / \ell_0$, we arrive at the expression

$$\underbrace{\frac{\partial \widetilde{\mathbf{u}}}{\partial \widetilde{t}} + (\widetilde{\mathbf{u}} \cdot \widetilde{\nabla}) \widetilde{\mathbf{u}}}_{\text{inertial terms}} = \underbrace{-\widetilde{\nabla} \widetilde{p}}_{\text{forcing term}} + \underbrace{\frac{1}{\mathrm{Re}} \widetilde{\nabla}^2 \widetilde{\mathbf{u}}}_{\text{viscous term}} \tag{1.57}$$

This is of the form of (1.13), except that we are now working with dimensionless parameters. Note that we have absorbed ρ into our definition of $\widetilde{p}$ on the right hand side. Then, the *Reynolds number* is defined as

$$\boxed{\mathrm{Re} = \frac{u_0 \ell_0}{\nu}} \tag{1.58}$$

This is a dimensionless parameter that characterises the flow. It is essentially a measure of the ratio of the magnitude of the inertial and viscous forces. In particular, we note two regimes:

- $\mathrm{Re} \ll 1$ - We can ignore the inertial term, as the flow will be dominated by small, viscous scales. Thus, we can approximate the scalings

$$\frac{\nabla p}{\rho} \approx \nu \nabla^2 \mathbf{u} \quad \longrightarrow \quad \Delta p \backsim \frac{\nu \rho u}{\ell} \tag{1.59}$$

- $\mathrm{Re} \gg 1$ - In this case, we can ignore the viscous term, as the system is dominated by large scale, inertial motions. In the steady state, this allows us to write that

$$(\mathbf{u} \cdot \nabla) \mathbf{u} \approx \frac{\nabla p}{\rho} \quad \longrightarrow \quad \Delta p \backsim \rho u^2 \tag{1.60}$$

Let us take a look at how this works in the case of example that we have already examined, that of the case of Poiseuille flow. Let us non-dimensionalise the expression that we obtained for the velocity along the pipe. Adopt the re-scalings:

$$\widetilde{u}_x = \frac{u_x}{u_0}, \quad \widetilde{y} = \frac{y}{a}, \quad \widetilde{p}_0 = \frac{p_0}{\rho u_0^2} \tag{1.61}$$

Substituting these into (1.45), we obtain the expression

$$\widetilde{u}_x = \mathrm{Re} \left(\frac{a \widetilde{p}_0}{2b} \right) \widetilde{y} (\widetilde{y} - 1) \tag{1.62}$$

It is clear from the above expression that, given some forcing and geometry determined by p_0, a and b, the dynamics of the flow is entirely determined by the Reynolds number.

Reynold's Experiment

In 1883, Osborne Reynolds performed an experiment whereby he injected dye into a flow through a glass tube, and observed the effects on the flow when he varied the velocity. This is evidently the case of Poiseuille flow above, except in a cylindrical coordinate system. He observed results similar to those shown in figure 1.3.

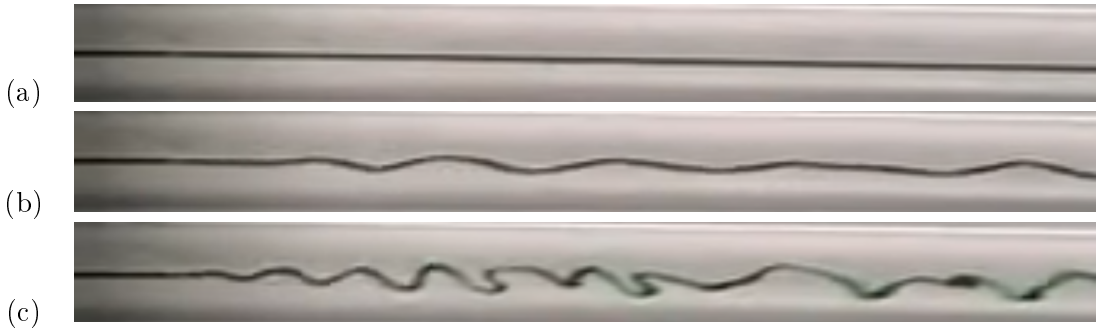

Figure 1.3: Experimental results for (a) Laminar flow (b) Transitional zone (c) Turbulent flow

He found that there were three different distinct regimes of flow behaviour. For $\mathrm{Re} \lesssim 1$, the flow lines seemed to follow a straight line path (with a slight blurring due to diffusive transport of the dye), which is known as *laminar flow*. For $1 \lesssim \mathrm{Re} \lesssim 1000$, there is a transitional zone in which the dye fluctuates, and there are 'surges' that travel with the flow. For $\mathrm{Re} \gtrsim 1000$, there is transverse mixing of the dye, and the flow line is no longer smooth. This is known as *turbulent flow*, but more on this in section 1.5.2. If Re is increased even further, then the turbulent eddies will begin to fill the entire pipe, until the flow lines break up and become undefined.

Dynamical Similarity

Suppose that two fluid flows satisfy the following conditions:

- They have the same Reynolds number Re
- All geometrical features of the flow are scaled in the same way
- All applied forces and pressure gradients are scaled similarly

Then, the behaviour and characteristics of the fluid flows are identical, and the flows are said to be *dynamically similar*. Note that this assumes that both flows can be described by the Navier-Stokes equation (1.13); if this is not the case, then other dimensionless parameters may be required in order to characterise the flow (such as the Magnetic Reynolds number, or the plasma beta).

In a wind tunnel, vortices are shed behind an object at a frequency of $0.5\ s^{-1}$*. The same plate is now placed in a water channel. Calculate the flow rate, as a function of that in the wind tunnel, to produce dynamically similar behaviour, and calculate the frequency of the vortex shedding.*

As both systems have the same geometry, and we assume the same forcing, they must have the same Reynolds number in order to achieve dynamical similarity. Suppose that the air

flow rate and kinematic viscosity are u_0 and ν respectively, and similarly u_0' and ν' for the flow in water. Applying the above condition:

$$\frac{u_0 \ell_0}{\nu} = \frac{u_0' \ell_0}{\nu'} \quad \longrightarrow \quad u_0' = \frac{\nu'}{\nu} u_0 \backsim \frac{1}{15} u_0 \tag{1.63}$$

Dimensionally, the vortex shedding rate must be proportional to some u/ℓ. This means that the rate will be smaller by the same factor of the velocity, leading us to conclude that $f' = 0.03\,\mathrm{s}^{-1}$.

1.3 Rotations and Vorticity

The *vorticity* of some flow velocity field $\mathbf{u}$ is defined by

$$\boxed{\boldsymbol{\omega} = \nabla \times \mathbf{u}} \tag{1.64}$$

Vorticity is a *local* measure of the rotation/spin of the fluid. The fact that it is local is important; this means that fluids that appear to have global rotation may actually have zero vorticity. Visually, we can get an idea of the vorticity of a particular flow by placing a small 'test cube' in a local area of the flow; if the cube itself rotates as it moves with the flow, then the vorticity is non-zero. Flows that have zero vorticity are said to be *irrotational*.

In two dimensions, the vorticity is given by two times the average angular velocity of two infinitesimal, mutually perpendicular, fluid elements. Consider the region surrounding a point where the velocity field is given by $\mathbf{u}_{(x,y)} = (u_x, u_y)$. We can expand in the region surrounding this point along two perpendicular axes:

$$\mathbf{u}_{(x+dx,y)} = \mathbf{u} + \frac{\partial \mathbf{u}}{\partial x}\, dx \tag{1.65}$$

$$\mathbf{u}_{(x,y+dy)} = \mathbf{u} + \frac{\partial \mathbf{u}}{\partial y}\, dy \tag{1.66}$$

The angular velocity of the fluid element at $(x + dx, y)$ is $\frac{\partial u_y}{\partial x}$, while the angular velocity of the fluid element at $(x, y + dy)$ is $-\frac{\partial u_x}{\partial y}$. The average angular velocity about (x, y) is thus given by

$$\frac{1}{2}\left(\frac{\partial u_y}{\partial x} - \frac{\partial u_x}{\partial y}\right) = \frac{1}{2}\nabla \times \mathbf{u} = \frac{1}{2}\boldsymbol{\omega} \tag{1.67}$$

For example, a shear flow of the form (1.23) has a non-zero vorticity; this is because while the fluid elements along the direction of the flow do not have angular velocity about some local point, the fluid elements perpendicular to the flow direction do. Overall, the fluid structure becomes 'stretched', almost as if it is rotating in the direction of the shear.

1.3.1 Vortices

Assume now that the flow that we are considering is purely azimuthal, such that $\mathbf{u} \cdot \widehat{\mathbf{r}} = 0$. We shall refer to flow fields of this time using the term *vortices*. Motivated by symmetry considerations, we propose a flow field of the form

$$\mathbf{u} = \Omega f(r)\, \widehat{\boldsymbol{\theta}} \tag{1.68}$$

where Ω is a constant that sets the magnitude of the velocity field, and $f(r)$ is some scalar function depending only on the radial coordinate r (for continuity reasons, it cannot depend on the azimuthal coordinates). Then, it is easy to show that the resultant vorticity is given by

$$\boxed{\boldsymbol{\omega} = \frac{\Omega}{r}\frac{\partial}{\partial r}\left(r f(r)\right)\, \mathbf{e}_z} \tag{1.69}$$

It is clear that in the case of $f(r) = r^{-1}$. then $\boldsymbol{\omega} = 0$, meaning that our test cube does not rotate as it moves around the centre of the vortex. However, the zero vorticity condition must break down in a small region around $r = 0$ in order to avoid divergent vorticity. A good model of this is the Rankine vortex, to be discussed in the next section.

The case of $f(r) = r$, $\mathbf{u}$ describes rigid body rotation with an angular velocity Ω, and vorticity $\boldsymbol{\omega} = 2\Omega\, \mathbf{e}_z$. This is similar to having a rotating disk.

The Rankine Vortex

The Rankine vortex is a type of vortex in a viscous fluid, characterised by a forced vortex in its central core, surrounded by a free vortex. The flow fields describing this vortex are given by

$$\mathbf{u} = \begin{cases} \Omega r\, \mathbf{e}_\theta & \text{for } r < a \\ \Omega \frac{a^2}{r}\, \mathbf{e}_\theta & \text{for } r > a \end{cases} \tag{1.70}$$

Clearly, we have rigid body rotation inside the vortex core, and an irrotational flow outside of it. This gives rise to the following velocity and vorticity profiles.

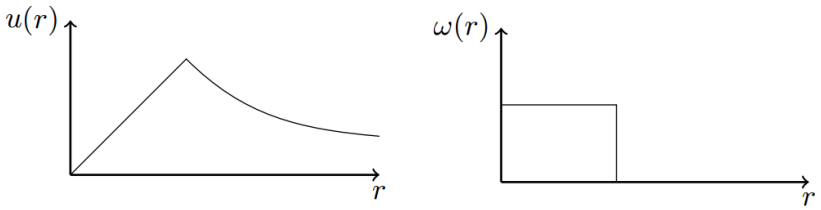

(a) (b)

Figure 1.4: The (a) flow field and (b) vorticity of the Rankine vortex

Given that there is only variation in r, the two components of the Navier-Stokes equation (1.13) (in cylindrical polars) that remain are

$$\frac{u_\theta^2}{r} = \frac{1}{\rho}\frac{\partial p}{\partial r}, \quad 0 = \frac{1}{\rho r}\frac{\partial p}{\partial \theta}, \quad -g = \frac{1}{\rho}\frac{\partial p}{\partial z} \tag{1.71}$$

The second of these makes it clear that $p = p(r, z)$. Explicit expressions for the pressure can be obtained by integrating the other components.

$$p(r,z) = \begin{cases} \frac{1}{2}\rho\Omega^2 r^2 - \rho g z + p_0 & \text{for } r < a \\ -\frac{1}{2}\rho\Omega^2 \frac{a^4}{r^2} - \rho g z + p_0 + \rho\Omega^2 a^2 & \text{for } r \geq a \end{cases} \tag{1.72}$$

where we have defined $p_0 = p(0,0)$ as the surrounding atmospheric pressure. Now, suppose that we wanted to find the height of the free water surface, such that $h = 0$ at $r = 0$. We know that along the boundary $z = h$, the pressure must be equal to the atmospheric pressure p_0. This gives us the height as

$$h(r) = \begin{cases} \frac{1}{2}\frac{\Omega^2}{g} r^2 & \text{for } r < a \\ \frac{\Omega^2 a^2}{g}\left[1 - \frac{a^2}{2r^2}\right] & \text{for } r \geq a \end{cases} \tag{1.73}$$

An impeller of radius 5 cm is located at the bottom of a tank of water, and is rotating at 120 revolutions per minute. The container is 1.5 m deep. What is the maximum rotation rate of the impeller if the upper surface of the water is not to expose the impeller to the air?

The maximum height of the water surface h_∞ occurs for $r \to \infty$. This means that the condition for the impeller not being exposed is

$$h_\infty = \frac{\Omega^2 a^2}{g} \leq 1.5\,\text{m} \quad \longrightarrow \quad \Omega \leq 76.7\ \text{rad s}^{-1} \tag{1.74}$$

1.3.2 The Vorticity Equation

Now that we have established the concept of vorticity, we shall now derive an associated conservation equation from the Navier-Stokes equation (1.13). For this, we need the vector calculus identities

$$(\mathbf{u}\cdot\nabla)\mathbf{u} = \nabla\left(\frac{\mathbf{u}^2}{2}\right) - \mathbf{u}\times(\nabla\times\mathbf{u}) \tag{1.75}$$

$$\nabla\times(\mathbf{u}\times\boldsymbol{\omega}) = (\boldsymbol{\omega}\cdot\nabla)\mathbf{u} - (\mathbf{u}\cdot\nabla)\boldsymbol{\omega} - \boldsymbol{\omega}(\nabla\cdot\mathbf{u}) \tag{1.76}$$

Note that the last term on the right hand side of the second identity is zero for incompressible fluids. When we take the curl of the Navier-Stokes equation, it is clear that the first term on the right-hand side of (1.75) will disappear, and we will be left with (1.76). Imposing the incompressibility condition, we arrive at

$$\frac{\partial\boldsymbol{\omega}}{\partial t} + (\mathbf{u}\cdot\nabla)\boldsymbol{\omega} - (\boldsymbol{\omega}\cdot\nabla)\mathbf{u} = \nu\nabla^2\boldsymbol{\omega} \tag{1.77}$$

Recalling (1.2), we can write this in the neat form

$$\boxed{\frac{d\boldsymbol{\omega}}{dt} = (\boldsymbol{\omega}\cdot\nabla)\mathbf{u} + \nu\nabla^2\boldsymbol{\omega}} \tag{1.78}$$

This is known as the *vorticity equation*. In a similar way to Navier-Stokes describing the conservation of momentum, the vorticity equation describes the conservation of angular momentum of such a fluid. Note that our body force term $\mathbf{f}$ is no longer present as it was assumed to be a conservative force, which is zero when taking the curl.

In the same way that we defined a streamline for our velocity field $\mathbf{u}$, we define a *vortex line* that is everywhere tangent to $\boldsymbol{\omega}$. *Vortex tubes* are bundles of vortex lines, and are actually persistent structures under certain conditions. Vorticity forms at the boundaries of a fluid where the no-slip boundary conditions result in viscous boundary layers which can become unstable due to vortex formation. This can also occur as a result of non-conservative forces, such as the Coriolis force.

The Evolution of Vorticity

But how does vorticity evolve? Without loss of generality, suppose that the fluid contains a vortex tube oriented along the z-axis, such that $\boldsymbol{\omega} = (0, 0, \omega_z)$. Then from (1.78), we can write that

$$\frac{d\boldsymbol{\omega}}{dt} = \underbrace{\omega_z\frac{\partial u_z}{\partial z}\mathbf{e}_z}_{\text{vortex stretching}} + \underbrace{\omega_z\frac{\partial u_\perp}{\partial z}\mathbf{e}_\perp}_{\text{vortex twisting}} + \underbrace{\nu\nabla^2\boldsymbol{\omega}}_{\text{viscous diffusion}} \tag{1.79}$$

The first term describes vortex stretching or shrinking. If the sign of the velocity derivative is negative, the vortex tube will elongate along $\mathbf{e}_z$, meaning that it becomes thinner, and so the vorticity must increase in order to conserve angular momentum. Evidently, there is a limit to this effect; the vortex tube will eventually become so thin that it encounters collisions (and thus viscosity) even in the inviscid limit, and will diffuse away.

The second term gives rise to vortex twisting; velocity gradients in $u_\perp$ creates perpendicular components of the vorticity $\boldsymbol{\omega}_\perp$. Lastly, the third term clearly leads to the diffusion and dissipation of vorticity, as controlled by the viscosity ν.

Kelvin's Circulation Theorem

We define the *circulation* Γ of a fluid as

$$\boxed{\Gamma = \oint_{C(t)} \mathbf{u} \cdot d\boldsymbol{\ell} = \int_{S(t)} d\mathbf{S} \cdot \boldsymbol{\omega}} \tag{1.80}$$

where $C(t)$ is some closed path following the flow, and $S(t)$ the surface spanning $C(t)$. We have included the second expression to make the relationship between circulation and vorticity explicit; the curve $C(t)$ is a vortex line, while $S(t)$ is the surface of the associated vortex tube.

Let us look at the time evolution of the circulation. We shall assume that the fluid is inviscid, incompressible, and subject to only conservative forces. Taking the time derivative:

$$\frac{d\Gamma}{dt} = \frac{d}{dt}\oint_{C(t)} \mathbf{u} \cdot d\boldsymbol{\ell} = \oint_{C(t)} \frac{d\mathbf{u}}{dt} \cdot d\boldsymbol{\ell} + \oint_{C(t)} \mathbf{u} \cdot \frac{d(d\boldsymbol{\ell})}{dt} \tag{1.81}$$

Note that we are able to take the time derivative within the integral as we are using the material derivative, and our closed path $C(t)$ has been defined as following the flow. Let us look at each of these terms separately.

$$\oint_{C(t)} \frac{d\mathbf{u}}{dt} \cdot d\boldsymbol{\ell} = -\frac{1}{\rho}\oint_{C(t)} (\nabla p + \nabla \chi) \cdot d\boldsymbol{\ell} = -\frac{1}{\rho}\oint_{C(t)} dp + d\chi = 0 \tag{1.82}$$

where we have used (1.13) with $\nu = 0$, and observed that both dp and $d\chi$ are exact derivatives integrated around a closed loop, which gives zero. For the second term:

$$\oint_{C(t)} \mathbf{u} \cdot \frac{d(d\boldsymbol{\ell})}{dt} = \oint_{C(t)} \mathbf{u} \cdot d\mathbf{u} = \frac{1}{2}\oint_{C(t)} d(\mathbf{u}^2) = 0 \tag{1.83}$$

as again $d(\mathbf{u}^2)$ is an exact derivative. Putting these terms together, it follows that

$$\boxed{\frac{d\Gamma}{dt} = 0} \tag{1.84}$$

This is known as *Kelvin's circulation theorem*, which describes how circulation is conserved in an inviscid, incompressible fluid that is subject only to conservative forces (these conditions bear repeating from above).

This has a few important consequences, which are sometimes collectively known as Helmholtz's vortex theorems:

- If $\Gamma = 0$ around any closed curve, then it will remain zero. This means that an irrotational flow will remain irrotational. This can also be deduced from the vorticity equation (1.78), as if we initially have $\boldsymbol{\omega} = 0$, then clearly $d\boldsymbol{\omega}/dt = 0$, and so no vorticity can develop
- Γ must be conserved for all cross-sections of the vortex tube, meaning that if the vortex tube is deformed such that $S(t)$ decreases, $\boldsymbol{\omega}$ must increase to compensate. This is a statement of the conservation of angular momentum
- A streamline which at any instant of time coincides with a vortex line will coincide with a vortex line forever. Put another way, the vortex lines can be said to be 'frozen in' to the flow field $\mathbf{u}$
- Vortex lines never end in the fluid. They either form closed loops or end at a fluid boundary, and the circulation is the same for every contour enclosing the vortex line

1.3.3 The Bernoulli Theorem

We define the *Bernoulli function* H as

$$\boxed{H = \frac{\mathbf{u}^2}{2} + \frac{p}{\rho} + \frac{\chi}{\rho}} \tag{1.85}$$

This is clearly related to the energy density given by (1.14). As gravity is often the force being considered, one will often see the potential χ written in the form $\chi = \rho g z$. Let us find the conditions under which the Bernoulli function is conserved. Using (1.75) on the Navier-Stokes equation (1.13), we obtain

$$\frac{\partial \mathbf{u}}{\partial t} + \nabla\left(\frac{\mathbf{u}^2}{2}\right) - \mathbf{u} \times \boldsymbol{\omega} = -\frac{\nabla p}{\rho} + \nu \nabla^2 \mathbf{u} + \frac{\mathbf{f}}{\rho} \tag{1.86}$$

Noting that $\mathbf{f} = -\nabla\chi$, and assuming incompressibility such that $\nabla\rho = 0$, we can collect all of the gradient terms on the left hand side

$$\frac{\partial \mathbf{u}}{\partial t} + \nabla \underbrace{\left(\frac{\mathbf{u}^2}{2} + \frac{p}{\rho} + \frac{\chi}{\rho}\right)}_{H} = \mathbf{u} \times \boldsymbol{\omega} + \nu \nabla^2 \mathbf{u} \tag{1.87}$$

Now, if H is to be constant along a streamline, then it must satisfy the condition that $(\mathbf{u} \cdot \nabla)H = 0$. Taking the dot product of (1.87) with $\mathbf{u}$, it follows that

$$(\mathbf{u} \cdot \nabla)H = \nu\, \mathbf{u} \cdot \nabla^2 \mathbf{u} - \mathbf{u} \cdot \frac{\partial \mathbf{u}}{\partial t} \tag{1.88}$$

Thus, for H to be constant along a streamline, we require that the flow is steady, and inviscid.

Now, let us suppose that the fluid is inviscid, and irrotational. Under these conditions, we can introduce the velocity potential defined by (1.37), allowing us to write that

$$\boxed{\nabla\left(H + \frac{\partial \phi}{\partial t}\right) = 0} \tag{1.89}$$

This implies that the quantity in brackets is conserved everywhere in the fluid, meaning that we can equate it at any two points, in a similar way to energy in a conservative system. Note that one usually assumes the the system is in the steady state, such that $\partial_t \phi = 0$.

We can apply the conservation of the Bernoulli function to find the pressure in certain flow cases. Let us consider a uniform flow of magnitude u_0 past a cylinder of radius a, as shown in figure 1.5 below. We assume that the flow is irrotational, incompressible, and inviscid, meaning that we can describe the flow field by the potential ϕ that must satisfy Laplace's equation

$$\nabla^2 \phi = 0 \tag{1.90}$$

This is solved via the normal methods, applying the boundary conditions that as $r \to \infty$, $\phi \to u_0 x = u_0 r \cos\theta$ and that $u_r = 0$ (non-tangential flow). Note that we cannot apply the no-slip condition as we are in the inviscid limit (the no-slip condition requires friction between adjacent fluid layers), though to do so would be over-constraining the solution in any case. This gives the flow potential

$$\phi = u_0 \left(r + \frac{a^2}{r}\right) \cos\theta \tag{1.91}$$

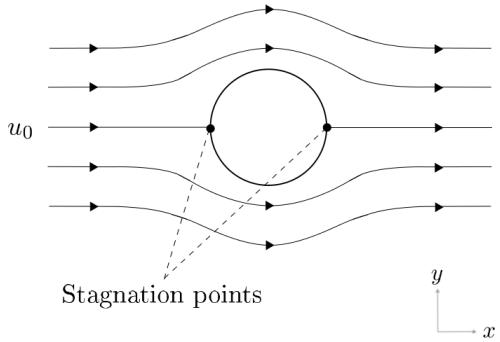

Figure 1.5: Uniform flow past a cylinder. We have labelled the location of the *stagnation points* where the velocity of the flow is zero at the surface of the cylinder

The resultant velocity field is

$$u_r = \frac{\partial \phi}{\partial r} = u_0 \left(1 - \frac{a^2}{r^2}\right) \cos\theta = \frac{1}{r}\frac{\partial \psi}{\partial \theta} \tag{1.92}$$

$$u_\theta = \frac{1}{r}\frac{\partial \phi}{\partial \theta} = -u_0 \left(1 + \frac{a^2}{r^2}\right) \sin\theta = -\frac{\partial \psi}{\partial r} \tag{1.93}$$

From this, it is very easy to find the stream function ψ, and thus streamlines. It is encouraging that we do indeed confirm that $u_r = 0$ on the sufrace of the cylinder.

As the flow is irrotational, incompressible, inviscid, and ϕ is time-independent, we know that H must be conserved throughout the flow. Thus, on the surface of the cylinder, we can write that

$$\frac{\mathbf{u}^2(a,\theta)}{2} + \frac{p(a,\theta)}{\rho} = \frac{p(a,0)}{\rho} \tag{1.94}$$

where we have chosen the pressure at the stagnation point $p(a,0)$ as the reference pressure. Noting that $u_\theta(a,\theta) = -2u_0 \sin\theta$, it follows that the pressure distribution on the surface of the cylinder is given by

$$p(a,\theta) = p(a,0) - 2\rho u_0^2 \sin^2\theta \tag{1.95}$$

The pressure towards the top and bottom of the cylinder is lower than for the sides as the fluid is moving faster here, meaning that by the conservation of the Bernoulli function, the pressure must decrease. However, there is no net lift (pressure the same on the top and bottom) and no net drag (pressure is the same on the front and back).

The Kutta-Joukouski Theorem

In actual fact, in order to have lift, we require non-zero circulation. To demonstrate this, consider an quasi-one-dimensional aerofoil surface (such as the wing of a plane) of length ℓ_0 that is inclined at a small angle to a uniform flow u_0 along the x-axis. We shall assume that the flow is irrotational, inviscid, and in the steady state, such that H is conserved throughout the fluid. Equating the H for the top and bottom of the aerofoil:

$$\frac{p_b}{\rho} + \frac{u_b^2}{2} = \frac{p_t}{\rho} + \frac{u_t^2}{2} \quad \longrightarrow \quad p_b - p_t = \frac{\rho}{2}(u_t^2 - u_b^2) \backsim \rho u_0 (u_t - u_b) \tag{1.96}$$

The last expression follows from the assumption that $u_t \backsim u_b \backsim u_0$. The lift L is then given by

$$L = \int_0^{\ell_0} dx\, p_b - p_t = \rho u_0 \int_0^{\ell_0} dx\, (u_t - u_b) \tag{1.97}$$

However, the circulation associated with the aerofoil is given by

$$\Gamma = \oint_{C(t)} \mathbf{u} \cdot d\boldsymbol{\ell} = \int_0^{\ell_0} dx\, u_b + \int_{\ell_0}^0 dx\, u_t = \int_0^{\ell_0} dx (u_b - u_t) \tag{1.98}$$

Comparison of these two expressions gives us that

$$\boxed{L = -\rho u_0 \Gamma} \tag{1.99}$$

This is the *Kutta-Joukouski theorem*, which demonstrates that in order to have lift, you need non-zero circulation. In fact, to have positive lift, then you must actually have negative circulation; this means that the flow speed across the top of the wing is higher than the flow speed across the bottom of the wing.

Astute readers will have noticed an apparent contradiction here: we assumed that the flow as irrotational, but now we have non-zero circulation. This is in fact not a contradiction; if the closed path $C(t)$ does not enclose the aerofoil, then $\Gamma = 0$. This is because when the aerofoil starts to move through the fluid medium, a starting vortex is formed on the trailing edge due to viscous effects in the boundary layer, which results in a non-zero circulation around the wing, but zero circulation for the entire system.

1.4 Some Specific Cases

In the first two chapters, we introduced the basic concepts and principles concerning fluid flows. We shall now have a look at some more specific cases of the application of these equations, with the aim of further increasing familiarity with this subject area.

1.4.1 Viscosity Dominated Flows

As the name suggests, this regime occurs where the effects of viscosity are dominant, for $\mathrm{Re} \ll 1$. This allows us to neglect the inertial terms in the Navier-Stokes equation (1.13), such that we are simply left with

$$\boxed{\nabla p = \eta \nabla^2 \mathbf{u} + \mathbf{f}} \tag{1.100}$$

This is known as the *Stokes' equation*. Viscous flows that can be described by this system include the creep of a glacier, treacle falling off a spoon, or microfluidics (involving observing and manipulating fluids on scales $\ell \ll \ell_0$).

Biological Mobility

Looking at (1.100), it is clear that is has the remarkable property of being kinematically reversible due to a lack of explicit time dependence. This has interesting consequences for biological mobility. More specifically, *Purcell's Scallop theorem* states that

> *To achieve propulsion at zero Reynolds number in Newtonian fluids, a swimmer must deform in such a way that is not invariant under time reversal*

Put another way, if the swimming stroke is invariant under time reversal, it must cover zero displacement; otherwise, time reversal would give the same physical system, but a different resultant displacement. This means that symmetrical motions, like the back-and-forth waving of a tail, cannot produce motion in such flows. At least three degrees of freedom are required in order to define a swimming stroke. One such method that cells have evolved in order to account for this is the use of flagella, which can move in a helical motion that is not invariant under time-reversal. In fact, in E-coli the resultant flow field is a dipole flow field; there is inwards flow in the directions perpendicular to the motion, and outwards flow in directions parallel to the motion.

Stokes' Drag

The Stokes' equation is linear, meaning that forces described by this equation are proportional to the flow velocities. More specifically, Stokes' drag is the force exerted on a sphere as it moves through such a medium, given by

$$\boxed{\mathbf{F}_s = 6\pi\eta a \mathbf{u}} \tag{1.101}$$

for a sphere of radius a. We can derive this by considering the stress tensor σ_i^j for the flow past a sphere of radius a in a uniform flow field u_0. In spherical polar coordinates, this can be shown to be

$$\sigma_i^j = \begin{pmatrix} \sigma_{rr} & \sigma_{r\theta} & \sigma_{r\phi} \\ \sigma_{\theta r} & \sigma_{\theta\theta} & \sigma_{\theta\phi} \\ \sigma_{\phi r} & \sigma_{\phi\theta} & \sigma_{\phi\phi} \end{pmatrix} = \begin{pmatrix} -p & -\frac{3\eta u_0}{2a}\sin\theta & 0 \\ -\frac{3\eta u_0}{2a}\cos\theta & -p & 0 \\ 0 & 0 & -p \end{pmatrix} \tag{1.102}$$

where we have evaluated the tensor at the surface of the sphere, and the pressure is given by

$$p = p_0 - \frac{3\eta u_0}{2a}\cos\theta \tag{1.103}$$

We are interested in forces along $\mathbf{e}_z$, which we choose to orient along the direction of the uniform flow. The relevant stress is found using (1.7):

$$t_z = \sigma_{rr}\cos\theta - \sigma_{r\theta}\sin\theta = -p_0\cos\theta + \frac{3\eta u_0}{2a} \tag{1.104}$$

One can then integrate this expression over the surface of the sphere to give the Stokes' drag, as above.

1.4.2 Thin-Film Approximation

In this case, we consider a thin layer of fluid on a surface, with perpendicular height h. Let the parallel velocity scale be u_0, and the corresponding length scale be ℓ, such that $h \ll \ell$. From incompressibility, we know that

$$\frac{\partial u_\perp}{\partial \mathbf{r}}\cdot\mathbf{e}_\perp + \frac{\partial u_\parallel}{\partial \mathbf{r}}\cdot\mathbf{e}_\parallel \backsim \frac{u_\perp}{h} + \frac{u_0}{\ell} \backsim 0 \quad\longrightarrow\quad u_\perp \backsim \frac{u_0 h}{\ell} \ll u_\parallel \tag{1.105}$$

This means that the perpendicular velocity scale is much smaller than the parallel velocity scale. Looking at the scaling of the other terms in the Navier-Stokes equation (1.13):

$$(\mathbf{u}\cdot\nabla)\mathbf{u} \backsim \frac{u_0^2}{\ell}, \quad \nu\nabla^2\mathbf{u} \backsim \frac{\nu u_0}{h^2}, \quad \frac{(\mathbf{u}\cdot\nabla)\mathbf{u}}{\nu\nabla^2\mathbf{u}} \backsim \frac{u_0^2}{\ell}\frac{h^2}{\nu u_0} = \mathrm{Re}\left(\frac{h}{\ell}\right)^2 \tag{1.106}$$

We can thus ignore the inertial term assuming that $\mathrm{Re}\, h^2/\ell^2 \ll 1$. This means we are simply left with the following expression

$$\rho\frac{\partial \mathbf{u}}{\partial t} + \nabla p = \eta\nabla^2\mathbf{u} \tag{1.107}$$

Let us now assume that the perpendicular direction is orientated along $\mathbf{e}_z$, while the parallel direction is orientated along $\mathbf{e}_x$. We shall further assume that there is translational symmetry along $\mathbf{e}_y$ such that there is no dependence on y. It is clear that the z component of the right-hand side of this equation will be smaller by a factor of h/ℓ, meaning that we can neglect it in comparison to the pressure term:

$$\frac{\partial p}{\partial z} \backsim 0 \quad\longrightarrow\quad p = p(x) \tag{1.108}$$

Assuming that the velocity u_z is small, then we can neglect the rate of change of the flow. This means that we are simply left with the following system of equations:

$$\boxed{\begin{aligned} \frac{dp}{dx} &= \eta\frac{\partial^2 u_x}{\partial z^2} && (1.109)\\ \frac{\partial u_x}{\partial x} + \frac{\partial u_z}{\partial z} &= 0 && (1.110)\end{aligned}}$$

This is known as the *thin-film* or *lubrication approximation*. It is valid in cases where there is a thin film of fluid between two surfaces, such as the in the lubrication of a ball bearing, or the spreading of paint across a surface.

A circular disk of radius a initially sticks to a flat ceiling at $z = 0$ by means of a thin film of viscous, incompressible liquid of dynamic viscosity η and thickness $h \ll a$. Define $W = \dot{h}$. Find the force required to pull the disk away from the ceiling, and hence estimate the time for which a mass m can be suspended.

This is clearly a problem that is solved using the thin-film approximation. In this case, it is sensible to work in cylindrical polar coordinates. Following similar scaling arguments as the above, it can be shown that the relevant equations are

$$\frac{\partial p}{\partial r} = \eta \frac{\partial^2 u_r}{\partial z^2} \tag{1.111}$$

$$\frac{\partial u_z}{\partial z} = -\frac{1}{r}\frac{\partial}{\partial r}\left(r u_r\right) \tag{1.112}$$

As $p = p(r)$, we can simply integrate the first of these equations to find an expression for u_r:

$$u_r = \frac{1}{2\eta}\frac{\partial p}{\partial r} z(z+h) \tag{1.113}$$

Note that we have applied the no-slip boundary condition at $z = -h$. We now apply the incompressibility condition (1.112) to find an expression for $W(t)$.

$$u_z = -\frac{1}{2\eta r}\frac{\partial}{\partial r}\left(r\frac{dp}{dr}\right)\int_{-h}^{0} dz\, z(z+h) = -W \tag{1.114}$$

One can then find the pressure $p(r)$ by integration, defining that $p = p_0$ at $r = a$, resulting in the expression

$$p - p_0 = -\frac{3\eta W}{h^3}(a^2 - r^2) \tag{1.115}$$

The resultant force required is then given by

$$F = \int dA\,(p_0 - p) = \int_0^{2\pi} d\theta \int_0^a dr\, r(p_0 - p) = \frac{3\pi}{2}\frac{\eta a^4 W}{h^3} \tag{1.116}$$

The force that is opposing the above force is simply that due to the weight of the object, meaning we write that

$$mg = \frac{3\pi}{2}\frac{\eta a^4 W}{h^3} \tag{1.117}$$

We now assume that the volume of the film remains constant such that $V = \pi a_0^2 h_0$, where a_0 and h_0 are initial radius and thickness of the film respectively. This allows us to write that

$$mg = \frac{3\eta}{2\pi}\frac{V^2}{h^5}\frac{dh}{dt} \quad \longrightarrow \quad \frac{1}{4h_0^4} - \frac{1}{4h^4} = \frac{2\pi mg}{3\eta V^2}t \tag{1.118}$$

We then take $h \to \infty$ as the time at which the mass has fallen, and is no longer being suspended, which yields the expression

$$t = \frac{3\eta\pi a_0^4}{8mgh_0^2} \tag{1.119}$$

We have arrived at this expression by assuming that the system is quasistatic, and incompressible; both of these assumptions will break down as the h increases. Furthermore, it no longer becomes valid to use the thin-film approximation when h becomes comparable to a ($h \backsim a$), as the approximations used to obtain the defining equations are no longer valid.

1.4.3 Waves

In the context of fluid flows, waves can simply be thought of as small density and pressure perturbations in the homogeneous background of the system. As such, we must relax our incompressibility assumption, as otherwise such waves cannot occur. This means that we take the mass conservation equation in its original form of (1.4).

Linear Waves

Let us suppose that we are in the inviscid limit, in the absence of any applied body forces. Then, we are working with the system of equations

$$\frac{\partial \rho}{\partial t} + \nabla \cdot (\rho \mathbf{u}) = 0 \tag{1.120}$$

$$\rho \left(\frac{\partial \mathbf{u}}{\partial t} + (\mathbf{u} \cdot \nabla)\mathbf{u} \right) + \nabla p = 0 \tag{1.121}$$

$$\left(\frac{\partial}{\partial t} + \mathbf{u} \cdot \nabla \right) \frac{p}{\rho^\gamma} = 0 \tag{1.122}$$

A simple solution to the above set of equations is $\mathbf{u} = 0$, $\rho = \rho_0$, and $p = p_0$, where both ρ_0 and p_0 are homogeneous constants. This is evidently a solution, but an un-interesting one. Let us instead suppose that we are looking at small perturbations around this state by letting

$$\mathbf{u} = \delta \mathbf{u}, \quad \rho = \rho_0 + \delta\rho, \quad p = p_0 + \delta p \tag{1.123}$$

where $\delta\mathbf{u}$, $\delta\rho$ and δp are vanishingly small. Substituting these solutions into the above set of equations, and ignoring terms of $\mathcal{O}(\delta^2)$ and above, we obtain the subsequent set of equations:

$$\frac{\partial \delta\rho}{\partial t} + \rho_0 \nabla \cdot \delta\mathbf{u} = 0 \tag{1.124}$$

$$\rho_0 \frac{\partial \delta\mathbf{u}}{\partial t} + \nabla \delta p = 0 \tag{1.125}$$

$$\frac{\partial}{\partial t} \left(\delta p - \gamma \frac{p_0}{\rho_0} \delta\rho \right) = 0 \tag{1.126}$$

We now assume that the equation of state of the system is a function of only density (as motivated by Kinetic theory); that is, $p = p(\rho)$. This means that we can expand the pressure about the equilibrium density ρ_0, allowing us to obtain

$$\nabla \delta p = \left. \frac{\partial p}{\partial \rho} \right|_{\rho=\rho_0} \nabla \delta\rho \tag{1.127}$$

Taking appropriate derivatives of the first two of these equations, and using the above condition, one can show that the density perturbations obey the wave-equation:

$$\boxed{\frac{\partial^2 \delta\rho}{\partial t^2} = c_s^2 \nabla^2 \delta\rho, \quad c_s^2 = \left. \frac{\partial p}{\partial \rho} \right|_{\rho=\rho_0}} \tag{1.128}$$

These are *sound waves*, with c_s being the phase velocity for the given medium in which the waves propagate; in other words, the speed of sound. These oscillations will do so without any damping as we have ignored the effects of viscosity on the system, making it non-dispersive.

To get an estimate for c_s by considering (1.126); in the steady state, it is clear that

$$\frac{\delta p}{\delta \rho} \approx \left.\frac{\partial p}{\partial \rho}\right|_{\rho=\rho_0} = \gamma \frac{p_0}{\rho_0} \tag{1.129}$$

This can also be obtained by recognising that sound waves are adiabatic perturbations, as they usually occur too quickly for heat to be able to flow, due to low thermal conductivity. This gives us the relationship between $p\rho^{-\gamma} = \text{constant}$, which is an equivalent condition to (1.122).

We are now in a position to re-visit the idea of incompressibility; under exactly what conditions can we approximate a gas as being incompressible? We have just showed that sound waves are small density perturbations around some equilibrium flow characterised by ρ_0 and p_0. Thus, an entirely sensible condition is that we require the pressure (or equivalently density) variations due to the flow are much less than the pressure variations due to the sound waves. Using (1.60), we can approximate $\Delta p \backsim \rho_0 u^2$ for the flow, while it is clear from the above that $\Delta p \backsim \rho_0 c_s^2$. This gives us the condition that

$$\boxed{\text{Ma} \ll 1, \quad \text{Ma} = \frac{u}{c_s}} \tag{1.130}$$

The quantity on the right hand side is known as the *Mach number*. This can be used to classify flows into subsonic and supersonic regimes. When a fast-moving object reaches $u \backsim c_s$, a large pressure difference is created in front of them. This abrupt pressure difference, called a *shockwave*, spreads backward and outward from the aircraft in a cone shape. It is this shockwave that creates the audible "sonic boom" that is heard.

Non-Linear Waves

Our derivation of (1.128) assumed that the perturbations around equilibrium were small initially, and indeed that they remained small as they propagate. However, the Navier-Stokes equation (1.13) is an inherently non-linear equation, and small perturbations will grow chaotically (more on this in section 1.5). Solving such non-linear equations is much more involved, and often not possible analytically. As such, we will consider what happens to a greatly simplified model with the defining equation

$$\frac{\partial u}{\partial t} + u\frac{\partial u}{\partial x} = 0 \tag{1.131}$$

This is solved by the ansatz $u = f(x - ut)$, which can be checked by direct substitution. It is clear that the amplitude of such a wave is proportional to the local flow velocity, meaning that it will steepen in real space, and transition to a shockwave type solution. The step-like structure shown in figure (1.6) can get quite steep if left unchecked. However, it will eventually be damped out by viscosity as the steepening in velocity is also accompanied by a shift towards smaller spatial scales at which viscosity becomes dominant. Thus, viscous dissipation increases with velocity gradients.

A particular type of non-linear wave is that of a surface water wave, which we will now look at as an example. Imagine that small amplitude waves are generated at the surface of a hollow channel of water that has been filled to a depth h. Assume that the flow is two-dimensional, inviscid and irrotational, such that we can characterise the flow by a velocity potential $\phi = \phi(x, z, t)$, $\nabla^2 \phi = 0$.

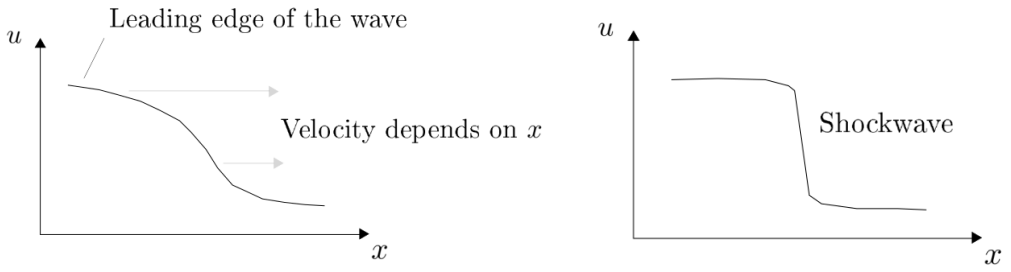

(a) (b)

Figure 1.6: The velocity profile of a non-linear wave at (a) early times (b) later times

These conditions also imply that the Bernoulli function is conserved throughout the flow, such that (1.89) is satisfied. This means that we can write that

$$\frac{\partial \phi}{\partial t} + H = \frac{\partial \phi}{\partial t} + gz + \frac{\mathbf{u}^2}{2} + \frac{p}{\rho} = \text{constant} \tag{1.132}$$

However, we can ignore the last two terms in this relationship, as we can absorb them into ϕ through a gauge transformation. Evaluating this expression at the surface of the fluid, we obtain the condition that

$$\frac{\partial \phi}{\partial t} + g\eta = 0 \quad \text{at } z = h \tag{1.133}$$

where η is the vertical displacement of the free surface of the water. The other two conditions that must be satisfied are

$$\frac{\partial \eta}{\partial t} - \frac{\partial \phi}{\partial z} = 0 \quad \text{at } z = h \tag{1.134}$$

$$\frac{\partial \phi}{\partial z} = 0 \quad \text{at } z = 0 \tag{1.135}$$

which come from the fact that the motion of the water of the boundary surface is governed by the vertical component of the flow, and that there must be no sources or sinks of the fluid along the solid boundary at the bottom of the channel.

Now, assume that the flow potential is separable in both coordinate directions, such that

$$\phi = f(x - ct)g(z) \tag{1.136}$$

where c is some constant velocity of the flow, and f and g are arbitrary functions. We can then solve Laplace's equation by separation of variables with separation constant k:

$$\frac{f''}{f} = -\frac{g''}{g} = -k^2 \tag{1.137}$$

This has general solution

$$\phi = \sum_k e^{i(kx - \omega t)} \left(c_1 e^{kz} + c_2 e^{-kz} \right) \tag{1.138}$$

where c_1 and c_2 are constants to be determined; (1.135) gives us that $c_1 = c_2$. We can then combine the two other boundary conditions at $z = h$ to give that

$$\frac{\partial^2 \phi}{\partial t^2} + g\frac{\partial \phi}{\partial z} = 0 \tag{1.139}$$

Substitution of the above solution yields the dispersion relation:

$$\boxed{\omega^2 = gk\tanh(kh)} \tag{1.140}$$

This gives rise to two cases:

- Shallow waves ($hk \ll 1$) - Physically, this limit occurs where the water is shallow compared to the wavelength of the wave. Wind waves approaching the shore, tides and tsunamis all behave like this limit, as the latter two have a wavelength much greater than the ocean depth. Under such conditions, we can expand the dispersion relation as
$$\omega \backsim \sqrt{gh}\left(k - \frac{k^3h^2}{6}\right) \tag{1.141}$$
- Deep waves ($hk \gg 1$) - This limit occurs where the water is very deep in comparison to the wavelength of the wave. Wind waves in the deep ocean obey this limit to a close approximation. In this case, the dispersion relation becomes
$$\omega \backsim \sqrt{gk}\left(1 - e^{-2hk}\right) \tag{1.142}$$

1.5 Instabilities and Turbulence

Some internal states of certain systems will grow without bound, leading to large amplitude effects. This is known as an *instability*. Not all systems are inherently unstable, but non-linear terms generally give rise to instabilities, as we saw in our consideration of a non-linear wave. Within a fluid, such instabilities often result in turbulent flow.

1.5.1 Fluid Instabilities

Rayleigh-Bernard

Consider a fluid between two parallel plates, with the upper plate being at a temperature T_1 and the lower plate being at a temperature T_2. In the case where $T_2 < T_1$, fluid of higher density remains at the bottom of the system, and so it remains stable. However, in the case that $T_2 > T_1$, then the lower density fluid is at the bottom of the system. Consider a fluid element that moves initially upwards from the bottom due to some random thermal fluctuation. If it does not cool down quickly enough, it will be surrounded by fluid of increasingly high density, resulting in an increasing buoyancy force and flow velocity. This causes convective 'rolls' to form in the fluid between the two plates.

This instability is controlled by a dimensionless parameter Ra known as the *Rayleigh number*. We can get an expression for this parameter through scaling arguments. Let d be the distance between the plates, ΔT the temperature different between them, ρ_0 the mean fluid density, κ the thermal conductivity, and

$$\alpha = -\frac{1}{\rho_0}\frac{dp}{dT} \tag{1.143}$$

the thermal expansivity of the fluid. Now, consider a roughly spherical fluid element of radius r_0, that acquires an initial upwards velocity u_0 due to random thermal motions. We then make the following scaling arguments:

- The thermal relaxation time of the particle τ_Q can be approximated from the heat diffusion equation
$$\kappa\nabla^2 T = \frac{\partial T}{\partial t} \quad \longrightarrow \quad \tau_Q \backsim \frac{r_0^2}{\kappa} \tag{1.144}$$
- The distance moved by particle over the thermal relaxation time
$$\delta z \backsim u_0 \tau_Q \tag{1.145}$$
- The difference in temperature between the fluid particle and the remainder of the fluid
$$\delta T = \frac{\partial T}{\partial z}\delta z \backsim \frac{\Delta T}{d} u_0 \tau_Q \tag{1.146}$$
- The change in density of the fluid element over the thermal relaxation time
$$\delta\rho = \frac{\partial \rho}{\partial T}\delta T \backsim \rho_0 \alpha \frac{\Delta T}{d}\frac{u_0 r_0^2}{\kappa} \tag{1.147}$$
- This results in a particular upthrust
$$\text{Upthrust} \backsim \delta\rho V g \backsim \rho_0 g \alpha \frac{\Delta T}{d}\frac{u_0 r_0^5}{\kappa} \tag{1.148}$$

- The upthrust must be balanced by the Stokes drag on the fluid element, which is given by

$$D \backsim \eta r_0 u_0 \backsim \rho_0 \nu r_0 u_0 \tag{1.149}$$

Thus, the condition for the Rayleigh-Bernard convection occurring is that the buoyancy force is greater than the Stokes drag, giving rise to the expression

$$\boxed{\mathrm{Ra} = \frac{\alpha \Delta T g d^3}{\kappa \nu} > \left(\frac{d}{r_0}\right)^4} \tag{1.150}$$

for the Rayleigh number. It is clear from the above expression that there is some critical Rayleigh number for the instability to occur, which can be show experientially to be $\backsim 1708$.

Rayleigh-Plateau

This instability explains as to why a falling stream of fluid breaks up into packets with the same volume, but smaller surface area. The driving force of the Rayleigh-Plateau instability is tendency of fluids to minimise their surface area due to surface tension.

Consider a vertical stream of water of a given thickness. No matter how smooth the stream is considered to be, there will always be small perturbations in the edge of the stream. If these are resolved into sinusoidal components, it can be shown that some of these grow, while others decay, with the behaviour being controlled entirely by the given wavenumber (number of peaks and troughs per centimetre) being considered and the original radius of the stream.

By assuming that all possible components exist initially in roughly equal (but vanishing) amplitudes, the size of the final drops can be predicted by determining by wave number which component grows the fastest. This is because this component will dominate at longer times, and will eventually be the one that pinches the stream into drops.

The radius of the stream can be written as

$$r(z) = r_0 + \sum_k a_k \cos(kz) + b_k \sin(kz) \tag{1.151}$$

where r_0 is the initial radius, and a_k, b_k are Fourier coefficients that are assumed to be small. It can be shown that the only modes that grow are those that satisfy the relationship $kr_0 < 1$. In fact, the fastest growing wavenumber is that satisfying $kr_0 \backsim 0.697$.

Rayleigh-Taylor

The Rayleigh-Taylor instability is that of an interface between two fluids of different densities which occurs where a denser fluid sits on-top of a less dense fluid under the influence of a gravitational field.

Consider a free interface between a fluid of density ρ_2 sitting ontop of a fluid of density ρ_2, such that $\rho_2 > \rho_1$. Orient the system such that $\mathbf{g} = -g\mathbf{e}_z$, and define the surface $z = \eta(x,t)$. Suppose that on the the surface there develops an initial perturbation given by

$$\eta(x,0) = \delta\eta \cos(kx) \tag{1.152}$$

where $\delta\eta$ is much less than the typical scale of z. Then, it can be shown that the solution evolves as

$$\eta(x,t) = \delta\eta \exp\left[\sqrt{gAk}t\right] \cos(kx) \tag{1.153}$$

where A is the *Atwood number* given by

$$A = \frac{\rho_2 - \rho_1}{\rho_2 + \rho_1} \tag{1.154}$$

Clearly, vanishingly small perturbations in along the boundary layer grow exponentially, creating 'mushroom' shaped spikes (structures of the heavy fluid into the light) and 'bubbles' (structures of the light fluid into the heavy). Eventually, growth becomes so unstable that the boundary layer becomes undefined and turbulent, breaking apart.

Kelvin-Helmholtz

This instability occurs where there is a velocity shear in a continuous fluid, or when there is a velocity difference at the interface between two fluids, such as the case of wind blowing over water, where the instability manifests on the water surface. This instability can also manifest itself in conjunction with the Rayleigh-Taylor instability along the interface that defines the structures between the two fluids of different densities.

The Kelvin-Hemholtz instability is controlled by the Richardson number Ri that is a ratio of the buoyancy term to the shear flow term:

$$\mathrm{Ri} = \frac{g}{\rho} \frac{\nabla \rho}{(\nabla u)^2} \tag{1.155}$$

1.5.2 Turbulence

Turbulence is a type of *deterministic chaos* that one should be able to describe by the Navier-Stokes equation (1.13). However, thermal fluctuations in the fluid are likely to be important due to a sensitive dependence on initial conditions. The result of turbulence is that the velocity and vorticity fields $\mathbf{u}$ and $\boldsymbol{\omega}$ fluctuate randomly, though this is not simply a gaussian white noise, as there are correlations between both fields.

Fluctuations around Equilibrium

Consider the Navier-Stokes equation in index notation form:

$$\partial_t u_i + (u_j \partial^j) u_i = -\frac{1}{\rho} \partial_i p + \nu \partial_j \partial^j u_i + \frac{f_i}{\rho} \tag{1.156}$$

We introduce the decomposition

$$\boxed{u_i = \langle u_i \rangle + \delta u_i} \tag{1.157}$$

where $\langle u_i \rangle$ is the mean flow velocity, and δu_i are fluctuations around this equilibrium, which we need not necessarily assume small. In fact, the nature of turbulence dictates that this will not remain small. The average is taken at a particular point over timescales much longer than the typical timescale of the flow. By construction, this means that $\langle \langle u_i \rangle \rangle = \langle u_i \rangle$, and $\langle \delta u_i \rangle = 0$. Substituting this decomposition into (1.156), and taking the average, we find that

$$\partial_t \langle u_i \rangle + \left(\langle u_j \rangle \partial^j \right) \langle u_i \rangle + \left\langle \left(\delta u_j \partial^j \right) \delta u_i \right\rangle = -\frac{1}{\rho} \partial_i p + \nu \partial_j \partial^j \langle u_i \rangle + \frac{\langle f_i \rangle}{\rho} \tag{1.158}$$

We see that this is just the same as the equation for the mean flow, except that we have an extra *eddy viscosity* term involving the fluctuations. However, the behaviour of this term is also not well understood, so doing this is just a way of obfuscating the problem, and does not get us much closer to a solution.

Kolmogorov Scaling

Kolmogorov scaling is a way of describing turbulence in terms of an energy cascade from large to small spatial scales (or rather, from low to high phase space in k), before the oscillations associated with the energy hit collisions, and are damped. That is, large scale structures are broken up into smaller ones until the scale reaches that at which collisionality becomes dominant. The *injection* range is associated with the largest structures in the fluid, characterised by a lengthscale ℓ and velocity scale u_ℓ. Likewise, the *dissipative* range is associated with small-scale collisional dissipation within the fluid, characterised by some lengthscale ξ and velocity scale u_ξ. The *inertial* range separates the injection and dissipative ranges, for which we wish to find an expression for the energy spectrum $E(k)$.

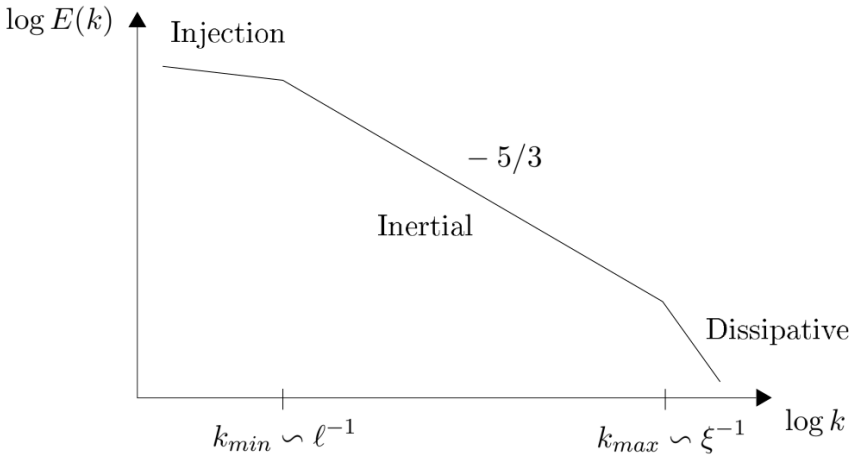

Figure 1.7: The energy spectrum associated with Kolmogorov scaling, showing the injection, inertial and dissipative ranges

Suppose that the rate of energy flow per unit mass in the inertial range is constant, and denoted by ε. By energy conservation, this must be equal to the rate at which energy is created in the injection range, allowing us to write that

$$\varepsilon \backsim \frac{u_\ell^2}{\ell/u_\ell} \backsim \frac{u_\ell^3}{\ell} \tag{1.159}$$

as we note that $[\varepsilon] = \mathrm{L}^2\mathrm{T}^{-3}$. Similarly, the rate at which energy arrives down the cascade to the dissipation range must be equal to the rate of energy dissipation due to viscosity:

$$\varepsilon \backsim \frac{u_\xi^3}{\xi} \backsim \nu \left(\frac{u_\xi}{\xi}\right)^2 \tag{1.160}$$

This allows us to define the *Kolmogorov length* and *Kolmogorov velocity* as

$$\boxed{\xi \backsim \nu^{3/4}\varepsilon^{-1/4}, \quad u_\xi \backsim (\nu\varepsilon)^{1/4}} \tag{1.161}$$

We expect dissipation to become important when $\mathrm{Re} \backsim 1$; is this indeed the case in the dissipative range? Using the above length and velocity scales, we write that

$$\mathrm{Re} \backsim \frac{u_\xi \xi}{\nu} \backsim \frac{\nu^{3/4}\varepsilon^{-1/4}(\nu\varepsilon)^{1/4}}{\nu} \backsim 1 \tag{1.162}$$

confirming our expectation. According to Kolmogorov, the energy spectrum in the inertial range can only depend on ε and k, and not ν, ξ or u_ξ as these are all dependent on viscosity that is absent in the inertial range. Noting that $[E(k)] = \mathrm{L}^3\mathrm{T}^{-2}$, we argue that $E(k) \backsim \varepsilon^{2/3}k^{-5/3}$ on dimensional grounds, as shown in figure 1.7 above.

2. *Dynamical Systems*

This chapter aims to cover the basic principles surrounding the rich and complex subject that is dynamical systems, including:

- Stability Analysis
- Bifurcations
- Some Examples
- Phase Space and Chaos

The concept of dynamical systems has its origins in Newtonian mechanics; such systems describe the time dependence of a point in a geometrical space, such as the end of a pendulum rod. However, many dynamical systems are usually not analytically solvable due to non-linearity, and so we have to content ourselves with the examination of trajectories in phase space.

2.1 Stability Analysis

The aim of this chapter is to solve systems of the form

$$\dot{\mathbf{r}} = \mathbf{f}(\mathbf{r}) \tag{2.1}$$

where $\mathbf{r} = (x_1, x_2, x_3, \dots)$ and $\mathbf{f}$ is, in general, some smooth non-linear function of $\mathbf{r}$. In most cases, these cannot be solved explicitly, and instead we content ourselves with attempting to find a rather more qualitative description of the behaviour of the system.

2.1.1 Fixed Points and Stability

To do this, we look at the behaviour of the system around *fixed points* at which the system does not change with time. That is, they are points $\mathbf{r}_0$ that satisfy $\mathbf{f}(\mathbf{r}_0) = 0$. We find the stability (or lack-thereof) associated with a fixed point by linearising about said point. Let $\mathbf{r} = \mathbf{r}_0 + \delta\mathbf{r}$ in (2.1):

$$\dot{\mathbf{r}} = \delta\dot{\mathbf{r}} = \mathbf{f}(\mathbf{r}_0 + \delta\mathbf{r}) \approx \left.\frac{\partial \mathbf{f}}{\partial \mathbf{r}}\right|_{\mathbf{r}=\mathbf{r}_0} \cdot \delta\mathbf{r} + \dots \tag{2.2}$$

where we have expanded to first order, and noted that $\mathbf{f}(\mathbf{r}_0) = 0$ by definition. We can write this as

$$\delta\dot{\mathbf{r}} = \mathcal{J}\delta\mathbf{r} \tag{2.3}$$

where we have defined the *Jacobian matrix*

$$\boxed{\mathcal{J}_{ij} = \frac{\partial r_i}{\partial r_j} = \begin{pmatrix} \frac{\partial \dot{x}}{\partial x} & \frac{\partial \dot{x}}{\partial y} \\ \frac{\partial \dot{y}}{\partial x} & \frac{\partial \dot{y}}{\partial y} \end{pmatrix}} \tag{2.4}$$

where all the derivatives are evaluated at the fixed point. The last expression above is the form of the Jacobian matrix in two dimensions (where $\mathbf{r} = (x, y)$), the case to which we shall restrict out consideration.

Suppose that $\mathcal{J}$ has eigenvalues λ_1 and λ_2, with corresponding eigenvectors $\mathbf{u}_1$ and $\mathbf{u}_2$. Note that in general the eigenvalues of $\mathcal{J}$ may be complex. As these span vector space associated with $\mathbf{r}$, we can write any state of the system as a linear combination of these eigenvectors. Namely, for arbitrary constants c_1 and c_2:

$$\begin{pmatrix} \delta x(0) \\ \delta y(0) \end{pmatrix} = c_1\mathbf{u}_1 + c_2\mathbf{u}_2 \quad \longrightarrow \quad \begin{pmatrix} \delta x(t) \\ \delta y(t) \end{pmatrix} = c_1\mathbf{u}_1\, e^{\lambda_1 t} + c_2\mathbf{u}_2\, e^{\lambda_2 t} \tag{2.5}$$

This means that the behaviour of the solution in the vicinity of the fixed point is determined by the eigenvalues of $\mathcal{J}$, while the dominant directions of the evolution of the system are determined by the eigenvectors.

2.1.2 Classifying Fixed Points

While we shall classify the various types of possible fixed points working only in two-dimensions, the phenomenological behaviour of the system will remain the same in higher dimensions; it will just take a different exact form of the flows in phase space. We will examine the following cases:

(a) λ_1, λ_2 real and positive - unstable node

(b) λ_1, λ_2 real and negative - stable node

(c) λ_1, λ_2 real with opposite signs - saddle node

(d) λ_1, λ_2 purely imaginary - stable orbit

(e) λ_1, λ_2 complex with positive real parts - unstable spiral

(f) λ_1, λ_2 complex with negative real parts - stable spiral

Phase space plots of examples of these different types of fixed points have been included in figure 2.2. Note that these figures are in the vicinity of the fixed points, where the linear approximation is still valid; to get the behaviour further from the fixed points, one has to resort to the fact that the phase-space lines must be continuous.

Clearly, the addition of imaginary parts to the eigenvalues simply creates 'rotation' in phase space; the direction of rotation can be determined by evaluating the equations of motion in the vicinity of the fixed point.

2.1.3 Limit Cycles

Limit cycles are phase space structures that are not included in our linear approximation used above as they are inherently non-linear. Stable limit cycles feature a stable orbit to which things decay, where as unstable limit cycles feature an orbit from which things decay. These are shown in figure 2.1 below. Limit cycles are generally associated with periodic solutions.

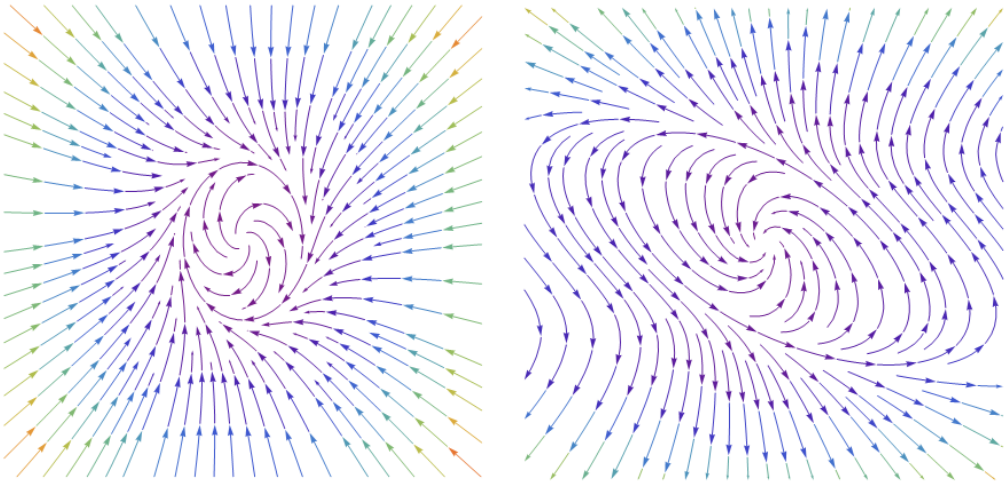

(a) (b)

Figure 2.1: Phase space plots showing examples of: (a) stable limit cycle (b) unstable limit cycle

If one can find a closed surface in phase space such that all trajectories along the surface point inwards, then this is known as a *trapping region*. The *Poincaré-Bendixson theorem* states that if such a trapping region exists, then it must contain an attractor. In two dimensions, this attractor will either be a stable fixed point, or a stable limit cycle. In higher dimensions, trajectories inside this region may wander around forever without reaching a fixed point, or a stable orbit; this is known as a *strange attractor*, an example of which we will examine in section 2.4.3.

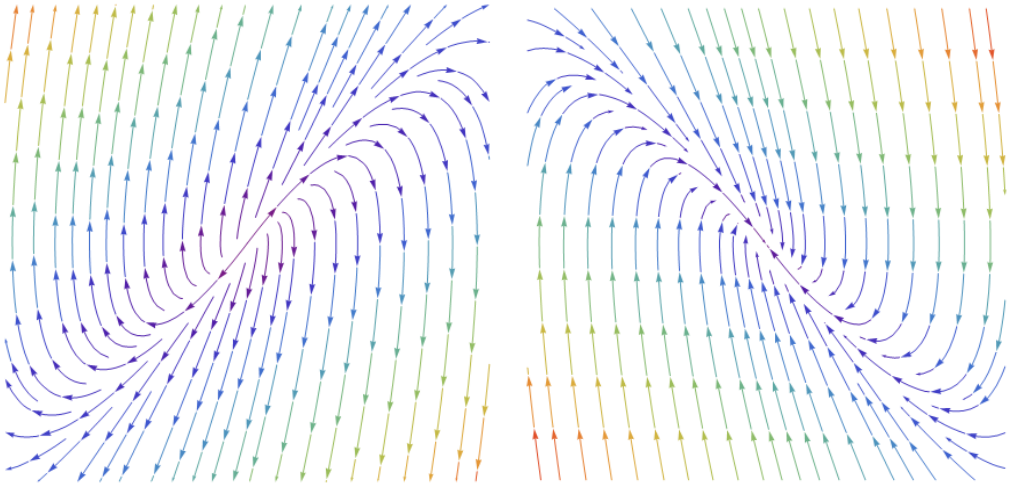

(a) (b)

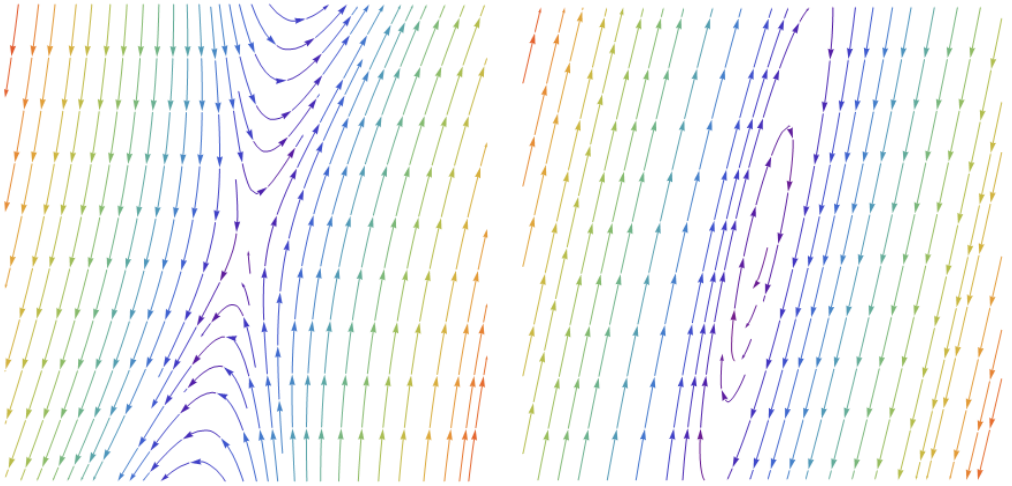

(c) (d)

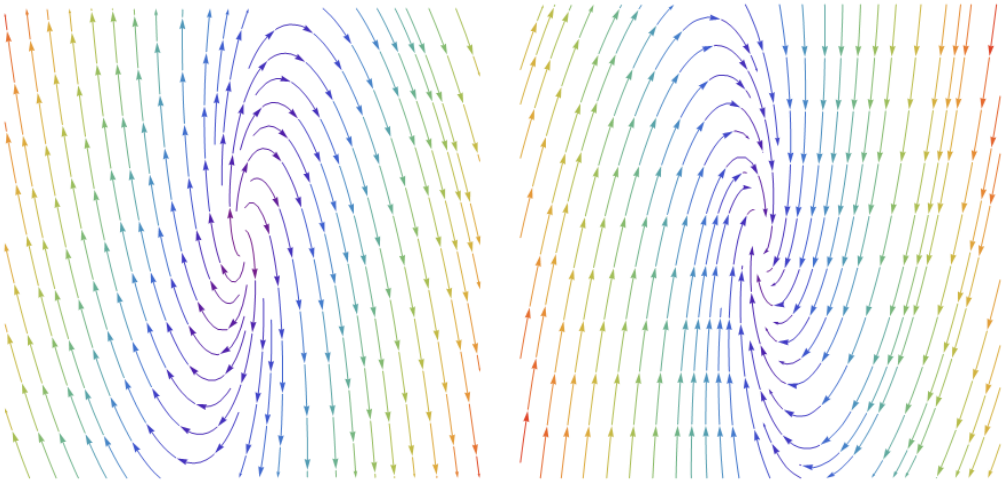

(e) (f)

Figure 2.2: Phase space plots showing examples of: (a) unstable node (b) stable node (c) saddle node (d) stable orbit (e) unstable spiral (f) stable spiral

2.2 Bifurcations

Bifurcations occur when the behaviour of a dynamical system changes - sometimes dramatically - as a parameter is varied. This may include the creation and destruction of fixed points, or a fixed point changing in stability. Note that the behaviour of many two-dimensional systems can be characterised by a single parameter with appropriate non-dimensionalisation. We can plot bifurcations on a *stability* or *bifurcation diagram*, which shows how the stability of fixed points changed as a parameter is varied. Note that the flows show on such diagrams must be continuous. In the following sections, we shall examine some of the animals of the bifurcation zoo for one-dimensional dynamical systems.

2.2.1 Saddle Node Bifurcation

A saddle node bifurcation occurs where two fixed points are produced/annihilated. This has the canonical form

$$\boxed{\dot{x} = r - x^2} \tag{2.6}$$

It is clear that this has stable points for

$$\dot{x} = 0 \quad \longrightarrow \quad x_0 = \pm\sqrt{r} \tag{2.7}$$

Using the stability analysis of section (2.1.2), it is clear that one of these is stable, while the other is unstable for $r > 0$, giving rise to the following.

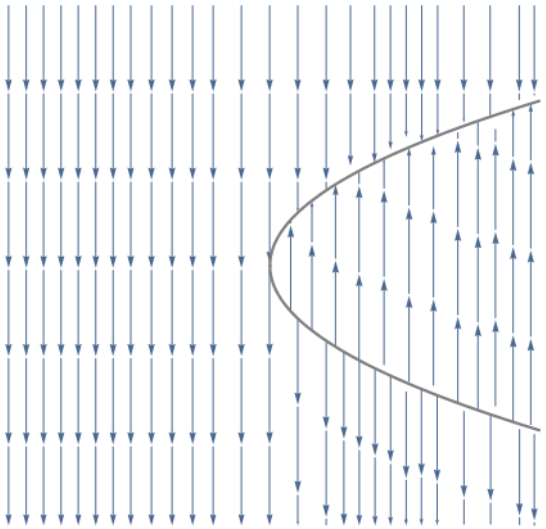

Figure 2.3: A stability diagram for a saddle node bifurcation. The parameter r is plotted on the horizontal axis, with the origin located at the centre of the diagram

2.2.2 Transcritical Bifurcation

A transcritical bifurcation is one in which a fixed point exists for all values of the parameter r, and is never destroyed. However, such a fixed point interchanges its stability with another fixed point as the parameter is varied. This has the canonical form

$$\boxed{\dot{x} = rx - x^2} \tag{2.8}$$

This has fixed points along $x_0 = 0$ and $x_0 = r$. Stability analysis reveals that neither curve is continuous in its stability; they in fact exchange stability at the origin.

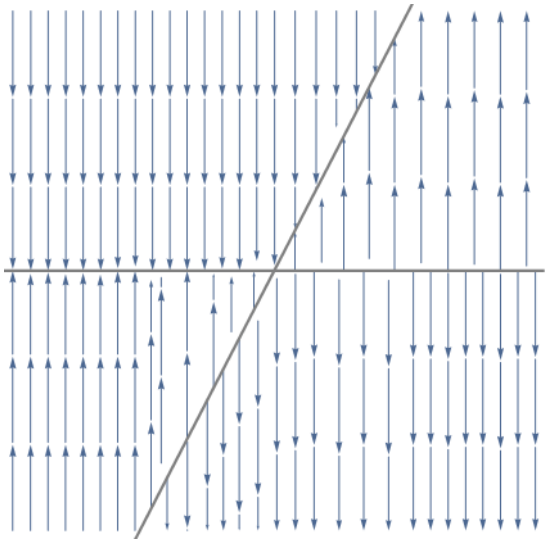

Figure 2.4: A stability diagram for a transcritical bifurcation. The parameter r is plotted on the horizontal axis, with the origin located at the centre of the diagram

2.2.3 Pitchfork Bifurcation

A pitchfork bifurcation occurs where the system transitions from having a single fixed point, to having three fixed points. Both supercritical and subcritical pitchfork bifurcations have symmetry in x; that is, they are unchanged under the parity inversion $x \leftrightarrow -x$. This symmetry is broken in the case of the imperfect pitchfork bifurcation.

Supercritical Pitchfork Bifurcation

The supercritical pitchfork bifurcation occurs when a stable fixed point becomes unstable, giving rise to two new stable fixed points, which form the 'prongs' of the pitchfork. It has the canonical form

$$\boxed{\dot{x} = rx - x^3} \tag{2.9}$$

with fixed points at

$$x_0 = 0, \quad x_0 = \pm\sqrt{r} \quad \text{for} \quad r > 0 \tag{2.10}$$

as shown in figure 2.5. The transition to convective rolls in Rayleigh-Bernard convection 1.5.1 is an example of such a bifurcation; the stable fixed points are the counter-rotating convective rolls, and the zero motion solution goes from being stable to unstable as the Rayleigh number passes its critical value. We will explore this more later in section 2.4.3.

Subcritical Pitchfork Bifurcation

Subcritical pitchfork bifurcations have two unstable fixed points that 'collide' with a stable one at $r = 0$, annihilating each other while the stable one looses its stability. This is almost the 'inverse' of the supercritical pitchfork, having the canonical form

$$\boxed{\dot{x} = rx + x^3} \tag{2.11}$$

with fixed points at

$$x_0 = 0, \quad x_0 = \pm\sqrt{-r} \quad \text{for} \quad r < 0 \tag{2.12}$$

However, it is clear from the right hand side of 2.5 that these solutions diverge to infinity for most values, meaning that it is unlikely to represent an actual physical system. We can

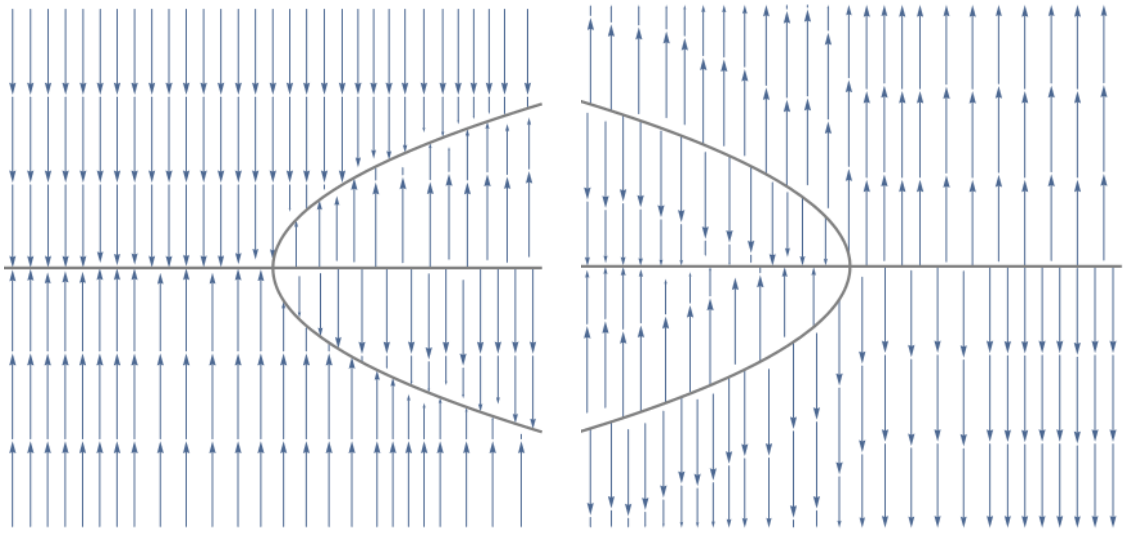

(a) (b)

Figure 2.5: A stability diagram for (a) a supercritical pitchfork bifurcation (b) a subcritical pitchfork bifurcation. The parameter r is plotted on the horizontal axis, with the origin located at the centre of the diagram

stabalise the equation by adding higher order terms, namely

$$\boxed{\dot{x} = rx + x^3 - x^5} \tag{2.13}$$

This looses the divergent property through the addition of two extra local saddle node bifurcations to the subcritical pitchfork. This model predicts hysteresis - a lack of reversibility as the control parameter r is varied - as shown in red in figure 2.6.

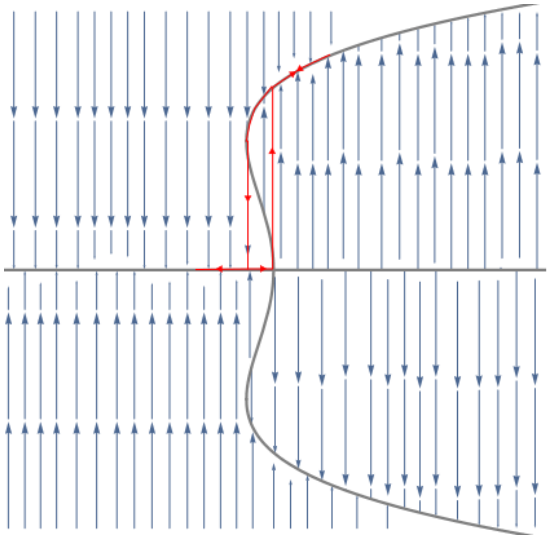

Figure 2.6: A stability diagram for a stable subcritical pitchfork bifurcation. The parameter r is plotted on the horizontal axis, with the origin located at the centre of the diagram. A hysteresis loop is shown in red

Imperfect Pitchfork Bifurcation

As previously stated, the symmetry of the supercritical and subcritical pitchfork bifurcations is broken in the imperfect pitchfork bifurcation by the addition of a small 'imperfection' parameter ϵ. This has the associated canonical form:

$$\boxed{\dot{x} = \epsilon + rx - x^3} \tag{2.14}$$

In order to construct a stability diagram for this system, let us examine how the curves are modified in the region of the fixed point $x_0 = 0$ for the pitchfork bifurcation. Let initially assume that x is small, such that

$$0 = \epsilon + rx - x^3 \backsim \epsilon + rx \quad \longrightarrow \quad x \backsim -\frac{\epsilon}{r} \tag{2.15}$$

But what exactly do we mean by 'x is small'? Well, we require that $x^3 \ll rx$, meaning that

$$x \ll \sqrt{r} \quad \longrightarrow \quad r \gg \epsilon^{2/3} \tag{2.16}$$

This means that in a region $r \gg \epsilon^{2/3}$ and $x \ll \sqrt{r}$, we have the curve $x = -\epsilon/r$. However, it is unclear what happens for $r \backsim \epsilon^{2/3}$, but we can complete the picture due to the fact that the curves have to be continuous, and tend to the normal pitchfork bifurcation for large x and r. This gives rise to figure 2.7.

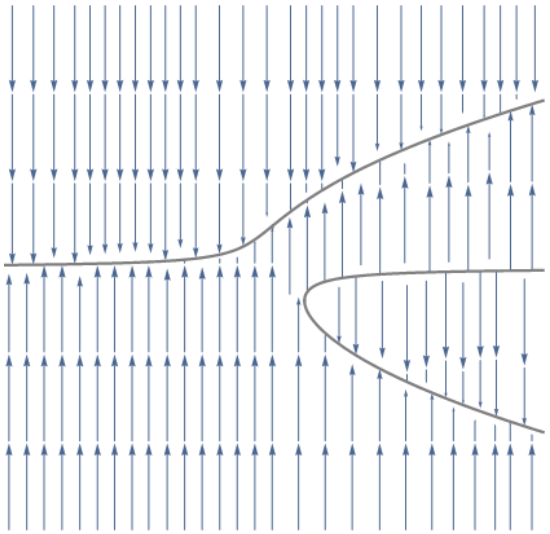

Figure 2.7: A stability diagram for an imperfect pitchfork bifurcation for $\epsilon = 0.5$. The parameter r is plotted on the horizontal axis, with the origin located at the centre of the diagram

How does this graph depend on the value of ϵ? We look for intersections between the curves $f(x) = rx - x^3$ and $g(x) = -\epsilon$. For $r \leq 0$, there is one stable fixed point for $x > 0$ as the curve is decreasing monotonically. For $r > 0$, there is a critical value ϵ_c, such that for $\epsilon \leq \epsilon_c$, there are three fixed points, and for $\epsilon < \epsilon_c$, there is one. We can find ϵ_c as it must occur at a minimum of $f(x)$:

$$\frac{d}{dx}(rx - x^3) = 0 \quad \longrightarrow \quad x_c = -\sqrt{\frac{r}{3}} \tag{2.17}$$

Then

$$\epsilon_c = \pm\frac{2r}{3}\sqrt{\frac{r}{3}} \tag{2.18}$$

It is thus possible to construct a diagram in the $\epsilon - r$ plane showing how the number of fixed points depends on the combination of these parameters.

2.2.4 Hopf Bifurcations

In a Hopf bifurcation, there is a switch in the stability of the system, and a periodic solution arises. More accurately, it is a local bifurcation in which a fixed point of a dynamical system looses stability as the linearised eigenvalues λ_1 and λ_2 cross the imaginary axis in the complex plane. This corresponds to the transition through a stable cycle, as they both become instantaneously purely imaginary.

Supercritical Hopf Bifurcation

A supercritical Hopf bifurcation features the transition from a stable spiral to a stable limit cycle. Physically, this represents a transition from oscillations that are decaying in time to oscillations that have constant amplitude in time.

Subcritical Hopf Bifurcation

In this bifurcation, an unstable limit cycle shrinks and engulfs the origin, which changes from a stable fixed point to an unstable one, meaning that trajectories that were originally inside the limit cycle becomes unbounded. Thus, small decaying oscillations suddenly become very large in amplitude, in a resonance-like effect. However, turning down the control parameter again does not destroy these large oscillations due to hysteresis, which can cause problems in mechanical and biological systems in which subcritical Hopf bifurcations occur.

2.3 Some Examples

As the title suggests, we will have a look at a couple of examples of dynamical systems in order to give the reader an idea of the general method that is used when tacking these sorts of systems. If the reader is already familiar with how to do this, it is recommended that they skip to section 2.4.

2.3.1 A Simple Pendulum

The first example that we will look at is that of the simple damped pendulum, with equation of motion given by

$$\ddot{\theta} + \gamma\dot{\theta} + \sin\theta = 0 \tag{2.19}$$

for some positive damping constant γ. At first glance, this does not appear to be in the form (2.1). However, we can convert higher-order differential equations such as this one into a dynamical system; in this case, we introduce $x = \theta$ and $y = \dot{\theta}$, such that we obtain the system:

$$\begin{aligned} \dot{x} &= y \\ \dot{y} &= -\gamma y - \sin x \end{aligned} \tag{2.20}$$

Fixed points occur at $\dot{x} = 0, \dot{y} = 0$. The first of these gives us that $y = 0$, meaning that all fixed points must occur along the x-axis. For $\dot{y} = 0$:

$$-\gamma y - \sin x = 0 \quad \longrightarrow \quad x = \pi n \quad \text{for integer } n \tag{2.21}$$

The Jacobian matrix at the fixed points is then given

$$\mathcal{J} = \begin{pmatrix} 0 & 1 \\ -\cos x & -\gamma \end{pmatrix} = \begin{pmatrix} 0 & 1 \\ \mp 1 & -\gamma \end{pmatrix} \tag{2.22}$$

where we have used the fact that $\cos \pi n = \pm$ for odd/even values of n. This has eigenvalues

$$\lambda = -\frac{\gamma}{2} \pm \sqrt{\left(\frac{\gamma}{2}\right)^2 \pm 1} \tag{2.23}$$

We thus have a few different cases, depending on the odd/even nature of n, and the value of γ:

- Odd n - In this case, the eigenvalues are given by

$$\lambda = -\frac{\gamma}{2} \pm \sqrt{\left(\frac{\gamma}{2}\right)^2 + 1} \tag{2.24}$$

  Interestingly, odd n always gives rise to saddle points regardless of the value of γ (something for the reader to check as an exercise). This is because this corresponds to the pendulum being inverted, which is an unstable fixed state of the system.

- Even n - In this case, the eigenvalues are given by

$$\lambda = -\frac{\gamma}{2} \pm \sqrt{\left(\frac{\gamma}{2}\right)^2 - 1} \tag{2.25}$$

  It is clear that $\gamma = 2$ is a critical value that determines the sign of λ.

  (i) If $\gamma \geq 2$, then all the eigenvalues are negative and real, meaning that we have stable nodes

(ii) If $\gamma < 2$, then all the eigenvalues are complex, with a negative real part. This results in stable spirals

Let us look at the phase portraits of this system for the various values of γ. For $\gamma = 0$, the system is reduced to that of the normal harmonic oscillator, consisting of just stable orbits. If a pendulum starts off on one of these trajectories, it will remain on that trajectory. For small, but finite γ, the system is under-damped; the stable spirals eventually bring the pendulum to rest at the bottom of the pendulum arc. For $\gamma = 2$, the system becomes critically damped, with all of the fixed points becoming stable. Lastly, $\gamma > 2$, the fixed points become greater and greater attractors, giving rise to an overdamped system.

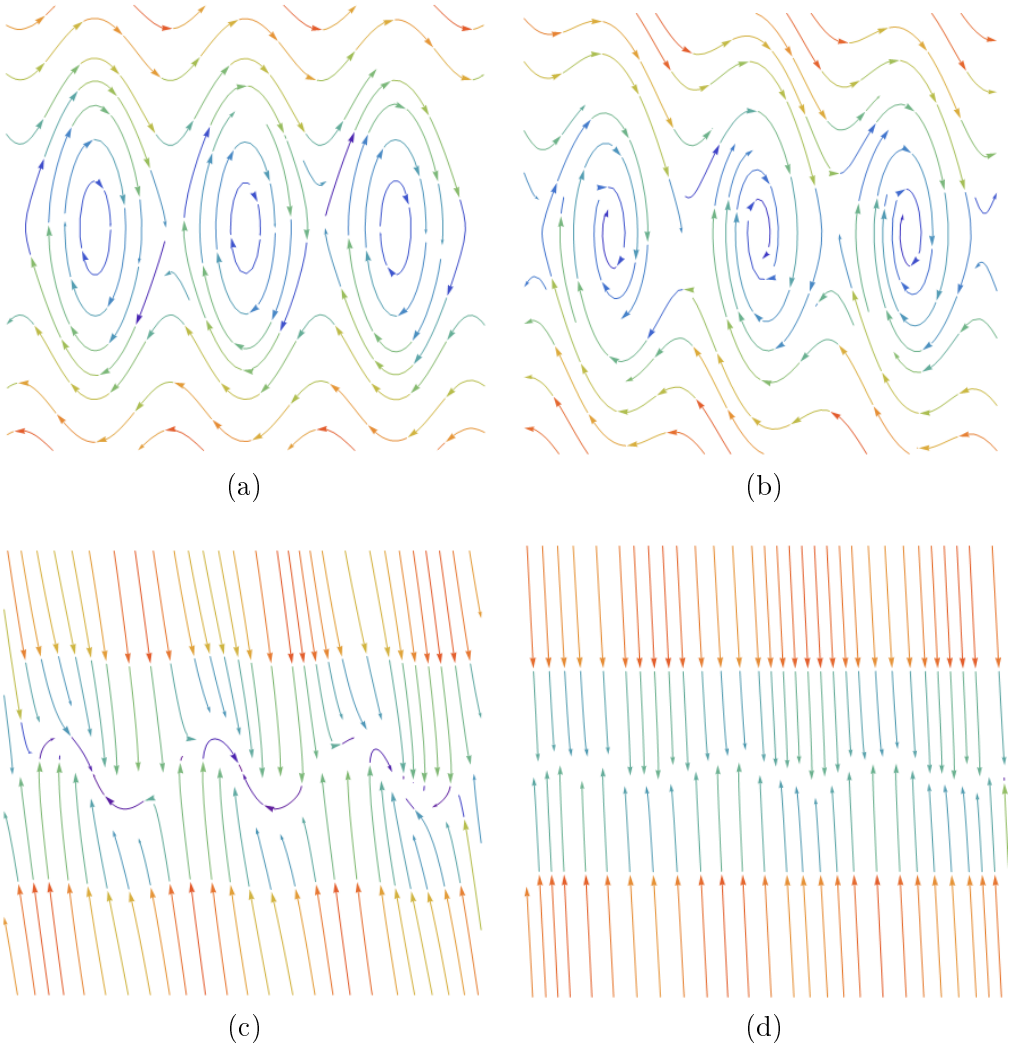

Figure 2.8: Phase space plots for the simple pendulum: (a) no damping ($\gamma = 0$) (b) small damping ($\gamma = 0.2$) (c) critical damping ($\gamma = 2$) (d) over damped ($\gamma = 6$). The x-axis corresponds to potential energy, and the y-axis to kinetic energy

2.3.2 Odell's Predator-Prey Model

In this example, we look at a particular model of predator-prey populations that is known as *Odell's predator-prey model*. Suppose that x is a non-dimensionalised variable that represents the prey population (of, say, rabbits), while y is a similar variable that represents the predator population (foxes). Then, according to this model, the differential equations

for the two populations are given by

$$\dot{x} = x\left(x(1-x) - y\right) \tag{2.26}$$
$$\dot{y} = y(x - r) \tag{2.27}$$

Before we perform our usual analysis, let us take a minute to motivate each of the terms in this equation. In (2.26), the x multiplying the bracketed term describes how the number of rabbits is proportional to their population size. Inside the brackets, the first term describes a combination of the fact that rabbits are polygamous, and that there is a natural constraint on their population (such as due to finite food resources). The second term is the offset due to predatory action, which manifests itself as a damping rate on the growth. Similarly, (2.27) shows proportionality between the two populations, as well as a natural cutoff due to the control parameter r.

In systems such as these, a useful first step is often to find the *nullclines*; these are the curves $\dot{x} = 0$ and $\dot{y} = 0$. The reason that this is useful is because the phase space trajectories must intersect these curves at right angles, which can serve to give an initial idea about their shape. In this case:

$$\dot{y} = 0 \quad \text{at} \quad y = 0,\ y = r \tag{2.28}$$
$$\dot{x} = 0 \quad \text{at} \quad x = 0,\ y = x - x^2 \tag{2.29}$$

We can then think of fixed points as being the intersection of the nullclines of each variable. These turn out to be

$$(0,0), \quad (1,0), \quad (r, r - r^2) \tag{2.30}$$

with the last only being possible for $0 < r < 1$ (as we cannot have negative numbers of either rabbits or foxes). These represent the cases of "no-one", maximum rabbits, and then somewhere in between. The Jacobian for this system is given by

$$\mathcal{J} = \begin{pmatrix} 2x - 3x^2 - y & -x \\ y & x - r \end{pmatrix} \tag{2.31}$$

with eigenvalues satisfying

$$\lambda^2 + (2x^2 - 3x + y + r)\lambda - 3x^3 + (3r + 2)x^2 + r(y - 2x) = 0 \tag{2.32}$$

One can either solve this as a quadratic, which is quite time-consuming, or put in the values of the fixed points before doing so. We shall do the latter.

- $(0,0)$ - $\lambda = 0, -r$. We thus have a linearly neutral, and stable fixed point
- $(1,0)$ - $\lambda = -1, 1 - r$. We have a saddle point for $0 < r < 1$, and a stable node for $r > 1$
- $(r, r - r^2)$ - This case is a little more complicated. The eigenvalues are given by

$$\lambda = r\left(\frac{1}{2} - r\right) \pm r\sqrt{r^2 - \frac{3}{4}} \tag{2.33}$$

  Clearly, $r = 1/2$ is a critical value that determines the stability of the fixed points, while $r = \sqrt{3}/2$ determines whether there is a any rotation in the trajectories.

  - $r < \sqrt{3}/2$ gives rise to a spiral with the following stability:
    (i) $r > 1/2$, stable

(ii) $r < 1/2$, unstable
(iii) $r = 1/2$, stable cycle

– $r > \sqrt{3}/2$ gives rise to fixed points with the following behaviour:
(i) $r > 1$, saddle (though this is un-physical and thus meaningless)
(ii) $\sqrt{3}/2 < r < 1$, stable node

Some phase space plots for different values of r are included in figure 2.9. We see that for a large value of the parameter r, no stable population of foxes can exist; they are too constrained by some external factor, and an initial population of rabbits will remain the same. For $r \gtrsim 1$, the foxes are too constrained to reach a stable population, but in this case they manage to reduce the rabbit population a little before dying out, at which point the rabbit population shoots up towards a maximum value of $x = 1$.

For $\sqrt{3}/2 < r < 1$, there is a fixed point that has a non-zero population of both foxes and rabbits, on which most trajectories converge; we still have the case of unchecked growth of rabbits in the cases where foxes cannot sustain a stable population. This stable node moves to decrease the number of rabbits and increase the number of foxes and forms a stable spiral as $r \to 1/2$.

As r continues to decrease, the system undergoes a supercritical Hopf bifurcation, forming a stable limit cycle with convergence from both sides. One can find the relevant trapping region by looking for a finite region for which $\dot{y} < 0$ for $x < r$; this simply involves finding a trajectory that passes through $x = a$ perpendicularly. With what frequency do the populations orbit the limit cycle? To answer this, we consider the behaviour of the system close to the bifurcation at $r = 1/2$. Linearising to first order yields:

$$x = a \backsim \frac{1}{2} \quad \longrightarrow \quad \delta\dot{x} = -\frac{1}{2}\delta y \tag{2.34}$$

$$y = a - a^2 \backsim \frac{1}{4} \quad \longrightarrow \quad \delta\dot{y} = \frac{1}{4}\delta x \tag{2.35}$$

It follows that

$$\delta\dot{x} = -\frac{1}{8}\delta x \tag{2.36}$$

meaning that the populations orbit the limit cycle at a frequency $\omega = (2\sqrt{2})^{-1}$.

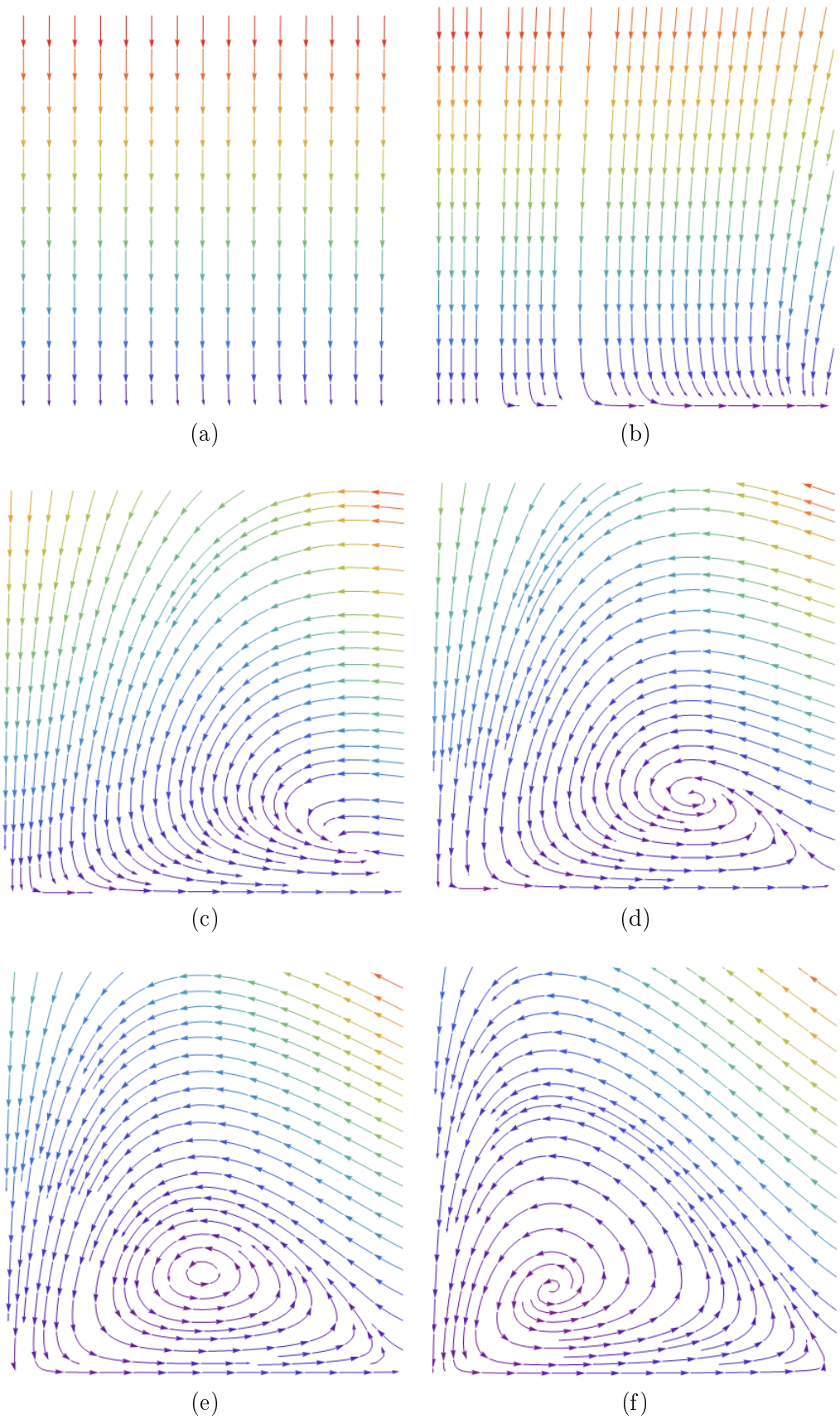

Figure 2.9: Phase space plots for Odell's predator-prey model: (a) $r = 100$ (b) $r = 6$ (c) $r = 0.88$ (d) $r = 0.65$ (e) $r = 0.5$ (f) $r = 0.3$. x has been plotted on the horizontal axis in the range $[0, 1]$, while y has been plotted on the vertical axis in the range $[0, 1]$

2.4 Phase Space and Chaos

We are now going to look more closely at the geometry of phase space, and the chaotic effects that certain systems can have on this phase space. Thus far, we have used the term *phase space* quite loosely to refer to the x-y plane in which we have been sketching our trajectories, and associated bifurcation diagrams. We shall now define the phase space of a dynamical system as follows:

> *A space in which all possible states of a dynamical system are represented, which each possible state corresponding to a unique point in phase space*

Then, the time evolution of the system traces a path through this space, known as a *phase space trajectory* (we have already been using this term, but it is worth clarifying it here). The phase space trajectory represents the set of states compatible with starting from one particular initial condition, located in the full phase space that represents the set of states compatible with starting from any initial condition. The dimensionality of the phase space equal to the number of independent parameters that are required to fully specify the instantaneous state of the system at any given time.

2.4.1 Volumes in Phase Space

We have been examining the stability of certain fixed points associated with trajectories in phase space. A similar question to ask about phase space is how volumes within it change with time, as changes in volume inform us about the local stability of the phase space. Recall the density continuity equation

$$\frac{\partial \rho}{\partial t} + \nabla \cdot (\rho \mathbf{u}) = 0 \tag{2.37}$$

that was derived by considering the density in some volume V of space, bounded by a closed surface S. As we made no assumptions about exactly what space we were working in, this equation remains valid in *any* phase space. Now, we make the assumption that the density ρ is proportional to inverse volume, such that $\rho \propto 1/V$. Then:

$$-\frac{1}{V^2}\frac{\partial V}{\partial t} + \frac{1}{V}\nabla \cdot \mathbf{u} - \frac{1}{V^2}(\mathbf{u} \cdot \nabla)V = 0 \tag{2.38}$$

where we have used by the chain rule, and the vector identity for dot products. It follows that

$$\boxed{\frac{dV}{dt} = V(\nabla \cdot \mathbf{u})} \tag{2.39}$$

We can thus see when the divergence of $\mathbf{u}$ is positive, the volume expands, while if it is negative, it contracts. Furthermore, in a way analogous to incompressible fluid flows, volumes in phase space are preserved if the divergence of the velocity is zero.

Hamiltonian Systems

In fact, volumes in phase space are preserved for any *Hamiltonian* system. Such a system is characterised by a Hamiltonian $\mathcal{H}(\mathbf{q}, \mathbf{p}, t)$ that satisfies the relations

$$\dot{\mathbf{p}} = -\frac{\partial \mathcal{H}}{\partial \mathbf{q}}, \quad \dot{\mathbf{q}} = \frac{\partial \mathcal{H}}{\partial \mathbf{p}} \tag{2.40}$$

where $\mathbf{p}$ and $\mathbf{q}$ are generalised coordinates of the same dimension, such that the system is completely described by the vector $\mathbf{r} = (\mathbf{p}, \mathbf{q})$ in phase space.

Then, by the definition of the total derivative

$$d\mathcal{H} = \frac{\partial \mathcal{H}}{\partial \mathbf{p}} \cdot d\mathbf{p} + \frac{\partial \mathcal{H}}{\partial \mathbf{q}} \cdot d\mathbf{q} \quad \longrightarrow \quad \frac{d\mathcal{H}}{dt} = \frac{\partial \mathcal{H}}{\partial \mathbf{p}} \cdot \frac{d\mathbf{p}}{dt} + \frac{\partial \mathcal{H}}{\partial \mathbf{q}} \cdot \frac{d\mathbf{q}}{dt} = 0 \tag{2.41}$$

Thus, a Hamiltonian system conserves the Hamiltonian by definition. If we also define $\mathbf{u} = \dot{\mathbf{r}} = (\dot{\mathbf{p}}, \dot{\mathbf{q}})$, then it follows that

$$\frac{dV}{dt} = V \nabla \cdot \mathbf{u} = V \left(\frac{\partial \dot{\mathbf{p}}}{\partial \mathbf{p}} + \frac{\partial \dot{\mathbf{q}}}{\partial \mathbf{q}} \right) = 0 \tag{2.42}$$

as derivatives commute. This allows us to conclude that a Hamiltonian also conserves volumes in phase space, though they may change in shape.

2.4.2 Fractals

A *fractal* is a mathematical set that exhibits a repeating pattern displayed at every length scale. If the replication is the same at every scale, then the pattern is said to be self-similar. Examples include the Von Koch curve (formed by replacing the middle third of all line segments with the other two sides of an equilateral triangle), and the Sierpinski carpet (formed by removing the central square from each larger square). The latter of these is of finite size, but has zero area.

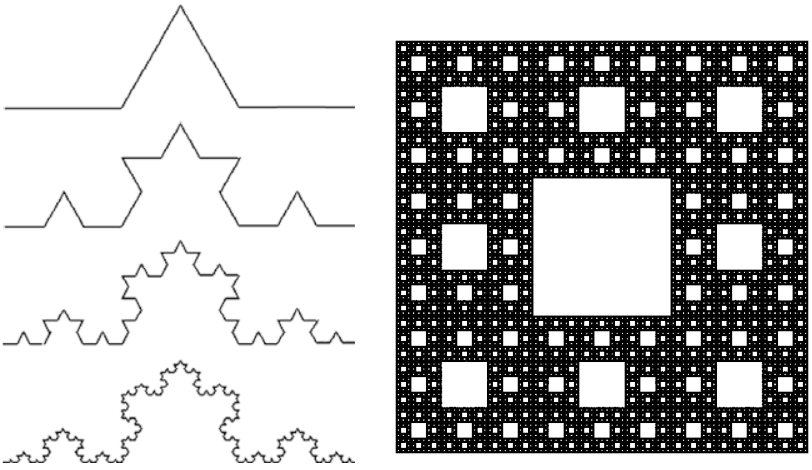

(a) (b)

Figure 2.10: Examples of fractals: (a) Von Koch curve (b) Sierpinski carpet

Fractals are different from other geometric figures due to the way in which they scale. For example, if the radius of a sphere is doubled, the volume scales by eight, or 2^3, as it resides in a three-dimensional space. However, if a fractal's one-dimensional lengths are all doubled, the spatial content of the fractal scales as a power that is not necessarily an integer. This means that we have to come up with another definition of dimension.

Similarity Dimension

This definition of dimension is used for fractals that are generated with regular algorithms, such as those displayed above. Suppose that m copies are created with a change in scale r. Then, the similarity dimension d is defined by

$$\boxed{m = r^d, \quad d = \frac{\log m}{\log r}} \tag{2.43}$$

For example, if we scale the lengths of a square by a factor of 2, it gives rise to 4 small squares; as expected, this gives $d = 2$ as a square is a manifestly two-dimensional object. For the two fractals shown above:

- Von Koch Curve - $m = 4$, $r = 3$, $d \approx 1.26$
- Sierpinski Carpet - $m = 3$, $r = 2$, $d \approx 1.585$

These clearly have non-integer dimensions of less than two, despite being apparently two-dimensional objects.

Correlation Dimension

On the other hand, physical fractals can be self similar, but only over a restricted range of lengthscales. Some examples include mountain ranges, lightning, and river deltas. In order to describe them, we need the correlation dimension. Consider a general surface of lengthscale ϵ, centred at some point $\mathbf{r}$ in phase space. In this context, a fractal is simply a set of points in phase space. Let $n(\mathbf{r}, \epsilon)$ be the number of points enclosed by the surface. Then, the correlation dimension $d(\mathbf{r})$ is defined as

$$n(\mathbf{r}, \epsilon) \propto \epsilon^{d(\mathbf{r})} \tag{2.44}$$

In general, n will have a very strong dependence on $\mathbf{r}$, and so in order to get anything sensible, we take a spatial average:

$$C(\epsilon) = \langle n(\mathbf{r}, \epsilon) \rangle_{\mathbf{r}} \propto \epsilon^{d} \tag{2.45}$$

where d can be a non-integer as before. If this relationship holds (approximately), then the set of points defines a fractal. This is usually found numerically by plotting $\log C = d \log \epsilon$. If this is a straight line for a sufficiently large range of ϵ, then we can define d.

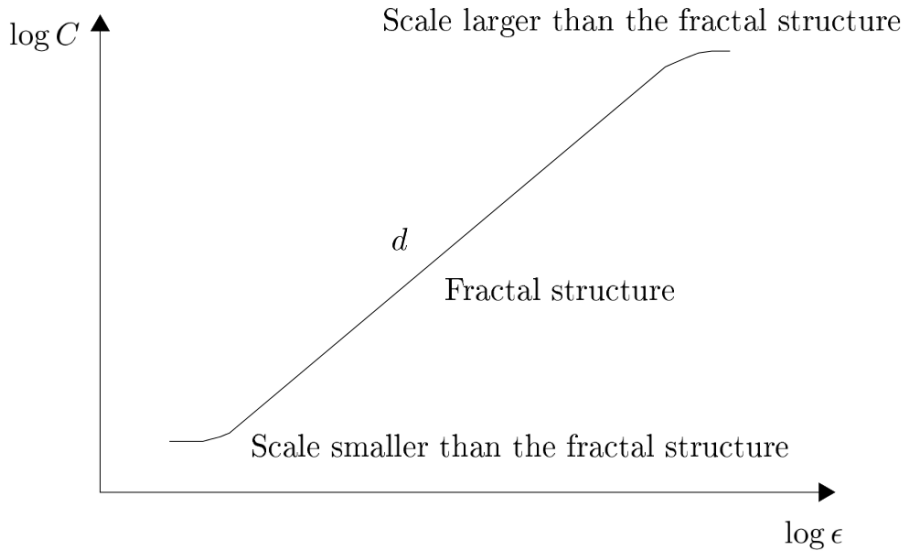

Figure 2.11: An example graph for finding the correlation dimension

2.4.3 The Lorenz Attractor

The Lorenz system is defined by the equations

$$\boxed{\begin{aligned}\dot{x} &= \sigma(y-x) \\ \dot{y} &= rx - y - xz \\ \dot{z} &= xy - bz\end{aligned}} \tag{2.46}$$

$$\dot{y} = rx - y - xz \tag{2.47}$$

$$\dot{z} = xy - bz \tag{2.48}$$

for positive real parameters r, σ and b. When this is used to model the atmosphere, σ is related to the *Prandtl number*, and r is related to the Rayleigh number. For certain values of these parameters, this system is actually a good model for Rayleigh-Bernard convection 1.5.1. Let us apply our usual dynamical systems analysis to this system to get a better idea about its behaviour.

Fixed Points and Stability

First, let us find and classify the fixed points in terms of their stability. Setting $\dot{\mathbf{r}} = 0$, we obtain the simultaneous equations

$$x - y = 0 \tag{2.49}$$

$$x(r - 1 - z) = 0 \tag{2.50}$$

$$x^2 - bz = 0 \tag{2.51}$$

which can be solved to yield the fixed points

$$\mathbf{r}_1 = (0,0,0), \quad \mathbf{r}_{2/3} = (\pm\sqrt{b(r-1)}, \pm\sqrt{b(r-1)}, r-1) \tag{2.52}$$

The associated Jacobian is given by

$$\mathcal{J} = \begin{pmatrix} -\sigma & \sigma & 0 \\ r-z & -1 & -x \\ y & x & -b \end{pmatrix} \tag{2.53}$$

For the fixed point at $(0,0,0)$, the eigenvalues are given by

$$\lambda = -b, \quad \lambda = -\frac{1}{2}(1+\sigma) \pm \frac{1}{2}\sqrt{1-(2-4r)\sigma+\sigma^2} \tag{2.54}$$

The first of these represents a globally stable fixed point; trajectories converge to zero along z at a rate b. In the case of the second set of eigenvalues, the point is stable for $r < 1$, but becomes a saddle point for $r > 1$. A bifurcation clearly occurs at $r_c = 1$. The symmetry of the system about z is suggesting that this might be a supercritical pitchfork bifurcation, but we need to do more to show this.

The other two fixed points have eigenvalues λ that satisfy the polynomial

$$\lambda^3 + \lambda^2(\sigma + b + 1) + \lambda b(\sigma + r) + 2\sigma b(r-1) = 0 \tag{2.55}$$

Let us look for solutions in the region of the bifurcation by letting $r \backsim 1+\epsilon$ (where $\epsilon \ll 1$), and $\lambda = \lambda_0 + \delta\lambda$. Then:

$$\lambda_0\left[\lambda_0^2 + \lambda_0(\sigma + b + 1) + b(\sigma + 1)\right] = 0 \tag{2.56}$$

The solution $\lambda_0 = 0$ implies that we need to look at higher order terms, and so keeping linear terms in ϵ and $\delta\lambda$:

$$\delta\lambda b(\sigma+1) + 2\sigma b(r-1) = 0 \quad \longrightarrow \quad \lambda = \delta\lambda = -\frac{2\sigma(r-1)}{\sigma+1} \tag{2.57}$$

which is clearly stable in the region of $r_c = 1$. It is easy to show that the other two solutions satisfy

$$\lambda = \lambda_0 = -b,\ -(\sigma + 1) \tag{2.58}$$

which are likewise stable. This means that we do indeed have a supercritical pitchfork bifurcation at $r_c = 1$

More Stability Changes

Now, we know that purely imaginary solutions correspond to a change in stability. This means that if we are going to have further stability changes, $\mathrm{Re}(\lambda)$ must become zero at some point. To find where this occurs, we let $\lambda = i\omega$.

$$i\omega^3 + \omega^2(\sigma + b + 1) - i\omega b(\sigma + r) - 2\sigma b(r - 1) = 0 \tag{2.59}$$

The real and imaginary parts of this expression must both be zero simultaneously. Setting the imaginary part to zero yields

$$\omega = 0,\ \pm\sqrt{b(\sigma + r)} \tag{2.60}$$

The solution $\omega = 0$ is in fact not a valid solution, meaning that the third point must be real, and thus stable. Setting the real part of (2.59) to zero allows us to find a second critical value for r of

$$\boxed{r_H = \frac{\sigma(\sigma + b + 3)}{\sigma - b - 1}} \tag{2.61}$$

This means that as r increases past r_H, the system will develop unstable spirals as $\mathrm{Re}(\lambda) > 0$ and $\mathrm{Im}(\lambda)$ for $r > r_H$. In order for this stability change to have occurred, there must have already been an unstable limit cycle that developed in the region $1 < r < r_H$, and so the bifurcation at $r = r_H$ is a subcritical Hopf bifurcation.

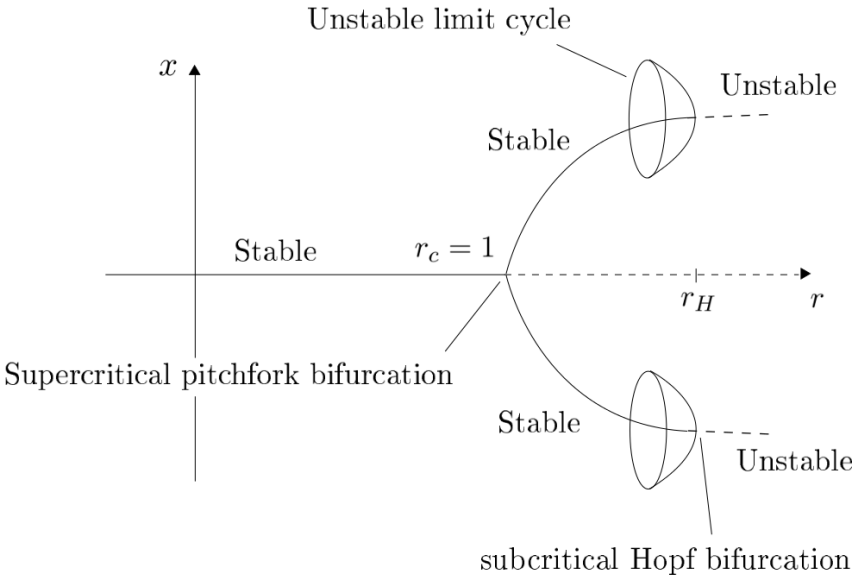

Figure 2.12: A bifurcation diagram for the Lorenz system in the x-r phase space plane

A Strange Attractor

It is clear that the system becomes globally unstable for $r > r_H$, which corresponds to the formation of turbulence in the case of Rayleigh-Bernard convection. So then how do trajectories not get kicked off to infinity? This is because there is a trapping region to which trajectories converge. Consider a volume element of phase space δV. Then by (2.39):

$$\frac{\delta \dot{V}}{\delta V} = \frac{\partial \dot{x}}{\partial x} + \frac{\partial \dot{y}}{\partial y} + \frac{\partial \dot{z}}{\partial z} = -(\sigma + 1 + b) \tag{2.62}$$

Thus, volumes in phase space collapse to zero at a rate $(\sigma + 1 + b)$ (which is in fact the sum of the eigenvalues).

Let us define a surface f in phase space such that

$$f(x, y, z) = rx^2 + \sigma y^2 + \sigma(z - 2r)^2 \tag{2.63}$$

This will define a trapping region provided that $\dot{f} < 0$. Taking the time derivative of the above, and substituting in (2.46), (2.47) and (2.48), we find that the condition that must be satisfied is

$$rx^2 + y^2 + b(z - r)^2 > br^2 \tag{2.64}$$

which confines motion to a particular region of phase space. When trajectories are plotted under a simulation, they follow a 'butterfly' like pattern, as shown in figure 2.13. The oscillations will switch unpredictably between each branch, and move on a particular surface without visiting every point on it. This means that the Lorenz attractor is actually a fractal structure; it has a correlation dimension $d = 2.055 \pm 0.004$.

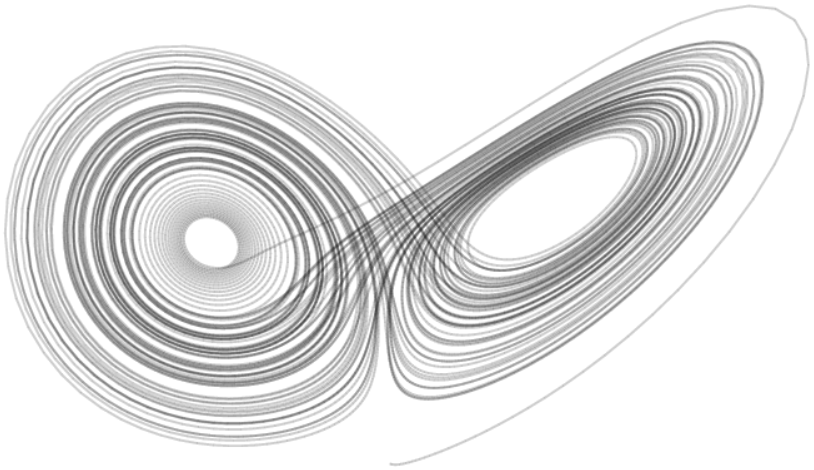

Figure 2.13: A example trajectory for the Lorenz attractor

Separation in Phase Space

Let us consider two points in phase space separated by $\delta\mathbf{r}$. How does this separation change with time? We first note that

$$\delta\dot{\mathbf{r}} = \mathcal{J}\delta\mathbf{r} \tag{2.65}$$

from (2.3). Then:

$$\frac{d}{dt}(|\delta\mathbf{r}|^2) = \frac{d}{dt}(\delta\mathbf{r}^T\delta\mathbf{r}) = \delta\mathbf{r}^T \cdot \frac{d(\delta\mathbf{r})}{dt} + \frac{d(\delta\mathbf{r})^T}{dt} \cdot \delta\mathbf{r} = \delta\mathbf{r}^T(\mathcal{J} + \mathcal{J}^T)\delta\mathbf{r} \tag{2.66}$$

Clearly, $\Lambda \equiv (\mathcal{J} + \mathcal{J}^T)/2$ is a symmetric matrix, meaning that it has real eigenvectors λ_i and orthogonal eigenvectors $\mathbf{u}_i$. Moving to this basis, we can write that

$$\boxed{\frac{d}{dt}(|\delta\mathbf{r}|^2) = 2\sum_i \lambda_i |\delta\mathbf{r}|^2} \tag{2.67}$$

The eigenvalues λ_i are known as *Lyapunov exponents*, which characterise the rate of separation of infinitesimally close trajectories. We can find these exponents at any point in space, and thus by evaluating the trace of Λ, it is possible to determine whether there is local divergence ($\mathrm{Tr}\Lambda > 0$) or convergence ($\mathrm{Tr}\Lambda < 0$). Let us consider the case of the Lorenz equations with $r = 28$, $\sigma = 10$ and $b = 8/3$. Suppose that we are located at the point $(0, 0, r - 2\sigma)$. Using (2.53), we find that

$$\Lambda = \begin{pmatrix} -\sigma & \frac{3}{2}\sigma & 0 \\ \frac{3}{2}\sigma & -1 & 0 \\ 0 & 0 & -b \end{pmatrix} \tag{2.68}$$

Using the parameter values given above, it is easy to show that this has eigenvalues and corresponding eigenvectors given by

$$\lambda_1 = -\frac{8}{3}, \qquad \mathbf{u}_1 = (0, 0, 1) \tag{2.69}$$

$$\lambda_2 = \frac{-11 + 3\sqrt{109}}{2}, \quad \mathbf{u}_2 = \left(\frac{-3 + \sqrt{109}}{10}, 1, 0\right) \tag{2.70}$$

$$\lambda_3 = \frac{-11 - 3\sqrt{109}}{2}, \quad \mathbf{u}_3 = \left(\frac{-3 - \sqrt{109}}{10}, 1, 0\right) \tag{2.71}$$

Thus, according to (2.67), we have slow decay perpendicular to the x-y plane (along z), and fast growth and decay parallel to the x-y plane at this point.

2.4.4 Chaos

The behaviour of the Lorenz attractor is an example of *deterministic chaos*. Chaotic systems are characterised by:

- Aperiodic long term behaviour - Trajectories in phase space do not settle into fixed points or periodic orbits, though they still may be confined to a fixed region of space (in the case of the strange attractor)
- Sensitive dependence on initial conditions - Chaotic systems will have at least one positive Lyapunov exponent, which will cause a slight error in initial conditions to grow almost without bound
- Deterministic - There is no randomness or stochasticity associated with chaotic systems; the irregular behaviour is a consequence of non-linear terms in the defining equations of motion

These ideas were summarised quite aptly by Edward Lorenz as

> *Chaos: When the present determines the future, but the approximate present does not approximately determine the future*

The attractor that bears his name is a particularly interesting chaotic system, as trajectories on the associated stranger attractor remain confined to the phase space trapping region, yet they will separate from one-another exponentially quickly. This behaviour can be thought of in terms of the continual stretching and folding of phase space that leads to fractal-like behaviour, allowing these separating trajectories to be confined to an apparently finite region.

A chaotic map

To demonstrate this behaviour of chaotic systems, we are going to examine the logistical map

$$x_{n+1} = 10x_n \pmod 1 \tag{2.72}$$

This map essentially shifts the training decimals of a non-integer to the 'left' by one. The integers involved cannot go out of the range $x \in [0, 1]$ due to the mod 1. The fixed points of a discrete map such as this one are those that map onto themselves; that is, the points for which $x_{n+1} = x_n$. Let us suppose that

$$x_n = a_0.a_1a_2a_3\ldots \tag{2.73}$$

where $a_0, a_1, a_2, a_3\ldots$ are integers in the range $x \in [0, 9]$. Then by the action of the map:

$$x_{n+1} = 0.a_2a_3\ldots \tag{2.74}$$

Then, the map is a fixed point if

$$0.a_2a_3\cdots = a_0.a_1a_2a_3\ldots \tag{2.75}$$

meaning that $a_0 = 0$ and $a_2 = a_3 = a_4 = \ldots$. The only numbers in the allowed range that satisfy this are

$$x = 0, \frac{1}{9}, \frac{2}{9}, \ldots, \frac{8}{9} \tag{2.76}$$

meaning that there are ten fixed points in total for the map.

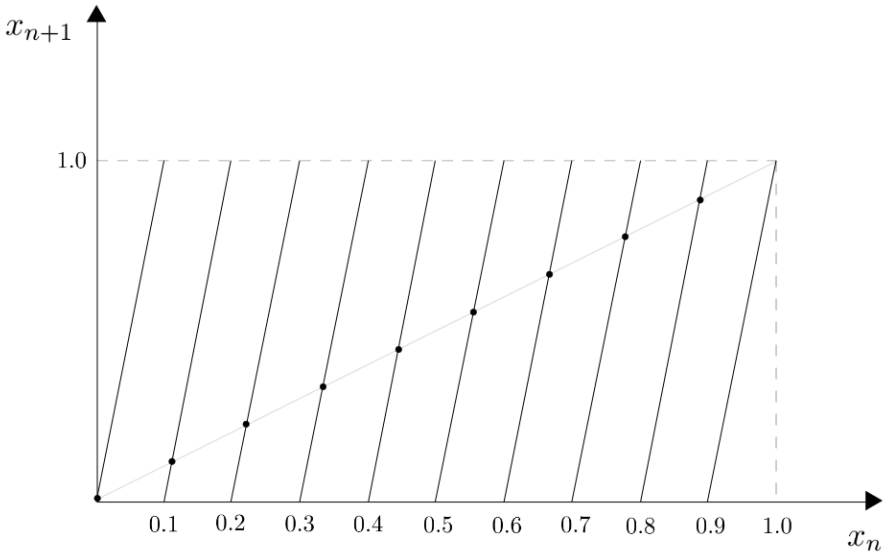

Figure 2.14: A example trajectory for the Lorenz attractor

Let us now look at the orbits of this map. Let x_p be a rational number consisting of all zeros, except that it contains some integer $1 < a_p < 9$ on the first position after the period, on the $(p+1)^{th}$ position after the period, on the $(2p+1)^{th}$ position and so on. It is clear that x_p is mapped onto itself after p iterations of the cycle, meaning that x_p gives a p-period orbit. As we can arbitrarily change p, we can create orbits of all periods. However, as $x_{n+1}/x_n = 10$, these orbits are all unstable, except for $x_n = 0$.

Similarly, an irrational number has an aperiodic decimal representation by definition, and so if x_n is irrational, the orbit will be aperiodic. Since both the reals and the rationals are

uncountable , the irrationals are also uncountable, meaning that we have infinitely many aperiodic orbits.

The sensitivity to initial conditions of this map is made clear when considering two points that are - initially - very close to one another. For example, consider the pair of initial conditions

$$x_0^{(1)} = 0.11111111110000\ldots \tag{2.77}$$
$$x_0^{(2)} = 0.11111111111111\ldots \tag{2.78}$$

which are clearly very close together as $x_0^{(1)} \approx x_0^{(2)}$. Consider their evolution under this map:

- $x_0^{(1)}$: $0.11111111110000 \to 0.11111111100000 \to 0.11111111000000 \to 0.11111110000000 \to 0.11111100000000 \to 0.111110000000000 \to 0.111100000000000 \to 0.111000000000000 \to 0.110000000000000 \to 0.100000000000000 \to 0.0000000000000$
- $x_0^{(2)}$: $0.11111111111111 \to 0.11111111111111 \to 0.11111111111111 \to \ldots$ as it is a fixed point

Thus, even though these points were initially separated by an amount of order $\mathcal{O}(11)$, they became separated by an $\mathcal{O}(1)$ difference after only 10 iterations of the logistical map. There is thus the exponential divergence that we associate with a sensitivity to initial conditions.

3. *Biophysics*

This chapter aims to cover some tenuously related concepts in Biophysics, including:

- Diffusion
- Polymer Chains
- Stochasticity and Fluctuations
- Molecular Motors
- Measurement Techniques

This section of the course seems very tacked-on, having little to do with the material covered in the previous two chapters. In any case, this author has tried to distil the relevant information from various sources in attempt to put it all in one place. An effort has also been made to separate the biology from the physics where possible, and only include the bare minimum when it comes to facts that have to be mindlessly memorised.

3.1 Diffusion

Many biological systems involve diffusion in some way, as this is the primary method of passive transport within gases and fluids. Students that studied biology during their secondary education would have already come across this; osmosis is simply diffusion across a semi-permeable membrane. We shall begin our discussion of diffusion by introducing the underlying physics associated with it, before applying this to biological processes and structures.

3.1.1 The Diffusion Equation

Suppose that at time t, the mean number density of some substance we are interested in within the fluid at the location $\mathbf{r}$ is given by $n(\mathbf{r}, t)$. We will it be at the same location after a small interval δt? During that time, so particles will move from $\mathbf{r}$ to other locations, and other particles will arrive to $\mathbf{r}$ from elsewhere. Therefore,

$$n(\mathbf{r}, t + \delta t) = \langle n(\mathbf{r} - \delta\mathbf{r}, t) \rangle \tag{3.1}$$

where $\mathbf{r} - \delta\mathbf{r}$ are positions where the particles that arrive at $\mathbf{r}$ at $t + \delta t$ were at at time t, and the average is an ensemble average over all these individual particle displacements. Let us take δt to be small enough so the corresponding particle displacements are much smaller than the scale of spatial variation of $n(\mathbf{r})$, namely that

$$|\delta\mathbf{r}| \ll \left(\frac{1}{n} |\nabla n| \right)^{-1} \tag{3.2}$$

We then Taylor expand (3.1) in small $\delta\mathbf{r}$:

$$n(\mathbf{r}, t) = \left\langle n(\mathbf{r}, t) - \delta\mathbf{r} \cdot \nabla n + \frac{\delta\mathbf{r}^2}{2} \nabla^2 n + \dots \right\rangle \approx n(\mathbf{r}, t) + \frac{\langle \delta\mathbf{r}^2 \rangle}{2} \nabla^2 n \tag{3.3}$$

where we have assumed that $\langle \delta\mathbf{r} \rangle = 0$ (no mean motion in any direction). Re-arranging this equation, we get

$$\frac{n(\mathbf{r}, t + \delta t) - n(\mathbf{r}, t)}{\delta t} = \frac{\langle \delta\mathbf{r}^2 \rangle}{2\delta t} \nabla^2 n \tag{3.4}$$

In the limit of $\delta t \to 0$, we find that n satisfies a diffusion equation, given by

$$\boxed{\frac{\partial n}{\partial t} = D \nabla^2 n, \quad D = \lim_{\delta t \to 0} \frac{\langle \delta\mathbf{r}^2 \rangle}{2\delta t}} \tag{3.5}$$

assuming that the limit exists such that D is finite. It is important to understand that $\delta t \to 0$ here means that δt is small compared to the time scales on which the diffusive evolution of n occurs, but it can still be long compared to the collisional timescales.

Random Walks

A random walk is a mathematical object that describs a path that consists of a succession of random steps on some mathematical space. In this context, 'random' refers to the fact that each step is un-correlated with the last; the step is not made with any information about the prior steps made. For a particle moving along a one-dimensional chain of discrete points, this means that it has an equal probability of moving forwards or backwards each time a point is reached. One can think of the diffusion equation as being the evolution equation for a particle undergoing a *random walk*; that is, it moves on a path that consists

of a succession of steps in real space that are uncorrelated with one another. This can be seen explicitly by taking the spatial Fourier transform of (3.5):

$$\frac{\partial \widetilde{n}}{\partial t} = -Dk^2\widetilde{n} \quad \longrightarrow \quad \widetilde{n}(\mathbf{k},t) = \widetilde{n}(\mathbf{k},0)e^{-k^2Dt} \tag{3.6}$$

where $\widetilde{n}$ is defined as the Fourier transform of n. Then, the final solution is given by

$$\begin{aligned} n(\mathbf{r},t) &= \frac{1}{(2\pi)^3}\int d^3\mathbf{r}'\, e^{-i\mathbf{k}\cdot\mathbf{r}'} n(\mathbf{r}',0) \int d^3\mathbf{k}\, e^{i\mathbf{k}\cdot\mathbf{r}}\, e^{-k^2Dt} \\ &= \int d^3\mathbf{r}'\, n(\mathbf{r}',0) \frac{1}{(4\pi Dt)^{3/2}} \exp\left[-\frac{(\mathbf{r}-\mathbf{r}')^2}{4Dt}\right] \end{aligned} \tag{3.7}$$

for some initial condition $n(\mathbf{r},0)$. For a random walk, the only possible initial condition is a delta function $n(\mathbf{r},0) = N\delta(\mathbf{r})$. This is as a result of the fact that having any spatial dependence within the initial condition would imply correlation between possible points within the random walk, which cannot be the case by definition. We have also ensured proper normalisation, as

$$\int d^3\mathbf{r}\, n(\mathbf{r},0) = N \tag{3.8}$$

where N is the total number of particles of the substance that we are interested in within our fluid. Substituting this into (3.7), we obtain the distribution:

$$n(\mathbf{r},t) = \frac{N}{(4\pi Dt)^{3/2}} \exp\left[-\frac{(\mathbf{r}-\mathbf{r}')^2}{4Dt}\right] \tag{3.9}$$

More generally, the form of the Green's function contained in (3.7) means that the probability of a particle undergoing a random walk to be within the interval $[\mathbf{r}, \mathbf{r}+d\mathbf{r}]$ at some time t is given by

$$\boxed{f(\mathbf{r},t) = \frac{1}{(4\pi Dt)^{3/2}} \exp\left[-\frac{(\mathbf{r}-\mathbf{r}')^2}{4Dt}\right]} \tag{3.10}$$

3.1.2 Diffusion and Cells

How does the physics of diffusion influence the nature of biological phenomena? The first thing that we can point to is that diffusion actually limits the size of living structures. We can use the expression for D in (3.5) to write that

$$x^2 \backsim 6Dt \quad \leftrightarrow \quad t \backsim \frac{x^2}{6D} \tag{3.11}$$

where the factor of 3 has come from assuming that the system is isotropic. Let us take the diffusion coefficient inside a cell to have value $D \approx 10\,\mu\text{m}^2\text{s}^{-1}$. Then:

$$x \backsim 10\,\mu\text{m} \quad \longrightarrow \quad t \backsim 10\,\text{ms} \tag{3.12}$$

$$x \backsim 1\,\text{cm} \quad \longrightarrow \quad t \backsim 10^6\,\text{s} \tag{3.13}$$

The scaling of t with x^2 means that diffusion timescales become very large even for relatively small displacements. This sets the limit on the size of a cell that can operate via diffusion alone, and still respond to changing surroundings on normal timescales. Solutions to this include active cellular transport, as well as compartmentalisation (as this will decrease the average overall diffusion time). This gives rise to two different cell types

- Prokaryotic - These operate via passive/diffusive transport, meaning that they are generally quite small ($\backsim$ 1-10 μm). They lack a nucleus, and often do not involve many internal components

- Eukaryotic - These operate via active transport, meaning that they can be much larger than prokaryotic cells ($\backsim$ 10-100 μm). These have a nucleus, and often feature internal structures, such as ribosomes (more on these later).

In section 1.4.1, we talked about how Purcell's Scallop Theorem limits the types of swimming strokes that are available to a cell at low Reynolds number. Diffusion also indirectly influences the way that a cell moves. If a cell is to be able to determine whether 'life' is getting better or worse in a particular direction (whether there are more or less food sources, for example), the cell must swim further in time t than the distance over which molecules reach it by diffusion. From (3.11):

$$x \backsim \sqrt{Dt} \quad \longrightarrow \quad v \backsim \frac{dx}{dt} \backsim \sqrt{\frac{D}{t}} \tag{3.14}$$

This is the speed that a cell has to be able to move at in order to out-run diffusion, which again limits the types of propulsion that cells can adopt.

Chemotaxis

Let us suppose that our theoretical cells can move at this speed. The movement of a mobile cell or organism in a direction corresponding to a gradient of a concentration in a particular substance is known as *chemotaxis*. But how do cells detect these changes in gradient? We can get a handle on this using the diffusion equation (3.5).

Consider a spherical cell of radius a immersed in a fluid, in which there is some substance of equilibrium concentration n_0. In the steady state, (3.5) becomes

$$\frac{1}{r^2}\frac{\partial}{\partial r}\left(r^2\frac{\partial n}{\partial r}\right) = 0, \quad j = -D\frac{\partial n}{\partial r} \tag{3.15}$$

with the associated boundary conditions

$$n(r \to \infty) = n_0 \tag{3.16}$$

$$n(a) = 0 \tag{3.17}$$

The second of these follows from the fact that the concentration is fully absorbed at the surface of the cell. By inspection, the solution is clearly

$$n(r) = n_0\left(1 - \frac{a}{r}\right), \quad j = -n_0 D\frac{a}{r^2} \tag{3.18}$$

The total absorption I_a at the surface is thus given by

$$I_a = \int d\mathbf{S}\cdot\mathbf{j} = 4\pi a n_0 D \tag{3.19}$$

The cellular needs will scale with it's volume ($\backsim a^3$), while it is clear that the amount that they absorb scales with a, which places a limit on the size of an individual bacterium.

The above calculation assumed that a cell can absorb at every point on it's surface, while most cells can only absorb substances at receptor sites that are tailored to said substance. We can model receptors on the surface of cells as small disks of radius b, with $b \ll a$. By analogy to the above result, the total absorption for each disk is given by $I_b = 4bn_0D$. Let the number of disks on the surface of the cell be N_b. Then,

$$N_b{}^{\max} = \frac{4\pi a^2}{\pi b^2} = \frac{4a^2}{b^2} \tag{3.20}$$

Let I be the absorption of a cell with a given number of receptor sites N_b, as in the above model. We know that the absorption must satisfy the following limits:

$$N_b \ll {N_b}^{\max}, \quad I \to N_b I_b \tag{3.21}$$

$$N_b \backsim {N_b}^{\max}, \quad I \to I_a \tag{3.22}$$

We can thus interpolate the concentration formula

$$\boxed{\frac{I}{I_a} = \frac{1}{1 + \frac{I_a}{N_b I_b}}} \tag{3.23}$$

Suppose that we require the absorption for a particular substance to be $I = \frac{1}{2} I_a$. Then, $N_b = I_a / I_b$, meaning that the ratio of the area covered by the disks to the total cell surface area is given by

$$\text{Area Ratio} = N_b \frac{\pi b^2}{4\pi a^2} = \frac{\pi}{4} \frac{b}{a} \backsim \frac{b}{a} \tag{3.24}$$

This means that for small receptor sites, only a very small amount of the total surface of the cell needs to be covered with receptor sites. This means that cells are able to have a large number of specialised, distinct receptor sites for different types of substances that can potentially be absorbed.

3.2 Polymer Chains

Polymer chains are particularly important within the biology of cells, as they play a central role in a diverse number of processes, from cell replication to ATP production. There are three particularly important polymers that we should know at least some detail about:

- Deoxyribonucleic acid (DNA) - A long chain polymer that carries the genetic instructions used in the functioning of all known organisms. It is made up of four nucleotides (AT:GC) that bind in pairs to form a double helix. In eukaryotic cells, the DNA of a cell is contained inside its nucleus
- Ribonucleic acid (RNA) - Another long chain polymer, consisting of a similar set of four nucleotides (AU:GC). Like DNA, it can encode information, but it can also act as a scaffold or a catalyst in chemical reactions
- Proteins - Molecules consisting of one or more long chains of amino acids (from a group of 20 possible). The sequence of amino acids that resides in a protein is defined by the sequence of base pairs contained within the DNA. As proteins can form very large macroscopic molecules, we can describe their structure at different levels:
  - Primary: The amino acid sequence itself
  - Secondary: The regularly repeating local structures stabilised by hydrogen bonds
  - Tertiary: The overall shape of the molecule, defined by the relationships between secondary structures
  - Quaternary: The structure formed by several protein molecules (a complex)

  Proteins play an incredibly crucial role in the functioning of cells, as they catalyse reactions, and regulate the rates at which many biological processes occur. Without proteins, cells would just be a cytoplasmic mass.

Within the cell, both DNA and RNA are responsible for the production of proteins. DNA in the nucleus is *transcribed* by RNA-polymerase to create messenger-RNA, using the sequence of amino acid pairs in the DNA as a template. A ribosome then *translates* the m-RNA, using the resultant information to create the proteins. Pictorially,

$$\text{DNA} \xleftrightarrow{\text{transcription}} \text{mRNA} \xrightarrow{\text{translation}} \text{Protein.} \tag{3.25}$$

The *central dogma* of molecular biology states that sequential information cannot be transferred back from a protein into either another protein or nucleic acid. That is, all information about the encoding of the protein structure is lost when it is formed. Essentially, this means that nucleic acids are required in order to produce proteins; a cell cannot replicate a protein give its structure. This information has been included in (3.25), in that we can have information exchange between DNA and mRNA, but not from proteins to mRNA.

If we take any of these polymers on a small enough scale, they look as if they are just single strands, with the complexity of the molecule being lost below the resolution that we are looking at. In other words, if you zoom out far enough, most things look like straight lines. Given this, we can adopt various models in order to explain the behaviour of polymers, which we will now investigate.

3.2.1 Freely-jointed Chain

Under this model, we consider the polymer to be made up of a chain of N segments of length b. Let $\mathbf{r}$ be the total end-to-end displacement of the chain, such that

$$\mathbf{r} = \sum_i^N \mathbf{r}_i \tag{3.26}$$

We assume that there is no preferred orientation for the segments, and that they are freely hinged where they touch. This allows us to write that

$$\langle \mathbf{r}_i \rangle = 0, \quad \langle \mathbf{r}_i \cdot \mathbf{r}_j \rangle = \delta_{ij} b^2 \tag{3.27}$$

It follows from these definitions that $\langle \mathbf{r} \rangle = 0$, and

$$\left\langle \mathbf{r}^2 \right\rangle = \sum_i^N \left\langle \mathbf{r}_i^2 \right\rangle + \sum_{i \neq j}^N \langle \mathbf{r}_i \cdot \mathbf{r}_j \rangle = Nb^2 \tag{3.28}$$

This means that the effective length of the polymer under the freely-jointed chain (FJC) model is given by $r_e = \sqrt{N} b$.

End-to-end Probability Distribution

As there is no correlation between the orientation of adjacent segments, we can think of the end of the chain as behaving as if has undergone some sort of random walk, making a step each time a new segment is added. By the central limit theorem, in the limit that $N \to \infty$, the quantity

$$X_i = \sqrt{N} \left(\frac{1}{N} \sum_i^N x_i - \langle x_i \rangle \right) \tag{3.29}$$

will have a normal (Gaussian) distribution with zero mean, and variance $\left\langle x_i^2 \right\rangle - \langle x_i \rangle^2 = r_e^2$:

$$f(X) = \frac{1}{\sqrt{2\pi r_e^2}} e^{-X^2/2r_e^2} \tag{3.30}$$

meaning that the probability of the end of the N segment chain being located in the interval $[\mathbf{r}, \mathbf{r} + d\mathbf{r}]$ is given by

$$\boxed{f(\mathbf{r}, N) = \left(\frac{3}{2\pi N b^2} \right)^{3/2} \exp\left[-\frac{3\mathbf{r}^2}{2Nb^2} \right]} \tag{3.31}$$

Comparing this expression with (3.10), it is clear that the number of segments N is directly analogous for the diffusion time t of a particle. In fact, we have the equivalence relationship that $b^2 = 6D$ between the two expressions.

We can use (3.31) to calculate the *cyclisation probability* (the probability that the ends will meet and fuse together) for an FJC. Assume that the ends of the chain are within a small displacement $\delta r \ll r_e$ of one another. Then, the associated probability is given by

$$p(0 < r < \delta r) = \int d^3\mathbf{r}\, f(\mathbf{r}, N) = \int_0^{\delta r} dr\, 4\pi r^2 \frac{1}{\left(\frac{2}{3}\pi r_e^2\right)^{3/2}} e^{-\frac{3\mathbf{r}^2}{2r_e^2}} \approx \frac{4\pi \delta r^3}{3\left(\frac{2}{3}\pi r_e^2\right)^{3/2}} \tag{3.32}$$

We have approximated the exponential factor to be roughly constant over the region of integration, as $\delta r \ll r_e$. The scaling of $p \backsim \delta r^3 / r_e^3$ means that the cyclisation probability will become much smaller for larger chains.

Elastic Properties

We can investigate the elastic properties of the chain using statistical mechanics. Suppose that we have some force f applied between the ends of the chain, orientated along $\mathbf{e}_z$. The energy associated with this force for each segment is given by

$$E_i = -\mathbf{f} \cdot \mathbf{r}_i = -fb\cos\theta \tag{3.33}$$

Note that this is not the actual energy contained within the chain; it is the energy that we have to expend to get the chain to sit at a particular extension, which is the quantity that we are concerned with statistically. The partition function is thus given by

$$Z = \int d^2 n_i \, e^{-\beta \sum_i E_i} = \prod_i \int d^2 n_i \, e^{-\beta E_i}, \quad \beta = (k_B T)^{-1} \tag{3.34}$$

If we recognise that the chain lengths are identical, we can use (3.33) to write that

$$Z = \left(\int d\Omega \, e^{-\beta E_i} \right)^N = \left(\int_0^{2\pi} d\phi \int_0^{\pi} d\theta \, \sin\theta e^{-\beta f b \cos\theta} \right)^N \tag{3.35}$$

such that

$$\boxed{Z = \left(4\pi \frac{\sinh\alpha}{\alpha} \right)^N, \quad \alpha = \frac{fb}{k_B T}} \tag{3.36}$$

As usual, the Gibbs free energy is given by $F = -k_B T \log Z$. Then, the resultant extension $\langle z \rangle$ is:

$$\langle z \rangle = \frac{\partial Z}{\partial(\beta f)} = -\frac{\partial F}{\partial f} = -\frac{b}{k_B T} \frac{\partial F}{\partial \alpha} \tag{3.37}$$

giving

$$\boxed{\langle z \rangle = Nb \left(\coth\alpha - \frac{1}{\alpha} \right)} \tag{3.38}$$

Evidently, this expression is non-linear. However, we can examine some asymptotic limits of this expression to further our understanding of the behaviour of the FJC.

- Low force limit ($\alpha \ll 1$) - Under this limit, we have that $\coth\alpha - 1/\alpha \approx \alpha/3$. Then:

$$\langle z \rangle \approx \frac{Nb}{3}\alpha \quad \longrightarrow \quad f \approx \frac{3k_B T}{Nb^2} \langle z \rangle \tag{3.39}$$

  This means that it appears to act as a linear, entropic spring, with effective spring constant $k_{\text{eff}} = 3k_B T/Nb^2$. This is because work has to be done to increase the entropy of the system upon the application of the force; there is a resistance against pulling it apart.

- High force limit ($\alpha \gg 1$) - Under this limit, $\coth\alpha \approx 1$, such that the non-linear extension is given by

$$\langle z \rangle \approx Nb \left(1 - \frac{1}{\alpha} \right) \quad \longrightarrow \quad f \approx \frac{k_B T}{b} \frac{1}{1 - \frac{\langle z \rangle}{Nb}} \tag{3.40}$$

  The asymptotic length of the system is clearly $\langle z \rangle \approx Nb \equiv \ell$, behaving like a straight rod. The force diverges as the extension approaches this value due to entropic considerations. Being at extension $\langle z \rangle = \ell$ corresponds to a single configuration of the system, and this means that the free energy cost required to stretch the spring becomes very large ($F = U - TS$ must always hold)

Looking at figure 3.1 below, it is clear that between these limits, the DNA polymer appears to follow the Worm-Like Chain model due to its elastic properties, which we shall expand on in section 3.2.3.

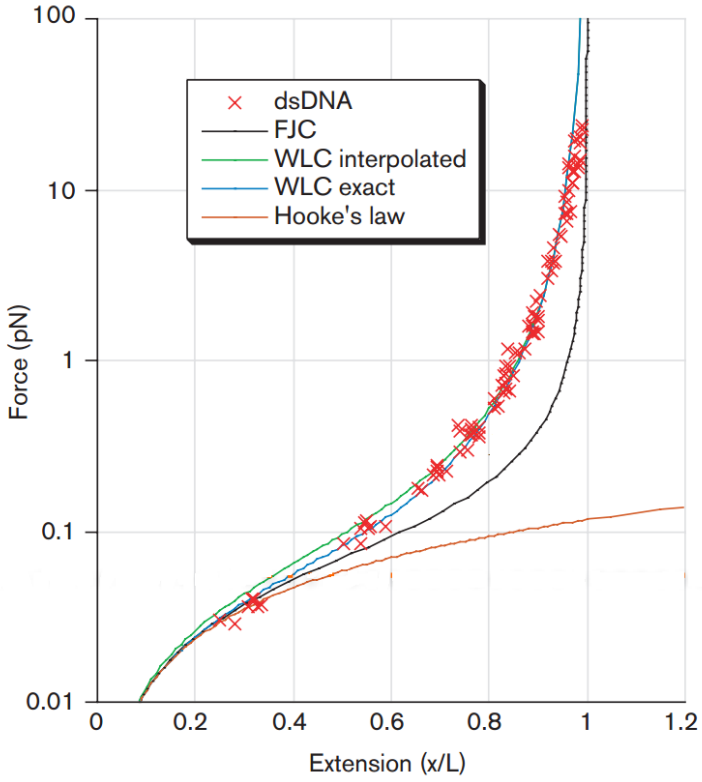

Figure 3.1: Force plotted against extension for various polymer models, where $\ell = Nb$ is the maximum possible length of the polymer

How do these results compare to if we had just used the random walk, end-to-end probability distribution for an FJC given by (3.31)? We know that the entropy S satisfies:

$$S = k_B \log W = \text{constant} + k_B \log f(\mathbf{r}, N) \tag{3.41}$$

where W is the number of possible configurations of a system. Using the definition of $f(\mathbf{r}, N)$ given by (3.31), the free energy is given by

$$F = U - TS = \text{constant} + \frac{3k_BT}{2Nb^2}\mathbf{r}^2 \tag{3.42}$$

The free energy is proportional to the square of the displacement, meaning that we once again obtain an entropic spring with the same effective spring constant as in the low force case. However, using (3.31) does not predict the high force limit, as it represents the probability distribution in an unforced, equilibrium state; we were considering diffusive behaviour, rather than some sort of forced system.

3.2.2 Freely-rotating Chain

The freely-rotating chain (FRC) model is similar to the freely jointed chain, except that we now take into account the angular correlation between adjacent segments, meaning that the FRC satisfies the following correlation functions

$$\langle \mathbf{r}_i \rangle = 0, \quad \langle \mathbf{r}_i \cdot \mathbf{r}_j \rangle = b^2(\cos\theta)^{|i-j|} \tag{3.43}$$

where θ is the (fixed) dihedral angle between the axes of two adjacent segments. Then, the mean-squared end-to-end distance is

$$\left\langle \mathbf{r}^2 \right\rangle = \sum_i^N \left\langle \mathbf{r}_i^2 \right\rangle + \sum_{i \neq j}^N \left\langle \mathbf{r}_i \cdot \mathbf{r}_j \right\rangle = Nb^2 \left[1 + \frac{1}{N} \sum_{i \neq j}^N (\cos\theta)^{|i-j|} \right] \tag{3.44}$$

Evaluating the second term in the brackets requires some attention. Letting $\zeta = \cos\theta$ (that has a nice ring to it....), we want to decompose the sum into a more tractable form.

$$\begin{aligned} \frac{1}{2} \sum_{i \neq j}^N \zeta^{|i-j|} &= \sum_{i=1}^N \sum_{j=1}^{N-i} \zeta^j = \sum_{i=1}^N \zeta \frac{1-\zeta^{N-i}}{1-\zeta} = \frac{\zeta}{1-\zeta} \sum_{i=1}^N 1 - \zeta^{N-i} = \frac{\zeta}{1-\zeta} \left[N - \zeta^N \sum_{i=1}^N \zeta^{-i} \right] \\ &= \frac{\zeta}{1-\zeta} \left[N - \zeta^N \zeta^{-1} \frac{1-\zeta^{-N}}{1-\zeta^{-1}} \right] = \frac{N\zeta}{1-\zeta} \left[1 - \frac{1}{N} \frac{1-\zeta^N}{1-\zeta} \right] \end{aligned} \tag{3.45}$$

Putting this expression pack into (3.44), and substituting back for ζ, this becomes

$$\left\langle r^2 \right\rangle = Nb^2 \left[\frac{1+\cos\theta}{1-\cos\theta} - \frac{2\cos\theta}{N} \frac{1-\cos^N\theta}{(1-\cos\theta)^2} \right] \tag{3.46}$$

In the limit of a long chain ($N \to \infty$), the second term in the expression vanishes, and we finally obtain

$$\boxed{\left\langle r^2 \right\rangle = Nb_{\text{eff}}^2, \quad b_{\text{eff}} = \sqrt{\frac{1+\cos\theta}{1-\cos\theta}}} \tag{3.47}$$

The quantity b_{eff} is called the *Khun length*, and can essentially be thought of as an effective segment length on comparison to the FJC model.

3.2.3 Worm-like Chain

Worm-like chains (WLC) are continuously flexible along their length, but retain some memory of the prior orientation of the chain along its length. Consider two points a and b along a chain of total length ℓ, at which we define tangent vectors $\mathbf{t}(a)$ and $\mathbf{t}(b)$ respectively. Then, we can write the correlation function:

$$\left\langle \mathbf{t}(a) \cdot \mathbf{t}(b) \right\rangle \backsim e^{-|a-b|/\xi_p} \tag{3.48}$$

The quantity ξ_p is known as the *persistence length*. This is essentially the lengthscale over which thermal fluctuations cause the chain to lose memory of its original direction. For DNA, $\xi_p \approx 50\,\text{nm}$. It can also be thought of as a lengthscale that parametrises the energy cost required to bend the chain into a circle of radius R, vis.

$$E_{\text{circ}} = k_B T \, \pi \frac{\xi_p}{R} \tag{3.49}$$

Once again, we want to calculate the mean-squared end-to-end distance:

$$\left\langle r^2 \right\rangle = \left\langle \int_0^\ell da \, \mathbf{t}(a) \cdot \int_0^\ell db \, \mathbf{t}(b) \right\rangle = \int_0^\ell da \int_0^\ell db \, e^{-|a-b|/\xi_p} \tag{3.50}$$

Evaluating both integrals with careful consideration of the absolute value, we arrive at the expression

$$\boxed{\left\langle r^2 \right\rangle = 2\xi_p^2 \left(e^{-\ell/\xi_p} - 1 + \frac{\ell}{\xi_p} \right)} \tag{3.51}$$

As with the FJC, let us evaluate some asymptotic limits of this expression.

- Short Persistence Length ($\xi_p \ll \ell$) - The chain appears to act like there are many segments, and so we should find that our expression reduces to that of the FJC. In this limit, we have that
$$e^{-\ell/\xi_p} \to 0, \quad \frac{\ell}{\xi_p} \gg 1 \tag{3.52}$$
such that
$$\left\langle r^2 \right\rangle \approx 2\xi_p^2 \frac{\ell}{\xi_p} \approx 2\xi_p \ell \tag{3.53}$$
Comparing this expression with (3.26), it is clear that in this limit, the WLC reduces to a FJC with Khun length $b_{\text{eff}} = 2\xi_p$.

- Long Persistence Length ($\xi_p \gg \ell$) - This limit describes a chain that is very resistant to deformation by bending.
$$\left\langle r^2 \right\rangle = 2\xi_p^2 \left(e^{-\ell/\xi_p} - 1 + \frac{\ell}{\xi_p} \right) \approx 2\xi_p^2 \left(1 - \frac{\ell}{\xi_p} + \frac{1}{2}\left(\frac{\ell}{\xi_p}\right)^2 - 1 + \frac{\ell}{\xi_p} \right) \approx \ell^2 \tag{3.54}$$
As expected, the WLC behaves like a straight rod of length ℓ, which can be seen in figure 3.1.

To find the force-extension curve, we need to consider both the energy taken to continuously deform the curve, as well as the energy resulting from the application of a force f (orientated along $\mathbf{e}_z$) to the ends of the molecular chain. Defining the tangent vector $\mathbf{t}$ as before, this energy is given by
$$E_{\xi_p} = \underbrace{\int_0^\ell ds\, \frac{\xi_p}{2\beta} \left| \frac{d\mathbf{t}(s)}{ds} \right|^2}_{\text{continuous deformation}} - \underbrace{\int_0^\ell ds\, f \cos[\theta(s)]}_{\text{applied force}} \tag{3.55}$$
where the angle $\theta(s)$ is defined by $\mathbf{t} \cdot \mathbf{e}_z = \cos[\theta(s)]$. That is, it is the angle between the direction $\mathbf{e}_z$ and the tangent vector at the point s along the curve. We could then theoretically compute the partition function, and take derivatives to find $\langle z \rangle$. However, this proves quite a hard integral to compute, and so instead, we shall simply quote the commonly used interpolation formula for the force-extension curve:
$$f = \frac{k_B T}{4\xi_p} \left[\left(1 - \frac{z}{\ell} \right)^{-2} - 1 + \frac{4z}{\ell} \right] \tag{3.56}$$
This interpolation formula agrees with the FLC in the low force limit, and displays similar divergent behaviour as $z \to \ell$.

3.3 Stochasticity and Fluctuations

Mathematically, a *stochastic* or random process is an object usually defined as a collection of random variables. Historically, the random variables were associated with or indexed by a set of numbers, usually viewed as points in time, giving the interpretation of the stochastic process as representing the numerical values for some system randomly changing over time. In physics, stochastic differential equations are used to describe processes that occur at some consistent rate, but with random fluctuations around said rate. The most common of these is the Langevin equation, which we shall now examine.

3.3.1 The Langevin Equation

The Langevin equation is a stochastic differential equation that describes the time evolution of a particle that is undergoing Brownian motion - the erratic random movement of microscopic particles in a fluid, as a result of continuous bombardment from molecules of the surrounding medium. It has the following form

$$\boxed{\frac{\partial \varphi}{\partial t} + \gamma\varphi = \eta(t)} \tag{3.57}$$

where φ is some field associated with the fluid particle that is subjected to a damping rate γ and to a Gaussian white-noise field η that satisfies

$$\langle \eta(t) \rangle = 0, \quad \langle \eta(t)\eta(t') \rangle = 2D\delta(t-t') \tag{3.58}$$

Note that the angle brackets denote the ensemble average; that is, the average over all possible trajectories associated with the field φ. We cannot analytically solve the entirety of this equation analytically by the definition of η as being a random field. However, we are able to solve for moments of the field φ, as we shall now do so.

Solution by direct integration

We begin our solution by letting $\varphi = \varphi_0 e^{-\gamma t}$, such that we obtain a differential equation for the amplitude φ_0:

$$\frac{\partial \varphi_0}{\partial t} = \eta e^{\gamma t} \quad \longrightarrow \quad \varphi_0 = \varphi(0) + \int_0^t dt'\, \eta(t') e^{\gamma t'} \tag{3.59}$$

Then our solution becomes

$$\boxed{\varphi(t) = e^{-\gamma t}\left[\varphi(0) + \int_0^t dt'\, \eta(t') e^{\gamma t'}\right]} \tag{3.60}$$

It is immediately obvious that $\langle \varphi(t) \rangle = 0$. This makes sense, as we expect that the net effect of random forcing is zero. In order to compute higher moments of φ, we need to calculate the following product:

$$\begin{aligned}\varphi(t_1)\varphi(t_2) = e^{-\gamma(t_1+t_2)}\Bigg[&\varphi(0)^2 + \varphi(0)\int_0^{t_1} dt'\, \eta(t') e^{\gamma t'} \\ &+\varphi(0)\int_0^{t_2} dt''\, \eta(t'') e^{\gamma t''} + \int_0^{t_1} dt' \int_0^{t_2} dt''\, \eta(t')\eta(t'') e^{\gamma(t'+t'')}\Bigg]\end{aligned} \tag{3.61}$$

Taking the average of this expression, and using (3.58), it follows that

$$\langle \varphi(t_1)\varphi(t_2)\rangle = \underbrace{\varphi(0)^2 e^{-\gamma(t_1+t_2)}}_{(1)} + \underbrace{\frac{D}{\gamma} e^{-\gamma(t_1+t_2)}\left(e^{2\gamma t_1}-1\right)}_{(2)} \tag{3.62}$$

At short times, the damped, ballistic motion included in the term (1) dominates. However, at longer times, the stochastic effects of (2) become more important. Astute readers will be querying what we mean by the terms 'long' and 'short'; in comparison to what? Well, it is clear that the field φ can be associated with a correlation time $\tau_c = \gamma^{-1}$ after which any knowledge of initial conditions is lost. This is an appropriate timescale to adopt. For long times such that $t_1, t_2 \gg \tau_c$, only the first order term will remain:

$$\langle \varphi(t_1)\varphi(t_2)\rangle \approx \frac{D}{\gamma} e^{-|t_1-t_2|/\tau_c} \tag{3.63}$$

We are able to write the absolute value in the exponent due to the fact that the two times are arbitrary, and their labels can simply be exchanged.

We can also perform a similar calculation for a quantity Φ, that we shall define as

$$\Phi = \int_0^t dt'\, \varphi(t') \tag{3.64}$$

For example, Φ would denote position in the case where φ corresponded to the particle velocity. Now, we shall assume that we are working at long times $\gg \tau_c$, such that we can make use of the simplified expression (3.63). It follows that

$$\langle \Phi(t_1)\Phi(t_2)\rangle = \int_0^{t_1} dt_1' \int_0^{t_2} dt_2' \left\langle \varphi(t_1')\varphi(t_2')\right\rangle = \int_0^{t_1} dt_1' \int_0^{t_2} dt_2' \frac{D}{\gamma} e^{-\gamma|t_1'-t_2'|} \tag{3.65}$$

$$= \frac{D}{\gamma}\left[\int_0^{t_2} dt_2' \int_{t_2'}^{t_1} dt_1'\, e^{-\gamma(t_1'-t_2')} + \int_0^{t_2} dt_2' \int_0^{t_2'} dt_1'\, e^{-\gamma(t_2'-t_1')}\right] \tag{3.66}$$

where we have assumed that $t_2 \leq t_1$. However, as these times are arbitrary, the resultant expression is also valid for cases where $t_2 \geq t_1$. Performing the integration, we find that

$$\langle \Phi(t_1)\Phi(t_2)\rangle = \frac{D}{\gamma^2}\left[2t_2 - \frac{1}{\gamma}e^{-\gamma t_1}\left(e^{\gamma t_2}-1\right) + \frac{1}{\gamma}\left(e^{-\gamma t_2}-1\right)\right] \tag{3.67}$$

Let us now look at the specific case where $\varphi = v$ and $\Phi = x$. Suppose that we are looking at times where $t_1, t_2 \gg \tau_c$, and then let $t_1 = t_2$. In this case, we obtain the expressions

$$\boxed{\left\langle v^2\right\rangle = \frac{D}{\gamma}, \quad \left\langle x^2\right\rangle = \frac{2D}{\gamma}t} \tag{3.68}$$

which are characteristic of Brownian motion. We can actually use these to find an approximate expression for the constant D. By equipartition:

$$m\left\langle v^2\right\rangle \backsim k_B T \tag{3.69}$$

Using the first expression in (3.68) above, it follows that

$$\boxed{D = \gamma\frac{k_B T}{m}} \tag{3.70}$$

This is the *fluctuation dissipation relation* for the case of Brownian motion. Both greater thermal energy and greater damping result in increased inter-particle collisions, and thus increased collisions with the particle in question; this increases the strength of the correlation between the velocity fields.

Solution by probability distributions

An alternative method to finding moments of the form $\langle v^n \rangle$ is to derive a probability distribution function for the velocity of the system. We define the function $f(v,t)$ as the probability of the particle having a velocity in the phase space cube $[v, v+dv]$ at a given time t. We denote the *actual* particle velocity as $\widetilde{v}(t)$, such that

$$f(v,t) = \langle \delta(v - \widetilde{v}) \rangle = \left\langle \widetilde{f} \right\rangle \tag{3.71}$$

From these definitions, it follows that

$$f(v,t) = \int d\widetilde{v}\, f(\widetilde{v}) \delta(v - \widetilde{v}) \tag{3.72}$$

where the integral is over all possible (actual) particle trajectories $\widetilde{v}(t)$. Differentiating the definition of $\widetilde{f}$:

$$\frac{\partial \widetilde{f}}{\partial t} = \delta'(v - \widetilde{v})(-\dot{\widetilde{v}}) = -\dot{\widetilde{v}} \frac{\partial \widetilde{f}}{\partial v} = -\frac{\partial}{\partial v}\left(\dot{\widetilde{v}} \widetilde{f}\right) \tag{3.73}$$

We are able to make the last step as the argument of the distribution v does not know anything about the actual velocity $\widetilde{v}$. We now use the definition of the Langevin equation (3.57) for $\varphi = v$ to write that

$$\frac{\partial \widetilde{f}}{\partial t} = -\frac{\partial}{\partial v}\left((-\gamma \widetilde{v} + \eta)\delta(v - \widetilde{v})\right) = -\frac{\partial}{\partial v}\left((-\gamma v + \eta)\widetilde{f}\right) = \gamma \frac{\partial}{\partial v}\left(v \widetilde{f}\right) - \frac{\partial}{\partial v}\left(\widetilde{f}\eta\right) \tag{3.74}$$

Formally integrating:

$$\widetilde{f} = \int^t dt' \left[\gamma \frac{\partial}{\partial v}\left(v \widetilde{f}(t')\right) - \frac{\partial}{\partial v}\left(\widetilde{f}(t')\eta(t')\right)\right] \tag{3.75}$$

Taking the correlation function with $\eta(t)$:

$$\left\langle \widetilde{f}(t)\eta(t) \right\rangle = \int^t dt' \left[\gamma \frac{\partial}{\partial v}\left(v \left\langle \widetilde{f}(t')\eta(t) \right\rangle\right) - \frac{\partial}{\partial v}\left(\left\langle \widetilde{f}(t')\eta(t')\eta(t) \right\rangle\right)\right] \tag{3.76}$$

Let us look at each of the terms in the integrand separately. With some thought, it becomes clear that $\widetilde{f}(t')$ cannot depend on some $\eta(t)$ at some future time t, allowing us to conclude that

$$\left\langle \widetilde{f}(t')\eta(t) \right\rangle = 0 \tag{3.77}$$

The second term looks quite complicated, as it is a triple correlator. However, by the same argument as above, $\widetilde{f}(t')$ can only depend on η at times before t', allowing us to break the correlator:

$$\left\langle \widetilde{f}(t')\eta(t')\eta(t) \right\rangle = \left\langle \widetilde{f}(t') \right\rangle \left\langle \eta(t')\eta(t) \right\rangle \tag{3.78}$$

From the definition (3.58), we write that

$$\left\langle \eta(t')\eta(t) \right\rangle = 2D\delta(t - t') = -\frac{\partial}{\partial v}(Df) \tag{3.79}$$

Taking the average of (3.74), we find that

$$\frac{\partial f}{\partial t} = \gamma \frac{\partial}{\partial v}(vf) - \frac{\partial}{\partial v}\left\langle \widetilde{f}\eta \right\rangle \tag{3.80}$$

However, we can obtain an expression for the average in the last term by combining (3.76), (3.77), (3.78), and (3.79), meaning that we obtain the equation:

$$\boxed{\frac{\partial f}{\partial t} = \gamma \frac{\partial}{\partial v}(vf) + D\frac{\partial^2 f}{\partial v^2}} \tag{3.81}$$

We thus obtain an evolution equation for the probability distribution function $f(v,t)$ that involves diffusion in phase space, parametrised by the constant D. This can be used to find evolution equations for moments of the distribution. For example:

$$\frac{\partial}{\partial t}\left\langle v^2\right\rangle = \int dv\, v^2 \frac{\partial f}{\partial v} = \gamma \int dv\, v^2 \frac{\partial}{\partial v}\left(vf\right) + D\int dv\, v^2 \frac{\partial^2 f}{\partial v^2} = -2\gamma\left\langle v^2\right\rangle + 2D \tag{3.82}$$

It is clear that in the steady state, this reduces to the relationship given by (3.68), as expected. A similar process can be used to obtain a probability distribution for the displacement, but the derivation shall not be detailed here.

3.3.2 Fluctuations in Gene Expression

We are now going to apply our knowledge of stochastic differential equations gained through our examination of the Langevin equation to the process of protein production outlined in (3.25). In particular, we shall examine the processes of transcription and translation.

Both mRNA and proteins are biological molecules with finite lifetimes, that we shall define as $\tau_R = \gamma_R^{-1}$ and $\tau_P = \gamma_P^{-1}$. Generally, proteins have very long lifetimes, and their degradation rate is due to the fat that replicating cells will eventually divide, which halves the number of proteins left in each cell. We find that

$$\begin{aligned}\tau_R &\leq \text{ cell cycle time}\\ \tau_P &\gtrsim \text{ cell cycle time}\end{aligned}$$

Transcription

Assume that mRNA is produced at a constant rate k_R through the process of transcription. Then, the mRNA population R can be described by the differential equation

$$\boxed{\frac{dR}{dt} = k_R - \gamma_R R + \eta_R} \tag{3.83}$$

where η_R is a white noise Gaussian field as in (3.58), with its strength parametrised by q_R:

$$\left\langle \eta_R(t)\right\rangle = 0, \quad \left\langle \eta_R(t)\eta_R(t')\right\rangle = q_R\delta(t-t') \tag{3.84}$$

The steady state concentration of mRNA is clearly given by

$$\left\langle R\right\rangle = \frac{k_R}{\gamma_R} \tag{3.85}$$

Let us expand around this steady state value by letting

$$R = \left\langle R\right\rangle + \delta R, \quad |\delta R| \ll |\left\langle R\right\rangle|, \quad \left\langle \delta R(t)\right\rangle = 0 \tag{3.86}$$

Our differential equation simply becomes

$$\frac{d}{dt}\delta R = -\gamma_R \delta R + + \eta_R \tag{3.87}$$

We want to find the spectrum $\left\langle |\delta R(t)|^2\right\rangle$. Motivated by this, we take the (time) Fourier transform of the above equation

$$-i\omega\delta\widetilde{R} = -\gamma_R\delta\widetilde{R} + \widetilde{\eta}_R \quad \longrightarrow \quad \delta\widetilde{R} = \frac{\widetilde{\eta}_R}{\gamma_R - i\omega} \tag{3.88}$$

where the tildes are used to indicate the Fourier transform quantities. The resultant spectrum is then given by the inverse Fourier transform:

$$\left\langle \delta R(t)\delta R(t')\right\rangle = \frac{1}{4\pi^2}\int d\omega d\omega'\, e^{-i(\omega-\omega')t}\frac{\langle \widetilde{\eta}_R(\omega)\widetilde{\eta}_R(\omega')\rangle}{(\gamma_R - i\omega)(\gamma_R + i\omega')} \tag{3.89}$$

This can be evaluated by noting that

$$\left\langle \widetilde{\eta}_R(\omega)\widetilde{\eta}_R(\omega')\right\rangle = \int dtdt'\, e^{i(\omega-\omega')t}\left\langle \eta_R(t)\eta_R(t')\right\rangle = q_R\int dt\, e^{i(\omega-\omega')t} = q_R\delta(\omega-\omega') \tag{3.90}$$

where we have made use of (3.84). Thus, letting $t = t'$, we have that

$$\left\langle \delta R^2\right\rangle = \int \frac{d\omega}{2\pi}\frac{q_R}{\gamma_R^2+\omega^2} = \frac{q_R}{2\gamma_R} \tag{3.91}$$

Now, we would expect that the fluctuations around equilibrium in such a chemical process to be roughly Poisson distributed; the Poisson distribution expresses the probability of a given number of events occurring in a fixed interval if these events occur with an average known rate, and independent of the interval since the last event. This means that we must have that $\left\langle \delta R^2\right\rangle = \langle R\rangle$, fixing the strength of the noise $q_R = 2k_R$.

Translation

The rate of translation is evidently linked to the population of mRNA, as the ribosomes read mRNA to produce proteins. We thus assume that the proteins are produced at a rate $k_P R$. Then, the protein population P can be described by the differential equation

$$\boxed{\frac{dP}{dt} = k_p R - \gamma_P P + \eta_P} \tag{3.92}$$

where η_P is once again a white noise Gaussian field as in (3.58), with its strength parametrised by q_P:

$$\langle \eta_P(t)\rangle = 0, \quad \left\langle \eta_P(t)\eta_P(t')\right\rangle = q_P\delta(t-t'), \quad q_P = \frac{2k_Pk_R}{\gamma_R} \tag{3.93}$$

The steady state concentration of proteins is given by

$$\langle P\rangle = \frac{k_P}{\gamma_P}\langle R\rangle = b\frac{k_R}{\gamma_P} \tag{3.94}$$

where $b = k_P/\gamma_R$ is called the *burst size* that describes the average number or proteins translated per mRNA. $\langle P\rangle$ behaves as we expect; it scales proportionally to the rates of production of both proteins and mRNA, and inversely with their rates of degradation. We shall again expand around this steady state value as in (3.86), such that

$$\frac{d}{dt}\delta P = -\gamma_P\delta P + k_P\delta R + \eta_p \tag{3.95}$$

Taking the Fourier transform as before

$$-i\omega\delta\widetilde{P} = -\gamma_P\delta\widetilde{P} + k_P\delta\widetilde{R} + \widetilde{\eta}_P \quad \longrightarrow \quad \delta\widetilde{P} = \frac{k_P\delta\widetilde{R} + \widetilde{\eta}_P}{\gamma_P - i\omega} \tag{3.96}$$

The resultant spectrum is then given by

$$\left\langle \delta P(t)\delta P(t')\right\rangle = \frac{1}{4\pi^2}\int d\omega d\omega'\, e^{-i(\omega-\omega')t}\frac{\left\langle (k_P\delta\widetilde{R} + \widetilde{\eta}_P)(k_P\delta\widetilde{R}^* + \widetilde{\eta}_P)\right\rangle}{(\gamma_P - i\omega)(\gamma_P + i\omega')} \tag{3.97}$$

where we have dropped the ω and ω' dependence for the sake of compactness. To simplify this expression, we expand the correlator:

$$\left\langle (k_P\delta\widetilde{R}(\omega)+\widetilde{\eta}_P(\omega))(k_P\delta\widetilde{R}^*(\omega')+\widetilde{\eta}_P^*)\right\rangle \tag{3.98}$$
$$= k_P^2\left\langle \delta\widetilde{R}(\omega)\delta\widetilde{R}^*(\omega')\right\rangle + \left\langle \widetilde{\eta}_P(\omega)\widetilde{\eta}_P^*(\omega')\right\rangle + k_P\left\langle \delta\widetilde{R}(\omega)\widetilde{\eta}_P(\omega')\right\rangle + k_P\left\langle \delta\widetilde{R}^*(\omega')\widetilde{\eta}_P(\omega)\right\rangle$$

Now, we argue that the last of these two correlators are zero as the concentration of R does not have any dependence on the stochastic field η_P. This means that we are only left with the terms

$$\left\langle (k_P\delta\widetilde{R}(\omega)+\widetilde{\eta}_P(\omega))(k_P\delta\widetilde{R}^*(\omega')+\widetilde{\eta}_P^*)\right\rangle = \left(q_R\frac{k_P^2}{\gamma_R^2+\omega^2}+q_P\right)\delta(\omega-\omega') \tag{3.99}$$

Substituting this in, and performing the integration yields

$$\boxed{\frac{\langle\delta P^2\rangle}{\langle P\rangle} = 1+\frac{b}{1+\gamma_P/\gamma_R}\approx 1+b} \tag{3.100}$$

The last approximation follows from the assuming that the proteins are much longer lived than the mRNA $\gamma_P/\gamma_R \ll 1$. It is thus clear that this process is non-Poissonian. This is because fluctuations in the protein population is slaved to the fluctuations within the mRNA population, such that a small number of mRNA leads to large fluctuations around the mean protein population, while a large number leads to small fluctuations.

A comment on noise

In the previous two sections, we have been using the word *noise* to describe the random fluctuations around an equilibrium state. While this usage is not incorrect, we have not been specific enough. In cellular biology, we often refer to two different types noise:

- Extrinsic noise - Caused by the differences between different cells, such as through the numbers of ribosomes, or the copy numbers of different proteins
- Intrinsic noise - Caused by stochastic fluctuations within the cells themselves. In the case of fluctuations in gene expression, the fields η_R and η_P describe intrinsic noise

We can measure noise by colour coding two almost identical types of genes (ensuring similar rates of replication), and plotting their abundance within a sample of cells as they replicate. Example data for this kind of experiment is shown below. The first set of graphs shows the populations in the presence of only extrinsic noise, while the second set shows the populations with both types of noise present.

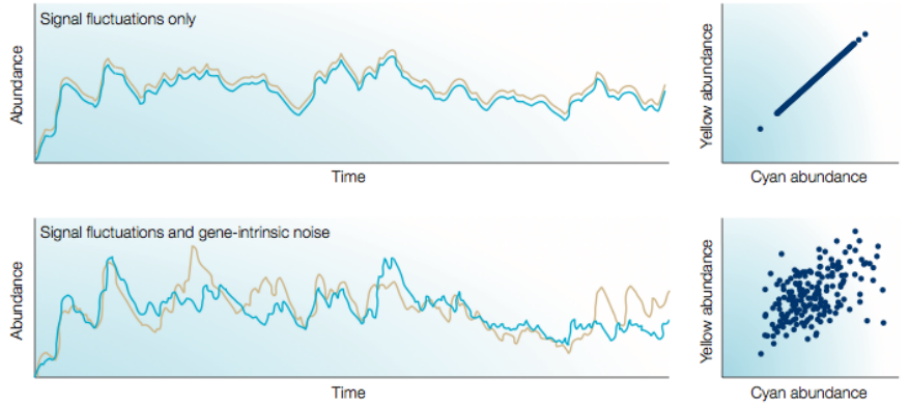

Figure 3.2: Relative populations (abundance) of two gene alleles, colour coded yellow and cyan

3.4 Active Transport

In section 3.1.2, we talked about how there is a scale separation between cells that operate internally via purely diffusive transport, and those that also employ active transport. In this model, we shall examine some theory surrounding active transport, and consider a basic model of active transport across a cell membrane.

3.4.1 The Fokker-Plank Equation

Consider the general case of a diffusion process occurring in a potential $U(\mathbf{r})$. Let $f(\mathbf{r},t)$ be the probability density of some random variable associated with the diffusion process at a time t, in the range $[\mathbf{r},\mathbf{r}+d\mathbf{r}]$. Let $\mathbf{j}$ be the associated probability current, where

$$\mathbf{j} = \mathbf{j}_{\text{ diffusion}} + \mathbf{j}_{\text{ potential}} \tag{3.101}$$

where we have written explicitly the parts associated with the diffusive transport and active transport (due to the potential) respectively. Now, we know that $\mathbf{j}_{\text{ diffusion}} \equiv \mathbf{j}_d$ must be some function of ∇f such that $\mathbf{j}_d = 0$ for $\nabla f = 0$, and that it must have the opposite site to ∇f by probability conservation. Then, assuming that ∇f is small:

$$\mathbf{j}_d(\nabla f) \approx \mathbf{j}_d(0) + \mathbf{j}_d'(0)\nabla f + \dots \tag{3.102}$$

meaning that to first order we can write that

$$\mathbf{j}_d = -D\nabla f \tag{3.103}$$

for some diffusion coefficient D. Consider some volume V bounded by a closed surface $S = \partial V$. Then, the rate of change of probability density within the volume is opposite and equal to the rate at which said probability density leaves the volume through the bounding surface.

$$\frac{\partial}{\partial t}\int_V dV\ f = -\int_{\partial V} d\mathbf{S}\cdot\mathbf{j} = -\int_V dV\ \nabla\cdot\mathbf{j} \tag{3.104}$$

As this must hold true for all volumes, we have the conservation of probability density $f(\mathbf{r},t)$ given by

$$\frac{\partial f}{\partial t} + \nabla\cdot\mathbf{j} = 0 \tag{3.105}$$

In equilibrium, we know that $\mathbf{j} = 0$ by definition, and that the resultant probability distribution will be Boltzmann distributed according to the potential $U(\mathbf{r})$. That is, we must have

$$f_{eq}(\mathbf{r}) \backsim e^{-\beta U(\mathbf{r})}, \quad \beta = (k_B T)^{-1} \tag{3.106}$$

Now, as $\mathbf{j} = 0$, we must also have that

$$\mathbf{j}_{\text{potential}} \equiv \mathbf{j}_p = -\mathbf{j}_d = D\nabla f_{eq} = D\beta f_{eq}\nabla U \tag{3.107}$$

This means that in general for non-equilibrium states, we have that

$$\mathbf{j} = -D\nabla f - D\beta f\nabla U \tag{3.108}$$

Substituting this result into (3.105) allows us to derive the *Fokker-Plank equation*:

$$\boxed{\frac{\partial f(\mathbf{r},t)}{\partial t} = D\nabla\left[\beta f(\mathbf{r},t)\nabla U(\mathbf{r}) + \nabla f(\mathbf{r},t)\right]} \tag{3.109}$$

This equation describes the evolution of a random variable f that is associated with a diffusive process occurring under some sort of forcing. We note that for $U(\mathbf{r}) =$ constant, this simply reduces to the simple diffusion equation.

3.4.2 The Molecular Ratchet

We shall now consider an example of active transport. Suppose that a translocating polymer (one being pulled across a membrane) of length ℓ has N binding sites spaced a distance d apart. On the inside of the membrane, there are binding proteins that irreversibly bind to the translocating polymer, which can locally (for lengths $\ll \xi_p$) be treated as a rigid rod. Once bound, these proteins prevent the polymer from moving further backwards out of the membrane. Lastly, suppose that there is some force F pulling against the translocation.

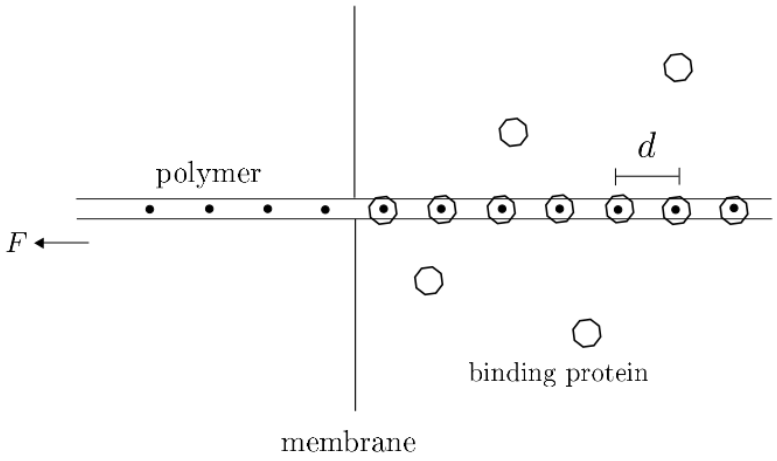

Figure 3.3: A schematic diagram of the molecular ratchet

We can apply the Fokker-Plank equation (3.109) to this problem. In this case, we restrict the problem to one-dimension, letting $f(x,t) = \int dx \int dy\, f(\mathbf{r},t)$, and $U = Fx$. It follows that

$$j_x = -\frac{DF}{k_B T} f(x,t) - D\frac{\partial f(x,t)}{\partial x} \tag{3.110}$$

In the steady state, $f(x,t) \to f(x)$, and $j_x = j_0 = \text{constant}$. The above equation is now a differential equation for $f(x)$. It is subject to the boundary condition that $f(d) = 0$, as if a protein binding site reaches a distance d from the pore, then another binding site emerges, which is now the site that we are considering. We obtain the solution that

$$f(\bar{x}) = \frac{\bar{F}}{1 + \bar{F} - e^{\bar{F}}} \left(1 - e^{-\bar{F}(\bar{x}-1)}\right) \tag{3.111}$$

where we have introduced the dimensionless variables $\bar{F} = Fd/k_B T$ and $\bar{x} = x/d$. Now, as the probability current is constant, we know that the associated velocity will be constant, such that $v = j_0/d$. Substituting our solution back into (3.110) yields

$$v(\bar{F}) = \frac{D}{d} \frac{\bar{F}^2}{e^{\bar{F}} - \bar{F} - 1} \tag{3.112}$$

Let us take a look at some limits of this expression:

- Low force limit ($\bar{F} \to 0$) - Expanding the exponential for small argument gives $v \approx 2D/d$. This is clearly the diffusion limit of the ratchet; even without a load, it takes some finite time for the polymer to diffuse from $x = 0$ to $x = d$, which is governed by the diffusion coefficient D
- High force limit ($\bar{F} \to \infty$) - In this case, $v \approx 0$. This is because even though there is a very large force being applied, the binding proteins in the ratchet mechanism stop it from being pulled out completely

3.5 Measurement Techniques

All of the above theoretical calculations are all very well and good, but in a practical subject such as biology, one has to be able to measure things, or at least know how to measure things. As such, we are going to spend this section discussing various measurement techniques used on very small scales that are applicable to biology.

3.5.1 Optical Tweezers

Optical tweezers use a highly focussed laser beam to provide an attractive (or repulsive) force to small - on the order of $\backsim 10^{-6}$ m - dielectric objects.

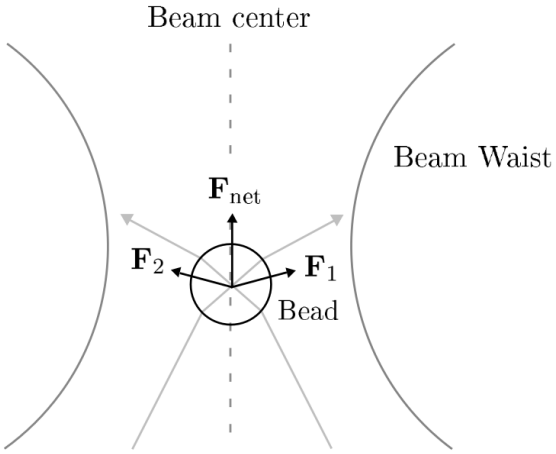

Figure 3.4: A schematic diagram showing the forces involved in the operation of optical tweezers

The incoming laser beam has an approximately Lorentzian profile, meaning that on-axis rays have a greater intensity than off-axis rays. The rays passing through the bead experience a change in momentum due to the difference in refractive index between the surrounding medium and the bead itself, causing a force to be applied to the bead. Suppose that the bead is displaced horizontally from the beam center. The larger momentum change associated with the greater intensity of the central rays causes the net force to be towards the center, ensuring that the bead remains aligned along the beam center. If it is displaced vertically away from the focus, the momentum change of the focussed rays applies a net force towards the focus, as shown in figure 3.4. The combination of these two 'restoring' forces ensures that the bead remains positioned in the focus of the laser beam, meaning that it can be moved around under motion of the laser.

We can model the forces on the bead by assuming it is polarisable, such that it can be treated under the electric dipole approximation. Consider the bead to be made of two charges of opposite signs at $\mathbf{r}_1$ and $\mathbf{r}_2$, such that $\mathbf{p} = q(\mathbf{r}_2 - \mathbf{r}_1)$. The net force on the bead is given by

$$\mathbf{F}_{\text{net}} = q\left(\mathbf{E}(\mathbf{r}_2) - \mathbf{E}(\mathbf{r}_1) + \frac{d(\mathbf{r}_2 - \mathbf{r}_1)}{dt} \times \mathbf{B}\right) \tag{3.113}$$

$$= q\left(\cancel{\mathbf{E}(\mathbf{r}_2)} + ((\mathbf{r}_2 - \mathbf{r}_1)\cdot\nabla)\mathbf{E} - \cancel{\mathbf{E}(\mathbf{r}_2)} + \frac{d(\mathbf{r}_2 - \mathbf{r}_1)}{dt} \times \mathbf{B}\right) \tag{3.114}$$

$$= \alpha\left((\mathbf{E}\cdot\nabla)\mathbf{E} + \frac{d\mathbf{E}}{dt} \times \mathbf{B}\right) \tag{3.115}$$

where we have assumed that the dielectric is linear $\mathbf{p} = \alpha\mathbf{E}$. We can make use of the identities

$$(\mathbf{E}\cdot\nabla)\mathbf{E} = \nabla\left(\frac{E^2}{2}\right) - \mathbf{E}\times(\nabla\times\mathbf{E}), \quad \nabla\times\mathbf{E} = -\frac{\partial\mathbf{B}}{\partial t} \tag{3.116}$$

such that we can write

$$\mathbf{F}_{\text{net}} = \alpha\left(\frac{1}{2}\nabla E^2 + \frac{d}{dt}(\mathbf{E}\times\mathbf{B})\right) \tag{3.117}$$

The second term in this expression is the time derivative of the Poynting Vector (up to multiplicative constants). Since this is constant for a laser when sampling over frequencies much smaller than the frequency of the laser light $\backsim 10^{14}\,\text{Hz}$, we can ignore this derivative. Noting that $E^2 = 2I(\mathbf{r})/cn\epsilon_0$, where $I(\mathbf{r})$ is the intensity of the laser beam as a function of position, the net force on the bead can be written as

$$\boxed{\mathbf{F}_{\text{net}} = \frac{\alpha}{cn\epsilon_0}\nabla I(\mathbf{r})} \tag{3.118}$$

Near the beam center, we can model the position of the bead using a Langevin-type equation

$$m\ddot{\mathbf{r}} + \gamma\dot{\mathbf{r}} + k\mathbf{r} = \boldsymbol{\eta}(t) \tag{3.119}$$

where $\boldsymbol{\eta}(t)$ is Gaussian white noise field as before. We assume that the forces exerted on the bead are very large, such that $\gamma, k \gg 1$, such that we can neglect the mass of the particle. Our equation thus becomes

$$\gamma\dot{\mathbf{r}} + k\mathbf{r} = \boldsymbol{\eta}(t) \tag{3.120}$$

We want to find the power spectrum associated with the trapped bead. Taking the Fourier transform as before, it is clear that

$$\widetilde{\mathbf{r}}(\omega) = \frac{\widetilde{\boldsymbol{\eta}}(\omega)}{k - i\gamma\omega} \tag{3.121}$$

From the fluctuation-dissipation relation, the power spectrum due to white noise is given by

$$|\widetilde{\boldsymbol{\eta}}(\omega)|^2 = 2\gamma k_B T \tag{3.122}$$

allowing us to derive the power spectrum of the bead:

$$\boxed{|\widetilde{\mathbf{r}}(\omega)|^2 = \frac{2k_B T}{\gamma}\frac{1}{\omega^2 + \omega_c^2}} \tag{3.123}$$

This is a Lorentzian of characteristic half-width $\omega_c = k/\gamma$ (the *corner frequency*), which can be used to find k by fitting this distribution to experimental data, and approximating γ by Stokes' Drag (1.101).

This optical tweezer set-up has many uses, given the precision with which it can be used to move small-scale objects. To the knowledge of this author, this was the technique that was used to measure the force-extension curves for the DNA strand shown in (3.1). It can also be used to measure the strength of 'molecular motors'. For example, if one attaches RNAp to one tweezer bead, and a strand of DNA to the other, one can measure the strength of the RNAp as it transcribes, assuming that the RNA strand is kept under constant force.

3.5.2 Magnetic Tweezers

Magnetic tweezers are used similarly to optical tweezers to enable the manipulation of cells and molecules through the application of controlled mechanical forces. The magnetic tweezers make use of a simple electromagnetic to operate; an electric current passing through a solenoid enclosing a ferromagnetic needle generates a magnetic field gradient that pulls a magnetisable bead towards the tip of the needle. Thus, manipulating the position of the needle allows the magnetic bead to be moved around.

Some applications of the magnetic tweezers include:

- Adhesion strength - Magnetic tweezers can be used to study cell adhesion strength. For this, magnetic beads are coated with an ECM (a collection of extracellular molecules secreted by cells that provides structural and biochemical support to the surrounding cells), which are then adhered to to cell surface. A controlled force is applied to a bead, and the percentage of the beads that remain attached to the cell under study is measured
- Cellular response to external stimuli - A magnetic bead is linked to an integrin receptor on the surface of a cell. The magnetic bead is made to oscillate at some known frequency through the application of the tweezers. When cells are submitted to a mechanical stimulus, they sense it, and stiffen the local areas where the stimulus was applied. This causes that amplitude of the oscillations to decrease over time, which can be measured
- Microrheology - This is the characterisation of mechanical properties of single cells or subcellular properties (cell or nuclear deformability). Using a bead attached strongly to the cell surface, it is possible to quantify several properties of cells, such as compliance and fluidity

3.5.3 Fluorescence Resonance Energy Transfer

Flourescence Resonance Energy Transfer (FRET) allows the detection of nanometre scale relative motions between two flurophores (chemical compound that can emit light upon excitation). It is based on the resonant coupling of two fluorophores attached to the molecule of interest. If the excitation spectrum of one of the fluorophores is sufficiently higher in energy than the acceptor, then it can be selectively excited by a laser, or a narrow-band of frequencies. When excited, this fluorophore can decay radiatively or non-radiatively; one of the non-radiative decay channels is the tranfer to energy by near-field dipole-dipole coupling to the other fluorophore. The rate of energy transfer, as per the Van-der-Waals force, scales as r^6, where r is the separation between the two fluorophores. This means that the efficiency of the transfer η scales as

$$\eta = \frac{1}{1 + (r/r_0)^6} \tag{3.124}$$

where η is estimated from the ratio between the florescence intensities at wavelengths characteristic of the two fluorophores. The *Förster Radius* r_0 is typically in the range $\backsim$ 2-6 nm, so displacements in the range $\backsim$ 1-10 nm can be observed. It depends on the overlap between the spectra of the fluorophores and on their relative orientations.

3.5.4 Atomic Force Microscope

The atomic force microscope (AFM) has a demonstrated resolution on the order of fractions of a nanometre, which is roughly three orders of magnitude better than the optical

diffraction limit. A needle tip with dimensions on the order of $\backsim \mu$m attached to a cantilever is passed over a microscopic surface. The vertical and lateral deflections of the cantilever due to the contours of the surface are measured using an optical laser that is reflected off the end of the cantilever into a photodiode. This allows startlingly detailed images of very microscopic surfaces to be produced.

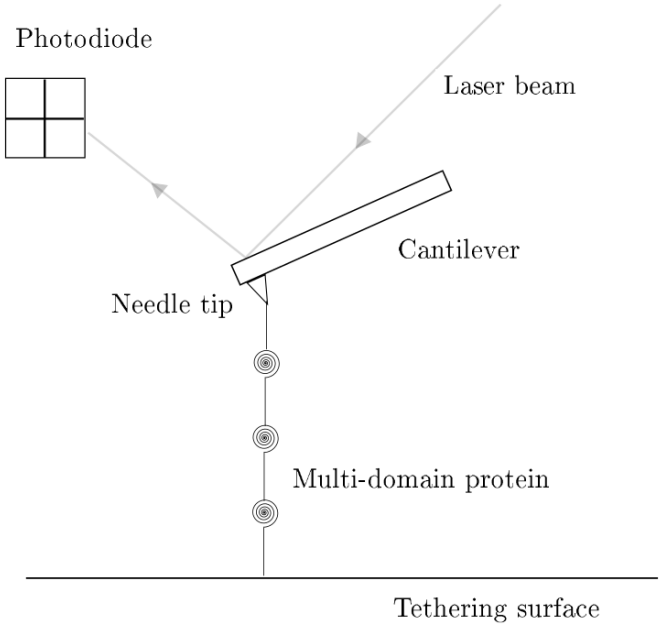

Figure 3.5: A diagram of the atomic force microscope when used as a cantilever

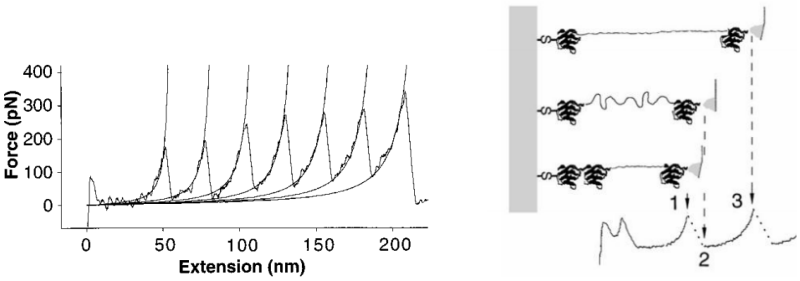

(a) (b)

Figure 3.6: The (a) force-extension curves and (b) unfolding of a multi-domain protein

The AFM can also be used to measure force extension curves. Mutli-domained proteins are long proteins that contain 'bunches' of the strand along its length; when these are subjected to enough force, they will un-ravel into a single strand. If one of these is attached to the tip of the AFM, and the other end tethered from this surface (figure 3.5), the force-extension curve can be measured, as in figure 3.6.